Femtosecond Cr^{4+}:forsterite Laser for Applications in Telecommunications and Biophotonics

Thesis presented for the degree of

Doctor of Philosophy

to the University of St Andrews

by

Alan McWilliam, MSci (Hons)

J. F. Allen Physics Research Laboratories
School of Physics and Astronomy
University of St Andrews
North Haugh
St Andrews
KY16 9SS
Scotland, UK

November 2006

Declarations

I, Alan McWilliam, hereby certify that this thesis, which is approximately thirty thousand words in length, has been written by me, that it is the record of work carried out by me and that it has not been submitted in any previous application for a higher degree.

       Signature of candidate   Date

I was admitted as a research student and as a candidate for the degree of Doctor of Philosophy in October, 2003; the higher study for which this is a record was carried out in the University of St Andrews between 2003 and 2006.

       Signature of candidate   Date

In submitting this thesis to the University of St Andrews I understand that I am giving permission for it to be made available for use in accordance with the regulations of the University Library for the time being in force, subject to any copyright vested in the work not being affected thereby. I also understand that the title and abstract will be published, and that a copy of the work may be made and supplied to any *bona fide* library or research worker.

       Signature of candidate   Date

I hereby certify that the candidate has fulfilled the conditions of the Resolution and Regulations appropriate for the degree of Doctor of Philosophy in the University of St Andrews and that the candidate is qualified to submit this thesis in application for that degree.

       Signature of supervisor   Date

*"The true delight is in the finding out
rather than the knowing."*

Isaac Asimov

Abstract

In this thesis, the development of a femtosecond Cr^{4+}:forsterite solid-state laser is described where the mode-locking procedure was initiated using two novel saturable absorbers. One was a GaInNAs quantum-well device and the other a quantum-dot-based saturable absorber. These devices had not previously been exploited for the generation of femtosecond pulses from a solid-state laser but in the course of this project, successful mode-locked laser operation in the femtosecond domain was demonstrated for both devices.

When the GaInNAs device was incorporated in the Cr^{4+}:forsterite laser, transform-limited pulses with durations as short as 62fs were obtained. The performance of this femtosecond laser was significantly superior to that for previous quantum-well based saturable absorbers in the 1300nm spectral region. The dynamics of the device were investigated with the aim of refining subsequent devices and to explore the potential to grow future devices for use at longer wavelengths.

At the outset of my research work quantum-dot based saturable absorbers had not be used for the mode locking of solid-state lasers in the femtosecond regime. The work presented in this thesis showed that quantum-dot structures could be exploited very effectively for this purpose. This was initially achieved with the quantum-dot element being inclined at an off-normal incidence within the cavity but experimental assessment together with further development of the device allowed for implementation at normal incidence. Reliable operation of the femtosecond laser was demonstrated very convincingly where transform-limited pulses of 160fs duration were generated.

Having developed practical femtosecond Cr^{4+}:forsterite lasers, the final part of the project research was directed towards exemplar applications for a laser operating in the 1300nm spectral region. These were biophotonics experiments in which assessments of both deep tissue penetration and two-photon chromosome cutting were undertaken. This work confirmed the suitability of the 1300nm laser radiation for propagation through substantial thicknesses of biological tissue (~15cm). The demonstration of highly localised two-photon cutting of Muntjac deer chromosomes also represented a novel result because single-photon absorption could be avoided effectively and the temporal broadening of the femtosecond pulses in the delivery optics arising from group velocity dispersion around 1300nm was minimal.

Contents

Chapter 1 – Introduction and Background

1.1   Introduction

"The solution looking for a problem", that was how the first laser built in 1960 was described [1]. Over the course of the following 45 years the range of available laser sources, from high average powered lasers [2, 3] to ultrashort-pulse lasers [4, 5], has grown tremendously and with them the number of applications for which lasers are now used. These applications encroach upon on many aspects of our lives from scanning barcodes, to CD and DVD players, through to the fields of communications, data storage, entertainment, medicine and surgery, materials processing, military technology and meteorology to name but a few.

Lasers are now usually designed and built with specific purposes in mind. The work described in this thesis was funded within a £12 million interdisciplinary research programme called the Ultrafast Photonics Collaboration (UPC). This collaboration combined the resources of seven leading UK universities and five industrial companies with the goal of delivering the enabling science and related technologies for future data communications based on femtosecond networks. As part of this programme, suitable sources for transmitting data were required. One feasible solution was an ultrafast laser that produces femtosecond pulses in the 1300nm spectral region and this forms the basis for this thesis.

Over the course of this chapter, I shall define femtosecond laser pulses, describe how they are produced and their various uses. However, first of all it is necessary to establish the length of a femtosecond. Ever since the first femtosecond pulses were produced, analogies have been used to try to impart an impression of just how short they are in comparison to a second. It is all very well saying that

$$1fs = 0.000000000000001s$$

but for most people this is just a number and difficult to appreciate. However, it can be said that the ratio of a femtosecond to a second is the same as one second to thirty-two million years. Alternatively, if you were to imagine a femtosecond to be the thickness of an average page of writing paper then a second's worth of pages piled on top of each other would be able to make the earth-moon trip five times!

There are four major characteristics of a femtosecond pulsed laser that can be exploited. These are the pulse duration, the broad spectrum, the pulse repetition frequency and the high peak power of the pulse [6]. The femtosecond pulse duration can provide exceptional temporal resolution. This allows for the observation of extremely fast processes such as the motion of electrons around the atom [7] or photosynthesis [8], which take place on picosecond time scales. Associated with this short pulse duration is the broad bandwidth of the pulse, which is desirable for use in the non-invasive imaging technique of optical coherence tomography (OCT) [9], and in the field of datacommunications with dense wavelength division multiplexing (DWDM) [10]. If this latter technique is used in conjunction with optical time division multiplexing (OTDM), which exploits the high pulse repetition frequency, then huge amounts of data, up to 1.36Tbits/s, can propagate down optical fibres [11]. Finally, femtosecond pulses have a high peak power that allows for the ablation of many materials. This ablation effect, turning a solid material directly into a gas, allows for holes or cuts to be made in materials, even tissue [12, 13], with virtually no heat damage to the surrounding area.

1.2 Applications of ultrashort lasers in the 1300nm spectral region

When considering femtosecond pulses at 1300nm there are two fields for which this wavelength regime is particularly suited; these are telecommunications and biophotonics. In the field of telecommunications the wavelengths are chosen based on how well they propagate in optical fibres [14].
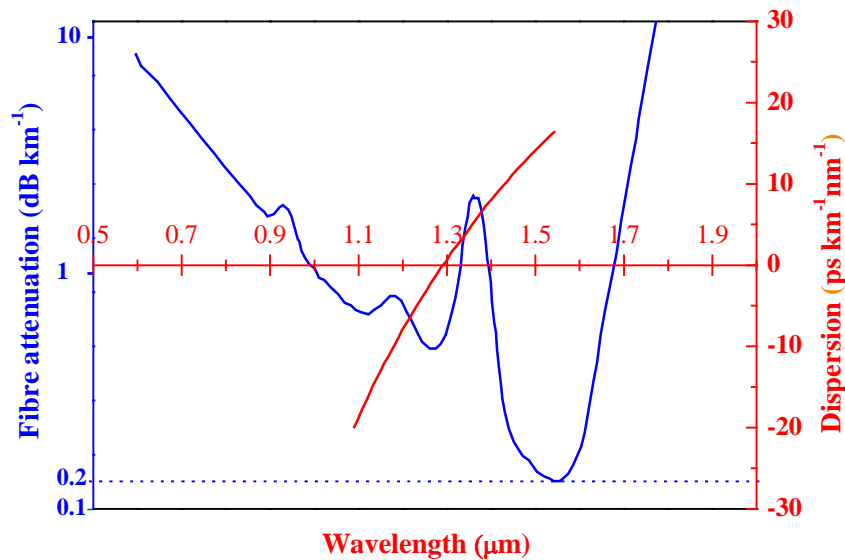
Fig. 1.1 Attenuation and dispersion properties of optical fibre.

Fig. 1.1 [15] shows the attenuation and dispersion for a typical optical fibre. This graph shows that a minimum of attenuation exists around 1550nm. Thus this is the wavelength regime that current long range (transoceanic) networks use and where the well-developed optical amplifiers are found. However, if pulses are to be used successfully then the dispersion characteristics of the fibre have to be considered. In the spectral region around 1300nm there is negligible dispersion; therefore these pulses will not broaden significantly as they propagate in an optical fibre. This is of particular importance in systems where DWDM is to be used [16], since as the pulse travels down an optical fibre it will broaden in time. If this is not counteracted then

the pulses will begin to overlap with their neighbouring pulses, causing the information on the individual pulses to become lost. Therefore for a data communications network based on femtosecond pulses, a wavelength that propagates with low dispersion in optical fibres is required.

A second area in which pulses around 1300nm are desirable is in the field of biophotonics [17]. Fig. 1.2 [18] shows that human skin has a transmission window centred around 1300nm [19].

Fig. 1.2 The attenuation of various constituents of biological tissue.

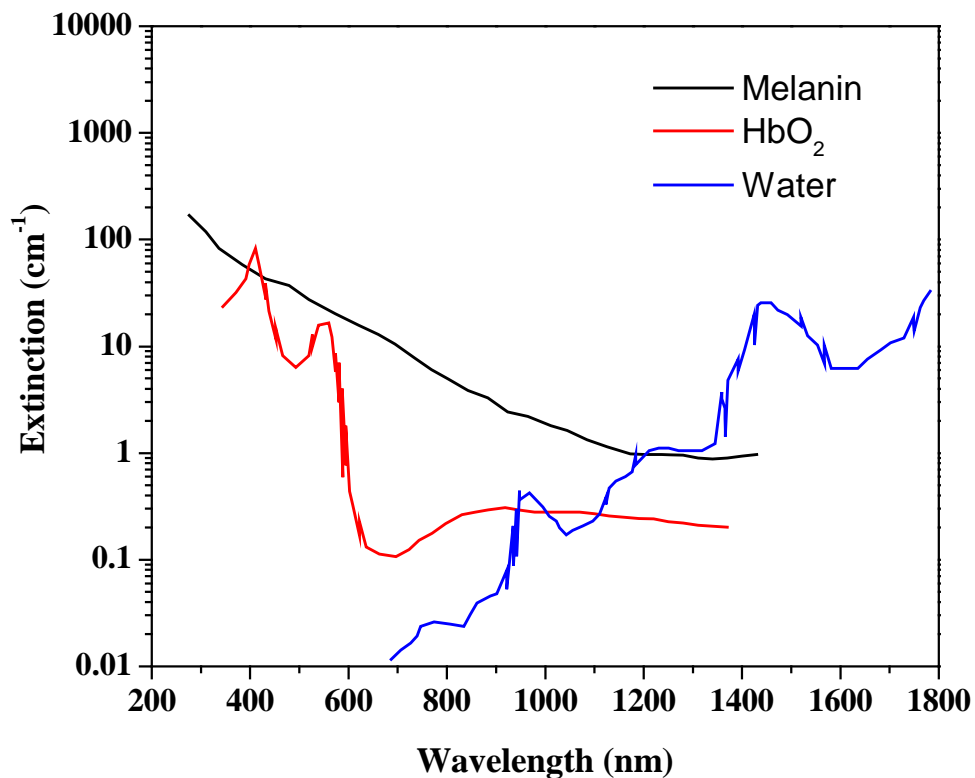The major constituents in biological tissue that absorb radiation include water, melanin and oxyhaemoglobin (HbO_2) for which the attenuation characteristics are shown. The graph shows that in the 1300nm region there is a minimum of absorption

between these three components and therefore this spectral region is ideal for therapeutic or diagnostic applications in medicine [20].

The topic of photodynamic therapy is of particular interest [21]. This is where a photo-sensitising agent is introduced into the tissue and illuminated by optical radiation, specifically laser radiation. This agent can be designed to fluoresce to aid in the diagnosis of disease, or to undergo a chemical change for therapeutic purposes. This technique is desirable for the diagnosis or treatment of a number of aliments, many of which require penetration through a thickness of tissue. As Fig. 1.2 shows, radiation around 1300nm can provide this required penetration depth.

The high peak powers generated from an ultrashort-pulse laser allow for the additional possibility of 2-photon absorption techniques to be utilised [22]. Due to the lack of absorption of radiation at 1300nm, minimal damage will be caused by the passage of this light through tissue. A chemical or dye that absorbs at half this wavelength could be introduced into the desired area of tissue. Then light from a femtosecond Cr^{4+}:forsterite laser, which operates in the 1300nm spectral regime, would be absorbed where it is needed without causing any damage to the surrounding tissue.

1.3 Pulse behaviour in dielectric materials

The way in which an optical pulse interacts with the various components within a laser resonator has advantages and disadvantages in the generation of ultrashort pulses. The nature of this interaction depends on the intensity of the pulse, with higher powers giving rise to a variety of nonlinear effects that can be exploited in the process of mode locking. The effects explained in this section have to be carefully controlled if the femtosecond regime is to be exploited.

By definition, a dielectric material under the influence of an electromagnetic field will produce an intensity-dependent polarisation response of the form,

$$P(E) = \varepsilon_o(\chi_{(1)}E + \chi_{(2)}E^2 + \chi_{(3)}E^3 + \ldots\ldots) \tag{1.1}$$

where ε_o is the permittivity of free space, E is the applied electric field and $\chi_{(n)}$ is the nth order susceptibility. If the electric field incident on the dielectric material is of low power then only the first-order term plays a role. $\chi_{(1)}$ is the linear susceptibility of the first order and is used to describe the effects of refraction, reflection and dispersion. With the associated high peak power of a circulating pulse then higher-order susceptibilities become relevant in the media within the laser cavity. These are weaker nonlinear effects and depend strongly on the underlying symmetry of the dielectric laser gain material. $\chi_{(2)}$ effects include second harmonic generation (SHG) and sum-frequency mixing (SFG), but these effects are only experienced in non-centrosymmetric materials [23]. The $\chi_{(3)}$ term describes third order nonlinear effects such as third harmonic generation (THG) and the optical Kerr effect. The $\chi_{(3)}$ term is experienced in centrosymmetric materials such as the gain media exploited in this project and these effects will be considered in Section 1.3.3.

It should also be noted that because of the peak power of an ultrashort pulse higher-order nonlinear effects would also be present. I shall look at the ideal case where only linear effects are considered prior to dealing with these nonlinear effects in Section 1.3.3.

1.3.1 Pulse propagation in a linear regime

Before I describe the effects that a pulse experiences as it propagates through a dielectric medium I shall introduce the mathematical description of this incident

pulse. An optical pulse has an associated time-dependent electric field *E(t)* that can be expressed as,

$$E(t) = \varepsilon(t)e^{i\phi(t)}e^{-i\omega_o t}$$

(1.2)

where $\varepsilon(t)$ is the time varying electric field envelope, $\phi(t)$ is the temporal phase variation across the pulse and ω_o is the optical carrier frequency [24]. Along with this time-dependent electric field, the shape of the pulse needs to expressed. Due to the pulse shaping that takes place inside the laser systems described in this thesis, the pulse amplitude has a temporal envelope represented by a sec*h* function of the form,

$$\varepsilon(t) = \varepsilon_o \sec h\left(\frac{1.763t}{\Delta\tau_p}\right)$$

(1.3)

Here $\Delta\tau_p$ is the full width half maximum of the pulse and ε_o is the real electric field amplitude. The intensity of the pulse takes a sech^2 pulse form and can be described as,

$$I(t) \approx |\varepsilon(t)|^2 = \varepsilon_o^2 \sec h^2\left(\frac{1.763t}{\Delta\tau_p}\right)$$

(1.4)

It is essential to know the pulse shape when measuring the pulse duration, and this will become evident in Section 1.5.

If a pulse of the form described above propagates through a linear dielectric material it will undergo a frequency-dependent phase change. For a dielectric material of length *L* this phase change is defined as,

$$\phi(\omega) = Ln_o(\lambda)\frac{2\pi}{\lambda} = \frac{\omega Ln_o(\omega)}{c} = \beta(\omega)L$$

(1.5)

where λ is the wavelength, ω is the angular frequency, *c* is the speed of light, $\beta(\omega)$ is the propagation constant and $n_o(\lambda)$ is the wavelength-dependent refractive index of the material [25]. The wavelength-dependent refractive index can be expressed as,

$$n_o(\lambda) = 1 + \frac{1}{2} \operatorname{Re}\left[\chi_{(1)}(\lambda) \right] \tag{1.6}$$

and shows the relationship between the first-order susceptibility and the wavelength of the optical pulse. It is this relationship between the wavelength and refractive index that leads to the dispersive effects experienced by an optical pulse. If equation 1.5 is expanded as a Taylor series centred around ω_o then the expanded terms can each be related to one of the various dispersive effects.

$$\beta(\omega) = \beta(\omega_o) + \beta'(\omega - \omega_o) + \frac{1}{2!}\beta''(\omega - \omega_o)^2 + \frac{1}{3!}\beta'''(\omega - \omega_o)^3 + ... \tag{1.7}$$

$\beta(\omega_o)$ is related to the phase velocity,

$$\beta(\omega_o) = \frac{\omega_0}{v_\phi} \tag{1.8}$$

The phase velocity is the velocity at which the central carrier frequency propagates. The second term in equation 1.7, $\beta'(\omega - \omega_o)$, describes the group velocity,

$$\beta' = \frac{d\beta}{d\omega} = \frac{1}{c}\left(n + \omega_o \frac{dn}{d\omega} \right) = \frac{1}{v_g} \tag{1.9}$$

and is the first derivative of the phase velocity. The group velocity is the velocity at which the pulse envelope propagates inside the dielectric material. The third term in equation 1.7 is the group velocity dispersion (GVD) and it is this term that describes the most significant pulse broadening effect. GVD is expressed as,

$$\beta'' = \frac{d\beta'}{d\omega} = \frac{1}{c}\left(2\frac{dn}{d\omega} + \omega_o \frac{d^2 n}{d\omega^2} \right) \tag{1.10}$$

This equation describes how the distribution of wavelengths across the bandwidth of a pulse will experience different group velocities as the pulse travels through a dielectric material. For the majority of dielectric materials the value for GVD is positive. As such the longer wavelengths components (red) of the pulse will travel

faster through a material than the shorter wavelength (blue) components. This is one of the pulse broadening effects that must be compensated for if ultrashort pulses are to be produced, along with self-phase modulation described in Section 1.3.3.2.

For completeness the fourth term in equation 1.7, β''', describes the third-order dispersion (TOD) in the system. TOD is not as dominant as the role of GVD and can usually be ignored unless dealing with pulses of ~20fs or shorter [26].

1.3.2 Dispersion compensation

To generate femtosecond pulses the dispersive effects described above have to be counteracted. This compensation, ideally, has to precisely counteract the positive dispersion that the pulse experiences as it passes through the dielectric gain material and other elements in the laser cavity, to allow for the creation of dispersion free pulses. As was explained above, in materials with positive GVD the longer wavelength (red) components of a pulse travel faster than the shorter wavelength (blue) components. Thus the pulses broaden in time. For ultrashort pulses to be realised, a net negative GVD has to be introduced into the cavity. Dispersion compensation in solid-state lasers is most simply provided by the insertion of a set of low-loss prisms into the cavity, as illustrated in Fig. 1.3.

Fig. 1.3. A two prism pair arrangement which can be used to generate negative GVD

The presence of the low-loss prism material introduces additional positive GVD into the system. As can be seen in Fig. 1.3, due to the wavelength dependent exit angle from the prisms, the longer (red) wavelength component travels a shorter path through the air than the shorter (blue) wavelength components. However the longer wavelength (red) component travels a longer path within the prism. By choosing the correct separation between the prisms an overall negative GVD can be introduced to the cavity where the shorter wavelength (blue) components will experience a shorter physical path length through the prism system.

Looking back at Fig. 1.3 it can be seen that the sequence of prisms is symmetric. By placing a mirror at the central position a single pair of prisms can provide the same value of negative GVD as a sequence of 4 prisms [27]. This single prism pair method is commonly used when dispersion compensation is implemented inside a standing wave laser cavity. This also highlights an advantage of using a standing wave resonator over a ring resonator. Since the intracavity beam inside a ring resonator travels in a ring a four-prism sequence will always be required and cannot be simplified to a single prism pair as in a standing wave resonator. Using a single pair of prisms will reduce the intracavity losses as well as simplifying the cavity.

Another widely used method of dispersion compensation uses chirped mirrors [28]. These reflect longer wavelengths from deeper inside the mirror compared to the shorter wavelengths on the surface of the mirror introducing negative GVD. Other approaches have utilised diffraction gratings [29], and Gires-Tournois interferometers [30], both of which provided the necessary negative GVD.

1.3.3 Pulse propagation in a nonlinear regime

Due to the centrosymmetric nature of the gain material and the high peak powers of the propagating pulse $\chi_{(3)}$ nonlinear effects take place. With a view towards ultrashort pulse generation, the third-order nonlinear effects of the optical Kerr effect, self-phase modulation and self focusing, are of most importance and shall be discussed in this section.

1.3.3.1 Optical Kerr effect

A sufficiently strong electromagnetic field, $E(t)$, incident on a dielectric material will experience a $\chi_{(3)}$ induced change of refractive index, Δn, in the material. This change in refractive index will depend upon the incoming intensity profile of the pulse and will reach a maximum at the peak of the pulse.

The refractive index of a material is the combination of the linear, n_o, and nonlinear, n_{2E}, index coefficients and can be expressed as,

$$n = n_o + n_{2E}\left|E(t)\right|^2 \tag{1.11}$$

n_{2E} is given by,

$$n_{2E} = \frac{3\chi_{(3)}}{8n_o} \tag{1.12}$$

For an ultrashort pulse the electromagnetic field is associated with the intensity of an optical pulse by,

$$I(t) \approx cn\left|E(t)\right|^2 \tag{1.13}$$

This allows equation 1.11 and 1.12 to be rewritten in terms of intensity,

$$n = n_o + n_{2I}I(t) \tag{1.14}$$

where,

11

$$n_{2I} = \frac{2n_{2E}}{\varepsilon_o c n_o} \tag{1.15}$$

n_{2I} is the related nonlinear refractive index coefficient and for most materials is positive. From the above equations it can be seen that for increasing pulse intensities the refractive index of the material will increase. It is this effect that gives rise to self focusing and the spectral broadening mechanism of self-phase modulation.

1.3.3.2 Self-phase modulation

The optical Kerr effect can be said to be essentially instantaneous in materials. As was discussed above, the refractive index change, Δn, reaches a maximum at the peak of the pulse profile. In materials having a positive nonlinear refractive index, n_{2I}, there is also an associated phase shift, $\Delta\phi(t)$, and with it a change in frequency, Δv, given by,

$$\Delta v = \frac{d}{dt}\Delta\phi(t) = \frac{d}{dt}\left(\frac{2\pi}{\lambda}Ln_{2I}I(t)\right) \tag{1.16}$$

Here L is the propagation length and I(t) is the pulse intensity. Equation 1.16 shows that as the leading edge of the pulse rises in intensity, the refractive index of the dielectric material increases and therefore the velocity of the pulse decreases. The frequency components in the leading edge of the pulse undergo a red-shift. Conversely, the frequency components in the trailing edge of the pulse undergo a blue-shift, Fig. 1.4, as the refractive index change of the material decreases with decreasing incident intensity.

This effect is often approximated as another form of linear dispersion and is compensated for using the techniques described earlier. Self-phase modulation (SPM) plays a hugely vital role in the generation of ultrashort pulses, allowing for the broadening of the spectral bandwidth by distributing the intracavity power over more

oscillating modes. SPM also plays a vital role in the formation of solitonic pulses. These effects will be discussed in more detail in Section 1.4.
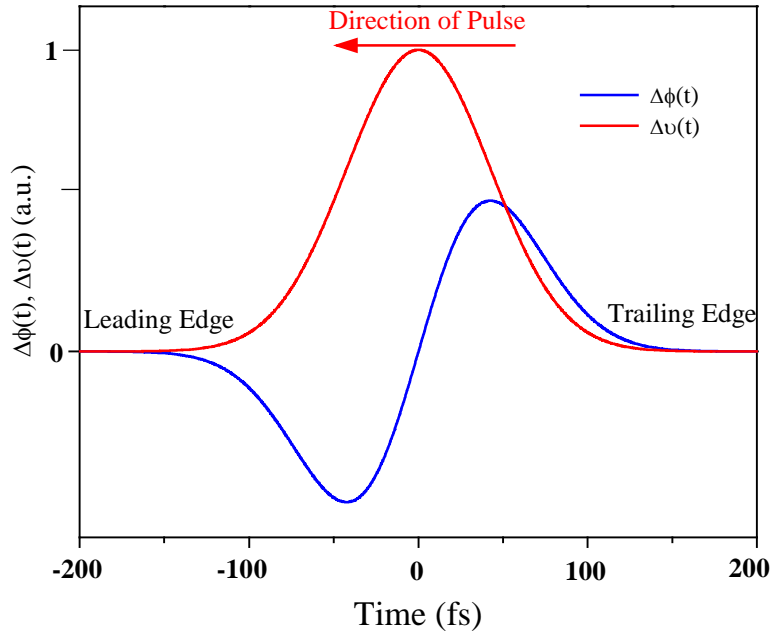

Fig. 1.4 Phase ($\Delta\phi$) and frequency ($\Delta\upsilon$) shift of the pulse undergoing self-phase modulation.

1.3.3.3 Self focusing effect

Consider a dielectric material that has a positive optical Kerr coefficient, through which a pulse having a Gaussian intensity profile is propagating. Due to the Gaussian intensity profile there is a higher intensity in the centre of the pulse than at the wings. Referring back to Equation 1.14 this will lead to a non-uniform change of the refractive index across the pulse profile.

Fig. 1.5 shows the phase fronts passing through such a material. The higher refractive index experienced at the centre of the pulse results in a lower phase velocity than in the wings. Therefore, the centre of the beam becomes retarded with respect to the wings, resulting in the beam undergoing an actual focusing. This is similar to the pulse passing through a weak positive lens. Since this effect is brought about by the

optical Kerr effect this is known as the Kerr-lens effect and is exploited in Kerr-lens mode locking[31].

Fig. 1.5. Self focusing of a pulse passing through a dielectric medium

1.4 Ultrashort pulse generation

The effects described in the previous section can be exploited to produce ultrashort pulses in a process known as mode locking. Other techniques for producing short pulses include Q-switching, gain switching and cavity dumping, but to generate femtosecond pulses mode locking remains the sole path.

There are several techniques for mode locking. Two will be described: Kerr-lens mode locking (KLM) and mode locking where semiconductor saturable absorbers are employed to create intensity-dependent loss mechanisms. Both of these are classed as passive mode locking techniques and rely on phase locking through amplitude modulation. Certain similarities exist between all mode-locking techniques in that all require a broadband gain material with a spectral bandwidth capable of supporting a large number of longitudinal modes. The longitudinal modes that a cavity can support will each have a slightly different wavelength separated by an integral number of half wavelengths given by Equation 1.17, which depends upon the cavity length. However, not all modes defined by this formula can exist within the cavity because they need to experience gain, therefore these modes have to fall under

the spectral bandwidth of the gain material. As such, Equation 1.17 and the spectral bandwidth of the gain material define the longitudinal modes that can exist in a given laser resonator.

$$\Delta \upsilon = \frac{c}{2nl} \qquad (1.17)$$

where 2nl is the round trip length of the cavity and c is the speed of light. The output from the laser as a function of time depends on the phase, frequencies and amplitudes of these individual longitudinal modes relative to each other. The phase, frequencies and amplitude of the modes vary independently and the total irradiance of the system is simply the sum of each individual mode's irradiance. If we can force all these modes to maintain a fixed phase relationship, oscillate in phase, then the laser is said to be mode locked. In such a system the individual modes add together constructively and destructively to produce a stream of ultrashort pulses, each separated by the cavity round trip time, 2nl/c, as shown in Fig. 1.6.
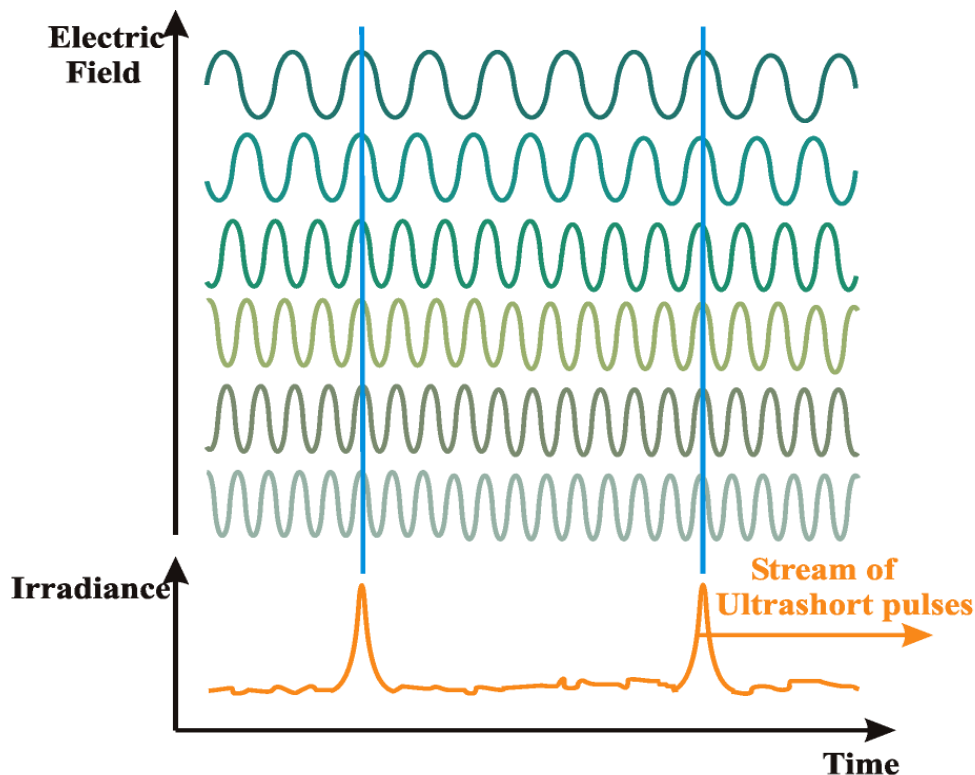

Fig. 1.6 Illustration of mode locking, where a number of oscillating modes are locked together in phase (blue lines) to generate a stream of ultrashort pulses.

It is the way in which the modes are forced into this fixed phase relationship that defines the various mode-locking techniques. Modulation has to be applied to the radiation within the laser cavity to force the modes into this fixed phase relationship. This can be done actively, by way of an acousto-optic modulator for instance, or, as is the case here, passively by introducing a nonlinear element into the cavity to provide an intensity dependent loss or gain mechanism. The gain or loss modulation can be thought of as a "shutter" which when closed provides loss in the cavity with no laser output. If opened every *2nl/c* seconds for a very brief period of time then a net-gain window will be open where the oscillating modes become fixed and a pulsed output will be generated. The laser can only sustain lasing while this net-gain window is open. This can be provided in one of three ways as described in the next section.

In passive mode locking this "shutter" is provided by an intracavity element with a non-linear intensity-dependent characteristic. It is these passive mode-locking techniques that have proved more successful than active techniques and allowed the shortest pulses to be produced.

1.4.1 Passive mode locking [32-36]

Passive mode locking utilises nonlinear effects to provide the necessary modulation to initiate the mode-locking process. This can be obtained with the use of a saturable absorber, here a loss or gain modulation is achieved through self-amplitude modulation (SAM), where a pulse saturates the absorber. This has desirable effects such as providing the opportunity for small-scale noise spikes to initiate the saturation process for mode locking. The parameters of the saturable absorber can be chosen to make this self-starting operation more favourable and in combination with the

recovery time of the gain, will create the "shutter" or short net-gain window required for mode locked operation. Three possibilities for this are shown in Fig. 1.7.
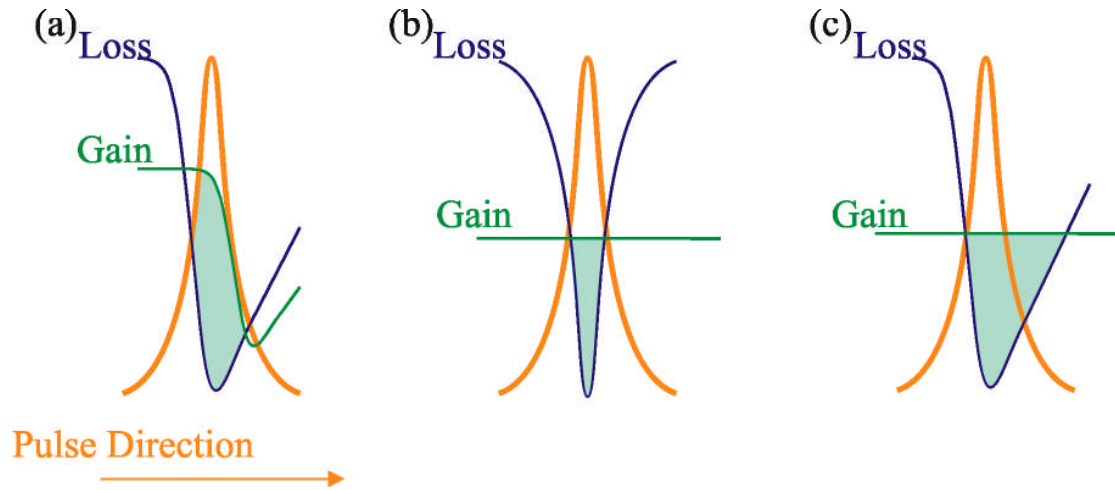

Fig. 1.7 Passive mode locking mechanism (a) Slow Saturable Absorption (SSA) (b) Fast Saturable Absorption (FSA) (c) Solitonic mode locking. The blue coloured area represents the net gain window.

If we first consider a saturable absorber with a recovery time that is long compared to the duration of the pulse then we have a slow saturable absorber (SSA) mechanism. This causes the front of the pulse to be suppressed while the tail of the pulse will pass through without attenuation. Since the recovery time is slow, this method relies on a fast recovery of the gain saturation between pulses to create this "shutter" effect. The combination of the long recovery time of the absorber and the gain saturation provides a short net gain window for mode locking, Fig. 1.7(a). For solid-state lasers the upper state lifetime is generally much longer than the pulse repetition frequency so there is insufficient gain saturation for this process to take place. Thus, we have to look to other techniques for mode locking in solid-state lasers. These are fast saturable absorber (FSA) mode locking, Fig. 1.7(b), and solitonic mode locking, Fig. 1.7(c).

Fast saturable absorber (FSA) mode locking requires a fast recovery time of the saturable absorber to create a suitably short net-gain window. Kerr lens mode locking has proved to be the most successful FSA technique so far, where the laser crystal itself acts effectively as the fast saturable absorber.

1.4.2 Kerr-lens mode locking

As the name suggests, this technique utilises the optical Kerr effect which will cause the intense pulse in the cavity to undergo self-focusing. The cavity is designed in such a way that a continuous wave, unmode-locked operation is discouraged. This is achieved either by means of hard aperture KLM where an intracavity slit is introduced to severely attenuate the continuous wave (CW) beam or by soft aperture KLM where the pump beam geometry is chosen to favour mode locked operation. The self-focusing effect of the mode locked pulses brings the intracavity beam into a more favourable environment for lasing, either focusing through the aperture or increasing the mode matching between the pump and intracavity beams. This acts as the intensity dependent gain mechanism to provide the modulation needed for mode locking.

The major advantage of KLM is its inherently broadband nature. The process of SPM causes the spectral components to broaden, allowing access to larger oscillating bandwidths and, as such, shorter pulses to be formed. Indeed, the shortest pulses have been realised from a KLM laser [37]. However KLM is not usually self-starting and requires an initial noise perturbation to grow into the pulse train. Tapping a mirror can provide this noise spike. Also the laser requires critical cavity alignment and is susceptible to environmental perturbations. When dealing with low gain materials such as Cr^{4+}:forsterite, the intracavity power instabilities can make the

starting and stabilisation rather difficult. For these reasons, and others, Kerr lens mode locking was not used in this research.

1.4.3 Solitonic mode locking [38-41]

Fig. 1.7 illustrates the three possible mechanisms that can give rise to femtosecond pulses. The third technique is known as solitonic mode locking. For solitonic mode locking the pulse shaping mechanism that leads to mode locked operation relies on the formation and propagation of soliton-like pulses. This is achieved by the careful balancing of the group velocity dispersion in the system with self-phase modulation. The mode locked pulse train builds up from background noise spikes. An additional loss mechanism, at the cavity round trip frequency, is required to initialise the mode locking and to stabilise the soliton. This loss mechanism can be active or passive but will typically take the form of a saturable absorber.

The short net-gain window for mode locking provided by SSA and FSA is not necessary in this case, as the soliton formation itself is the dominant mechanism for pulse shaping. This means that solitonic mode locking can have a much longer gain window as shown in Fig. 1.7(c). This allows saturable absorbers with much longer recovery times to be used with recovery times of up to 10 times the pulse duration being acceptable.

There is some active debate over the primary mechanism involved in solitonic mode locking and whether this is completely independent from the KLM process. The use of a saturable absorber to initiate and stabilise solitonic mode locking as described here results in ultrashort pulses which will inevitably lead to the presence of Kerr non-linearity within the cavity. Whether this plays a role in solitonic mode locking or is just a secondary effect is a matter of opinion.

1.4.4 Semiconductor saturable absorbers [42-46]

For passive mode locking using saturable absorbers two possible devices are typically used: a *se*miconductor *s*aturable *a*bsorber *m*irror (SESAM) or a *s*aturable *B*ragg *r*eflector (SBR). Both provide an intensity-dependent reflectivity to administer the necessary loss/gain modulation and therefore the intense pulses in mode locked operation are favoured over the continuous wave, unmode-locked operation of the laser. Both devices exhibit similar characteristics, with layers of high and low index semiconductor materials to act as a Bragg reflector with a saturable absorber layer near the top of the device. The saturable absorber provides the modulation for mode locking to take place, initially noise spikes in the laser act to bleach the saturable absorber before building up into the mode locked pulse train, with the intense pulses acting to saturate the absorption. These devices are designed to provide broad flat reflectivity for the broadband circulating intracavity radiation.

Any difference between the two devices can be found in the semiconductor layer structure and also the growth technique and post processing of the device. Generally, the absorber layer for a SESAM has been grown at a lower temperature than that of a SBR; this affects the spectral and temporal responses of the device with SESAMs displaying a much broader profile than SBRs where the spectral and temporal characteristics tend to be sharply peaked. With advances in epitaxial growth techniques such as molecular beam epitaxy (MBE), these devices can be grown with greater precision and with specific characteristics in mind, making for highly desirable mode locking elements. The range of research [47-51] in which SESAMs or SBRs are used for mode locking shows the versatility of these devices and the range of wavelengths and pulse durations, from picosecond to sub-10 femtoseconds, over which self-starting mode locking can be initiated and maintained.

There are five important macroscopic properties of semiconductor saturable absorbers that determine the operation of a passively mode-locked laser. These are impulse recovery time, τ_A, modulation depth, ΔR, non-saturable loss, ΔR_{NS}, saturation fluence, F_{sat}, and the spectral bandwidth, $\Delta\lambda$.

The impulse recovery time, τ_A, is the time the device takes to recover after an intense incident pulse has saturated the device [42]. A suitable recovery time is essential for the appropriate mode locking mechanism. For fast saturable absorption mode locking this must be of the order of the pulse duration. For solitonic mode locking the impulse recovery time can be up to ten times the duration of the pulse.

The modulation depth, ΔR, is the maximum change in reflectivity of the device between a low intensity incident pulse and a high intensity pulse that bleaches the absorber. To become bleached the incident pulse needs a fluence (defined as energy density per unit area) much larger than the saturation fluence of the absorber. The larger the modulation depth, the shorter the duration of the pulse that can be supported and the greater the likelyhood of self-starting operation. The drawback of having a larger modulation depth is the increased chance of Q-switching instabilities, so a balance must be found. To alter the modulation depth the reflectivity of the front surface can be altered, or the thickness of the absorber. Typically ΔR is 1-2%.

Non-saturable losses, ΔR_{NS}, are any losses that are present after an intense pulse has bleached the absorber. These losses include a less than 100% reflectivity of the Bragg stack, scattering losses and residual absorption. The design and growth of the device influences the amount of non-saturable losses present. Absorbers grown at low temperatures tend to display a significantly higher non-saturable loss than a high temperature growth device such as a typical SBR. For use in low gain systems, such as the laser described in this thesis, the non-saturable losses were kept as low as

possible and indeed the GaInNAs device discussed in Chapter 3 displayed negligible non-saturable losses [48].

Saturation fluence, F_{sat}, is defined as the energy density per unit area, and is a measure of the minimum energy density per unit area upon the saturable absorber required to fully saturate it. This property should ideally be kept as small as possible so that the device can be operated while fully saturated minimising any residual losses and allowing access to the available modulation depth. Also, with high saturation fluence, Q-switched mode locking is more likely to take place, and the possibility of damaging the structure is increasing likely with higher fluence. The saturation fluence of the device can be controlled in a number of different ways, during growth of the device structure the reflectivity of the top layer can be altered. Alternatively the position of the absorber in the device could be varied.

Another property of a saturable absorber is its spectral bandwidth. This is the range of wavelengths that are reflected from the Bragg stack and as such this places certain constraints on the minimum pulse duration that can be produced. The spectral bandwidth of the device can be determined from the index contrast between the layers of the Bragg stack and from the thickness of these layers. This property of the system along with the gain bandwidth of the gain crystal will determine the range of wavelengths over which lasing can be sustain. From this the minimum pulse duration can be determined.

Throughout this project, saturable absorber devices were used to initiate mode locking. These have included a GaInNAs device (Chapter 3) and a quantum-dot based saturable absorber (Chapter 4). The particular properties of these devices and the advantages their use has over the previously tried saturable absorber devices in the 1300nm spectral region will be discussed in greater detail in these later chapters.

1.5 Pulse measurement [23, 52-54]

The measurement of the duration of ultrashort pulses is not a trivial problem. Ideally, to measure the time duration of any given event you have to compare it to another event with a known shorter duration. Ultrashort pulses are the fastest man-made events, which raises the problem of how the duration of these pulses can be measured. The answer is to compare the pulses against themselves through a technique called autocorrelation.

As mentioned earlier, it is important that we know the shape of the pulse. This is vital because the shape of the pulse will determine the constants and conversion factors required to correctly calculate the pulse duration.
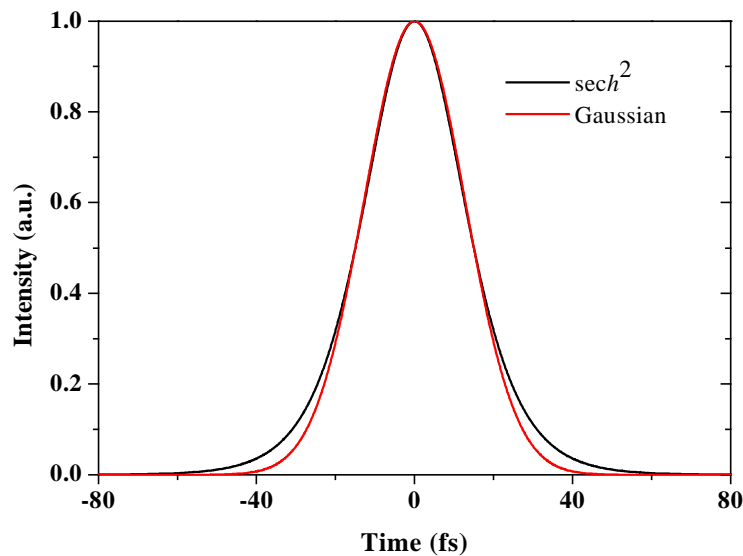

Fig. 1.8 Comparison of the Gaussian and sech^2 pulse shapes.

Fig. 1.8 illustrates the difference between the most commonly assumed pulse shapes of Gaussian and sech^2. These two pulse shapes may seem very similar but both will give rise to very different mathematical descriptions for a pulse.

The mathematical description of the propagating pulse shape was described in Section 1.3.1 and from these equations a further fundamental property of the pulse can be introduced. The temporal and spectral characteristics of a pulse are related

through the Fourier transform. The Fourier transform of the temporal pulse, *I(t)*, in real space gives the spectral pulse, *I(ω),* in reciprocal space [32]. This means that the temporal and spectral bandwidths of an ultrashort pulse cannot vary independently and leads us to the bandwidth theorem where,

$$\Delta v \Delta \tau_p \geq TBP \qquad (1.18)$$

Here, $\Delta \upsilon$ is the full width half-maximum spectral bandwidth of a pulse, $\Delta \tau_p$ is the full width half-maximum of the pulse duration and TBP is the time-bandwidth product. For a Gaussian pulse the TBP is 0.44 and for a sech^2 pulse is 0.32. For an ideal pulse, then, the TBP will be equal to these values. When this happens the pulse is said to be transform limited, or bandwidth limited, and the pulse will have the shortest possible pulse duration for a given spectral bandwidth. If a chirp was present on the pulse then the value for the TBP would be larger. This value gives an indication of whether the dispersion compensation of a cavity is sufficient. Chirp can be understood as the time dependence of the pulse's instantaneous frequency. More specifically, an up chirp describes a pulse in which the instantaneous frequency increases with time and is brought about by dispersion in propagating through a dielectric medium as described above. The shortest pulse durations are obtained for a pulse without any chirp, hence the requirement to introduce dispersion compensation into the laser cavity.

1.5.1 Two-photon absorption autocorrelation

The two-photon absorption autocorrelation technique is perhaps the simplest of a wide variety of different autocorrelation methods.
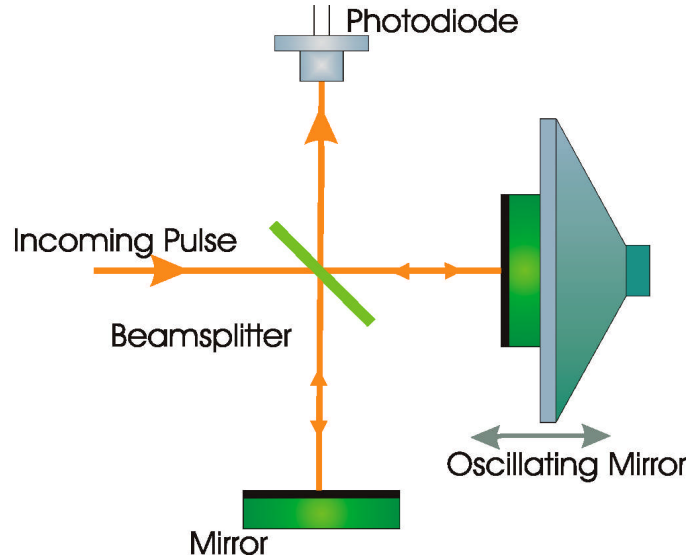

Fig. 1.9 A two-photon absorption autocorrelator

Fig. 1.9 is a representative schematic of a two-photon absorption autocorrelator. The incident incoming pulse is split into two equal intensity components, both of which are directed down paths of equal optical lengths and are recombined on the detector. One pulse is reflected from a static mirror and the other from an oscillating mirror that introduces a delay causing the pulses to be scanned across each other and monitored at the detector. For this autocorrelator set-up to work the detector must have a quadratic response to the incident intensity. This was first achieved by using second harmonic crystals but these are expensive, difficult to align and consideration needs to be made about their phasematching bandwidth. The same quadratic response can be achieved by the use of semiconductor materials such as LEDs or simple photodiodes [55, 56]. These provide a much simpler and cheaper alternative as the two-photon absorption in a semiconductor exhibits this necessary quadratic response. An incident photon of greater energy than the semiconductor bandgap energy, E_g, will be absorbed

linearly with respect to incident power. However, if the incident intensity of photons is high enough, as in the high peak intensity of an ultrashort pulse, then photons of energy $1/2E_g<E<E_g$ can undergo a relatively efficient two-photon absorption process. The photocurrent produced from this has the desired quadratic response to the incident intensity. For the Cr^{4+}:forsterite laser described in this thesis, a cheap and widely available silicon diode was used to measure pulse durations.

If the two-photon detector is calibrated for a relatively slow frequency response then a time-averaged intensity autocorrelation is recorded. This is defined as,

$$G_i(\tau) = 1 + 2g(\tau) \qquad (1.19)$$

where g(τ) is the background free autocorrelation function and is expressed as,

$$g(\tau) = \frac{\int\limits_{-\infty}^{\infty} I(t)I(t-\tau)dt}{\int\limits_{-\infty}^{\infty} I(t)^2 dt} \qquad (1.20)$$

It can be seen from the previous two equations that no functions of phase are included. Therefore, no information about the chirp on the pulse is included in the autocorrelation trace. Also, for the autocorrelation to provide valid information then the correct contrast ratio must be achieved. For values of $\tau=0$, $\pm\infty$ then respective values of 1 and 3 for $G_i(\tau)$ are found. So for the two-photon intensity autocorrelation to provide accurate information then a contrast ratio of 3:1 must be achieved, Fig. 1.10 (a).
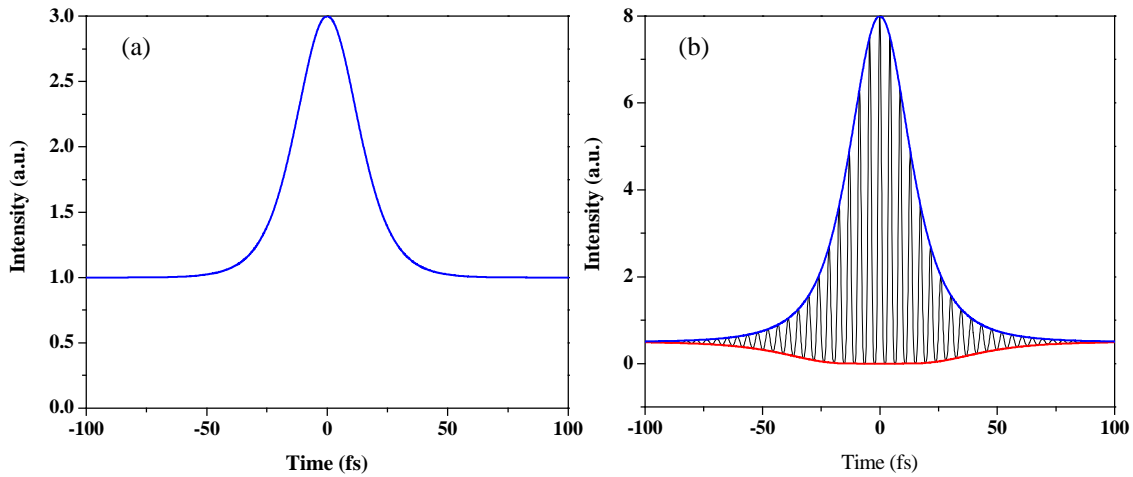
Fig. 1.10 Representative two-photon autocorrelation traces: (a) intensity (b) interferometric

The FWHM of the autocorrelation trace does not directly provide the pulse duration of the ultrashort pulse. To calculate the pulse duration a conversion factor has to be used. This factor depends on the assumed pulse shape and this relation takes the form,

$$\Delta\tau_p = \frac{\Delta t}{k} \qquad (1.21)$$

Here k is the conversion factor, which for a $\sec h^2$ pulse shape is 1.542 or for Gaussian pulse shapes is 1.414.

By adapting the response time of the detector, an interferometric autocorrelator can be built. The oscillation of the speaker also has to be increased. The main difference between the intensity autocorrelator and the interferometric autocorrelator is that the individual fringes that are created on the beamsplitter can be resolved. Each fringe is separated by a delay of $\Delta\tau = \pi/\omega$ and information about the amount of chirp presented on the pulse is supplied using this method.   A representative interferometric autocorrelation trace is shown in Fig. 1.10 (b).

27

1.6 Conclusion

In this chapter an outline of ultrashort pulse generation, characterisation and potential applications has been given. The effects of the propagation of an ultrashort pulse through a dielectric material were described and ways of exploiting these effects in various mode-locking techniques were discussed. The technique of autocorrelation, which provides a method for measuring the duration of these pulses, was also discussed. This chapter represents a foundation upon which the work undertaken in this project was built. In the subsequent chapters the design of a Cr^{4+}:forsterite laser system incorporating saturable absorbers to initiate mode locking will be described together with new saturable absorber devices that were evaluated. Some potential applications of this laser system will also be discussed in Chapter five.

1.7 References

1.   Maiman, T.H., "*Stimulated optical radiation in ruby*", Nature, 1960. **187**(4736): p. 493-494.

2.   Jones-Bey, H.A., "*High-power lasers - airborne laser achieves lethal antimissile power levels*", Laser Focus World, 2006. **42**(2): p. 31-33.

3.   Lundstrom, E., G. Brodin, J. Lundin, M. Marklund, R. Bingham, J. Collier, J.T. Mendonca, and P. Norreys, "*Using high-power lasers for detection of elastic photon-photon scattering*", Physical Review Letters, 2006. **96**(8).

4.   Kryukov, P.G., "*Ultrashort-pulse lasers*", Quantum Electronics, 2001. **31**(2): p. 95-119.

5.   Sorokin, E., S. Naumov, and I.T. Sorokina, "*Ultrabroadband infrared solid-state lasers*", IEEE Journal of Selected Topics in Quantum Electronics, 2005. **11**(3): p. 690-712.

6.   Keller, U., "*Recent developments in compact ultrafast lasers*", Nature, 2003. **424**(6950): p. 831-838.

7.   Zewail, A.H., "*Femtochemistry: Atomic-scale dynamics of the chemical bond*", Journal of Physical Chemistry A, 2000. **104**(24): p. 5660-5694.

8.   Lakhno, V.D., "*Dynamical theory of primary processes of charge separation in the photosynthetic reaction center*", Journal of Biological Physics, 2005. **31**(2): p. 145-159.

9.   Podoleanu, A.G., "*Optical coherence tomography*", British Journal of Radiology, 2005. **78**(935): p. 976-988.

10.   Mollenauer, L.F., P.V. Mamyshev, J. Gripp, M.J. Neubelt, N. Mamysheva, L. Gruner-Nielsen, and T. Veng, "*Demonstration of massive wavelength-division multiplexing over transoceanic distances by use of dispersion-managed solitons*", Optics Letters, 2000. **25**(10): p. 704-706.

11.   Chai, Y.J., C.G. Leburn, A.A. Lagatsky, C.T.A. Brown, R.V. Penty, I.H. White, and W. Sibbett, "*1.36-Tb/s spectral slicing source based on a Cr4+-YAG femtosecond laser*", Journal of Lightwave Technology, 2005. **23**(3): p. 1319-1324.

12.   Hammer, D.X., R.J. Thomas, G.D. Noojin, B.A. Rockwell, P.K. Kennedy, and W.P. Roach, "*Experimental investigation of ultrashort pulse laser-induced breakdown thresholds in aqueous media*", IEEE Journal of Quantum Electronics, 1996. **32**(4): p. 670-678.

13.   Loesel, F.H., M.H. Niemz, J.F. Bille, and T. Juhasz, "*Laser-induced optical breakdown on hard and soft tissues and its dependence on the pulse duration: Experiment and model*", IEEE Journal of Quantum Electronics, 1996. **32**(10): p. 1717-1722.

14.   Knox, W.H., "*Ultrafast technology in telecommunications",* IEEE Journal of Selected Topics in Quantum Electronics, 2000. **6**(6): p. 1273-1278.

15.   Agrawal, G.P., "*Nonlinear Fiber Optics".* 1995: Academic Press.

16.   Dennis, T., Curtis, E.A., Oates, C.W., Hollberg, L., Gilbert S.L., "*Wavelength References for 1300-nm Wavelength-Division Multiplexing",* Journal of Lightwave Technology, 2002. **20**(5): p. 776-782.

17.   Svanberg, S., "*Some applications of ultrashort laser pulses in biology and medicine",* Measurement Science & Technology, 2001. **12**(11): p. 1777-1783.

18.   Cheong, W.F., P.S. A., and A.J. Welch, "*A review of optical properties of biological tissues",* IEEE Journal of Quantum Electronics, 1990. **26**(12): p. 2166-2185.

19.   Sun, C.K., C.C. Chen, S.W. Chu, T.H. Tsai, Y.C. Chen, and B.L. Lin, "*Multiharmonic-generation biopsy of skin",* Optics Letters, 2003. **28**(24): p. 2488-2490.

20.   Fischer, P., A. McWilliam, C.T.A. Brown, K. Wood, M. MacDonald, W. Sibbett, and K. Dholakia, "*Deep tissue penetration of radiation: modelling and experiments",* Paper CL-4-Wed, European Conference on Lasers and Electro-Optics (ECLEO), Munich, Germany, 2005.

21.   Pogue, B.W. and T. Hasan, "*Targeting in photodynamic therapy and photo-imaging",* in *Optics and Photonics News.* 2003. p. 37-43.

22.   Chen, I.H., S.W. Chu, C.K. Sun, P.C. Cheng, and B.L. Lin, "*Wavelength dependent damage in biological multi-photon confocal microscopy: A micro-spectroscopic comparison between femtosecond Ti : sapphire and Cr : forsterite laser sources",* Optical and Quantum Electronics, 2002. **34**(12): p. 1251-1266.

23.   Cormack, I.G., "*Rapid techniques for ultrashort optical pulse characterisation",* in *School of Physics and Astronomy.* 2001, PhD Thesis, University of St Andrews.

24.   Wilson, J. and J. Hawkes, "*Optelectronics - An introduction".* 3rd ed. 1998, London: Prentice Hall.

25.   Walmsley, I., L. Waxer, and C. Dorrer, "*The role of dispersion in ultrafast optics",* Review of Scientific Instruments, 2001. **72**(1): p. 1-29.

26.   Chudoba, C., J.G. Fujimoto, E.P. Ippen, H.A. Haus, U. Morgner, F.X. Kartner, V. Scheuer, G. Angelow, and T. Tschudi, "*All-solid-state Cr:forsterite laser generating 14-fs pulses at 1.3μm",* Optics Letters, 2001. **26**(5): p. 292-294.

27.   Fork, R.L., O.E. Martinez, and J.P. Gordon, "*Negative dispersion using pairs of prisms",* Optics Letters, 1984. **9**(5): p. 150-152.

28.   Szipocs, R., A. Kohazi-Kis, S. Lako, P. Apai, A.P. Kovacs, G. DeBell, L. Mott, A.W. Louderback, A.V. Tikhonravov, and M.K. Trubetskov, "*Negative dispersion mirrors for dispersion control in femtosecond lasers: chirped dielectric mirrors and multi-cavity Gires-Tournois interferometers",* Applied Physics B: Lasers and Optics, 2000. **70**: p. S51-S57.

29.   Treacy, E.B., "*Optical pulse compression with diffraction gratings",* IEEE Journal of Quantum Electronics, 1969. **5**(9): p. 454-458.

30.   Robertson, A., U. Ernst, R. Knappe, R. Wallenstein, V. Scheuer, T. Tschudi, D. Burns, M.D. Dawson, and A.I. Ferguson, "*Prismless diode-pumped mode-locked femtosecond Cr : LiSAF laser",* Optics Communications, 1999. **163**(1-3): p. 38-43.

31.   Spence, D.E., P.N. Kean, and W. Sibbett, "*60-fsec pulse generation from a self-mode-locked Ti-sapphire laser",* Optics Letters, 1991. **16**(1): p. 42-44.

32.   Siegman, A.E., "*Lasers".* 1986, California: University Science Books.

33.   Keller, U. "*Advances in Lasers and Applications: Ultrashort pulse generation".* in *Proceedings of the 52nd Scottish Universities Summer School in Physics*. 1998. St Andrews, Scotland: Scottish Universities Summer School in Physics & Institute of Physics Publishing.

34.   Haus, H.A., "*Mode-locking of lasers",* IEEE Journal of Selected Topics in Quantum Electronics, 2000. **6**(6): p. 1173-1185.

35.   DiDomenico, M., Jr., J.E. Geusic, H.M. Marcos, and R.G. Smith, "*Generation of ultrashort optical pulses by mode locking the YAIG: Nd laser",* Applied Physics Letters, 1966. **8**(7): p. 180-183.

36.   Mocker, H.W. and R.J. Collins, "*Mode competition and self-modelocking effects in a Q-switched ruby laser",* Applied Physics Letters, 1965. **7**(10): p. 270-273.

37.   Jung, I.D., F.X. Kartner, N. Matuschek, D.H. Sutter, F. MorierGenoud, G. Zhang, U. Keller, V. Scheuer, M. Tilsch, and T. Tschudi, "*Self-starting 6.5-fs pulses from a Ti:Sapphire laser",* Optics Letters, 1997. **22**(13): p. 1009-1011.

38.   Keller, U., "*Semiconductor Nonlinearities for Solid-State Laser Modelocking and Q-Switching",* Semiconductors and Semimetals, 1998. **59**: p. 211-285.

39.   Jung, I.D., F.X. Kartner, L.R. Brovelli, M. Kamp, and U. Keller, "*Experimental-verification of soliton mode-locking using only a slow saturable absorber",* Optics Letters, 1995. **20**(18): p. 1892-1894.

40.   Kartner, F.X., I.D. Jung, and U. Keller, "*Soliton mode-locking with saturable absorbers",* IEEE Journal of Selected Topics in Quantum Electronics, 1996. **2**(3): p. 540-556.

41.   Taylor, J.R., "*Optical solitons - theory and experiment"*, C.U. Press, Editor. 1992.

42. Tsuda, S., W.H. Knox, S.T. Cundiff, W.Y. Jan, and J.E. Cunningham, "*Mode-locking ultrafast solid-state lasers with saturable Bragg reflectors*", IEEE Journal of Selected Topics in Quantum Electronics, 1996. **2**(3): p. 454-464.

43. Keller, U., K.J. Weingarten, F.X. Kartner, D. Kopf, B. Braun, I.D. Jung, R. Fluck, C. Honninger, N. Matuschek, and J.A. der Au, "*Semiconductor saturable absorber mirrors (SESAM's) for femtosecond to nanosecond pulse generation in solid-state lasers*", IEEE Journal of Selected Topics in Quantum Electronics, 1996. **2**(3): p. 435-453.

44. Craig, B. and A. Krueger, "*Saturable Bragg reflectors simplify modelocking*", Laser Focus World, 2000. **36**(8): p. 227-228.

45. Keller, U., D.A.B. Miller, G.D. Boyd, T.H. Chiu, J.F. Ferguson, and M.T. Asom, "*Solid-state low-loss Intracavity saturable absorber for Nd-YLF lasers - an antiresonant semiconductor fabry-perot saturable absorber*", Optics Letters, 1992. **17**(7): p. 505-507.

46. Honninger, C., R. Paschotta, F. Morier-Genoud, M. Moser, and U. Keller, "*Q-switching stability limits of continuous-wave passive mode locking*", Journal of the Optical Society of America B-Optical Physics, 1999. **16**(1): p. 46-56.

47. Wang, Y.S., H.J. Liu, Z. Cheng, W. Zhao, Y.G. Wang, X.Y. Ma, and Z.G. Zhang, "*Self-starting mode-locked femtosecond Ti : sapphire laser using saturable, Bragg reflector(SBR)*", Acta Physica Sinica, 2005. **54**(11): p. 5184-5188.

48. McWilliam, A., A.A. Lagatsky, C.G. Lebum, P. Fischer, C.T.A. Brown, G.J. Valentine, A.J. Kemp, S. Calvez, D. Burns, M.D. Dawson, M. Pessa, and W. Sibbett, "*Low-loss GaInNAs saturable Bragg reflector for mode-locking of a femtosecond Cr4+: Forsterite-laser*", IEEE Photonics Technology Letters, 2005. **17**(11): p. 2292-2294.

49. Lagatsky, A.A., C.G. Leburn, C.T.A. Brown, W. Sibbett, and W.H. Knox, "*Compact self-starting femtosecond Cr4+: YAG laser diode pumped by a Yb-fiber laser*", Optics Communications, 2003. **217**(1-6): p. 363-367.

50. Lagatsky, A.A., E.U. Rafailov, W. Sibbett, D.A. Livshits, A.E. Zhukov, and V.M. Ustinov, "*Quantum-dot-based saturable absorber with p-n junction for mode-locking of solid-state lasers*", Ieee Photonics Technology Letters, 2005. **17**(2): p. 294-296.

51. McWilliam, A., A.A. Lagatsky, B. C.T.A., W. Sibbett, A.E. Zhukov, V.M. Ustinov, A.P. Vasil'ev, and E.U. Rafailov, "*Quantum-dot-based saturable absorber for femtosecond mode-locked operation of a solid-state laser*", Optics Letters, 2006. **31**(10): p. 1444-1446.

52. Armstrong, J.A., "*Measurement of picosecond laser pulse widths*", Applied Physics Letters, 1967. **10**(1): p. 16-18.

53. Reid, D.T., W. Sibbett, J.M. Dudley, L.P. Barry, B. Thomsen, and J.D. Harvey, "*Commercial semiconductor devices for two photon absorption*

autocorrelation of ultrashort light pulses", Applied Optics, 1998. **37**(34): p. 8142-8144.

54. Trebino, R. and D.J. Kane, "*Using phase retrieval to measure the intensity and phase of ultrashort pulses - frequency-resolved optical gating",* Journal of the Optical Society of America a-Optics Image Science and Vision, 1993. **10**(5): p. 1101-1111.

55. Lochbrunner, S., P. Huppmann, and E. Riedle, "*Crosscorrelation measurements of ultrashort visible pulses: comparison between nonlinear crystals and SiC photodiodes",* Optics Communications, 2000. **184**(1-4): p. 321-328.

56. Reid, D.T., M. Padgett, C. McGowan, W.E. Sleat, and W. Sibbett, "*Light-emitting diodes as measurement devices for femtosecond laser pulses",* Optics Letters, 1997. **22**(4): p. 233-235.

Chapter 2 – Initial characterisation of a Cr^{4+}:forsterite laser

2.1 Introduction

In this chapter a brief summary of reported research undertaken on Cr^{4+}:forsterite lasers will be presented. This will outline the background upon which the work described in this thesis has been built. The properties of the gain material, Cr^{4+}:forsterite, will then be described to show its suitability for mode locking and the production of ultrashort, and particularly femtosecond, pulses. To set the scene, the design and construction of a continuous wave Cr^{4+}:forsterite cavity is detailed and the characterisation of the laser is outlined. It is this laser that was used as a test bed for the saturable absorber devices used to initiate mode locking (Chapters 3 and 4) and for the biophotonics experiments described later in Chapter 5.

2.2 Cr^{4+}:forsterite: a history

Chromium is a transition metal that can be used as a dopant in a host lattice to produce a practical laser gain medium. There are several possible gain materials that chromium plays a role in including Cr:YAG, Cr:forsterite, Cr:LiSaf, Cr:ZnSe and Cr:sapphire. For these to be considered as suitable laser gain media certain criteria must be satisfied, such as chemical and mechanical stability, good heat conductivity and a long upper state lifetime. The lasing action and the relationship between the energy levels of the lasing ion depends on the host medium. Host materials can include garnets [1], fluorides [2], phosphate/silicate glasses [3] and sapphire [4]. In Cr^{4+} doped forsterite (Mg$_2$SiO$_4$) the lasing transition takes place between the electronic energy levels of the 3d electrons. The active laser ions are not shielded from the surrounding host lattice and, as such, strong electron-phonon coupling will

take place and give rise to a broadly tunable output [5]. In general, gain bandwidths in excess of 30nm and upper state lifetimes greater than 3μs are typically found in such materials.

Forsterite was discovered by and named after the German naturalist Johann Forster. It belongs to a crystal class called olivines [6] that make up a large proportion of the earth's mantle. The name refers to the greenish colour of the family members and, indeed, mankind has known the apple green member of the forsterite family, *peridot,* for centuries, Fig. 2.1.

Fig. 2.1. The apple green *peridot,* the most commonly known member of the forsterite family.

The forsterite crystal has the chemical composition Mg_2SiO_4. It was this crystal that played the role of the host lattice for the chromium ions to create the gain material for these experiments. Lasing action in the Cr^{4+}:forsterite gain material was first reported in 1988 [7, 8]. At this time uncertainty existed over the nature of the lasing ion and trivalent chromium (Cr^{3+}) was conjectured to be responsible for the lasing action. However, through spectroscopic analysis [9, 10] it was found that both Cr^{3+} and Cr^{4+} were taken into the host material with the Cr^{3+} taking the place of the octahedrally coordinated Mg^{2+} sites and Cr^{4+} substituting into tedrahedrally coordinated Si^{4+} sites. This spectroscopic analysis supported the theory that Cr^{4+} was the lasing ion and showed that the presence of Cr^{3+} in the host lattice actually

decreased the efficiency of the laser due to two-photon absorption of the pump wavelength [11].

Mode-locked operation of Cr^{4+}:forsterite in the picosecond domain (31ps pulses) was first achieved in 1991 using an intracavity loss modulator in the form of an acousto-optic device [12]. To achieve shorter pulses, passive techniques must be used, and in 1992 150fs pulses from a Cr^{4+}:forsterite laser were realised using additive pulse mode locking [13]. This technique was not pursued further due to the development of Kerr-lens mode locking and semiconductor saturable absorbers. Both of these provide a more versatile and simpler path into the femtosecond domain.

The technique of Kerr-lens mode locking initiated by a acousto-optic modulator was used to mode lock a Cr^{4+}:forsterite laser producing pulses initially of 60fs [14] before careful management of the dispersion compensation allowed 36fs [15] pulses to be realised. This mode locked operation was sustained even after the acousto-optic modulator was turned off indicating that the laser was self-mode locked. Kerr-lens mode locking has also provided the shortest pulses from a Cr^{4+}:forsterite laser, with the crystal cooled to -10°C and, using a combination of chirped mirrors and prisms to compensate for higher-order dispersion, pulses of 14fs in duration could be produced [16].

More relevant to this thesis is the previous work undertaken with Cr^{4+}:forsterite lasers that were mode locked using semiconductor saturable absorbers. These provide self-starting operation and have been used extensively to mode lock Cr^{4+}:forsterite lasers over the past ten years. The first report of the exploitation of a saturable absorber was published in 1996. The saturable absorber used consisted of 25 periods of GaAs/AlAs quarter wave layers followed by two InGaAs quantum wells and allowed the generation of 110fs pulses [17]. Alternatively, saturable absorbers

grown on an InP substrate with InGaAsP quantum wells have been used [18]. In subsequent studies pulses as short as 40fs have been produced but these relied on cooling the crystal to ~0°C [18, 19]. Both of these saturable absorbers have drawbacks and their presence has a detrimental effect to the laser performance. Their disadvantages and the identification of new GaInNAs saturable absorbers that improve on these results will be described in the following chapter.

2.3 Cr^{4+}:forsterite as a laser gain material

The emission and absorption spectra of a Cr^{4+}:forsterite crystal is included as Fig. 2.2, this is for a crystal cut along the a-axis as the Cr^{4+}:forsterite crystal used in these experiments was.
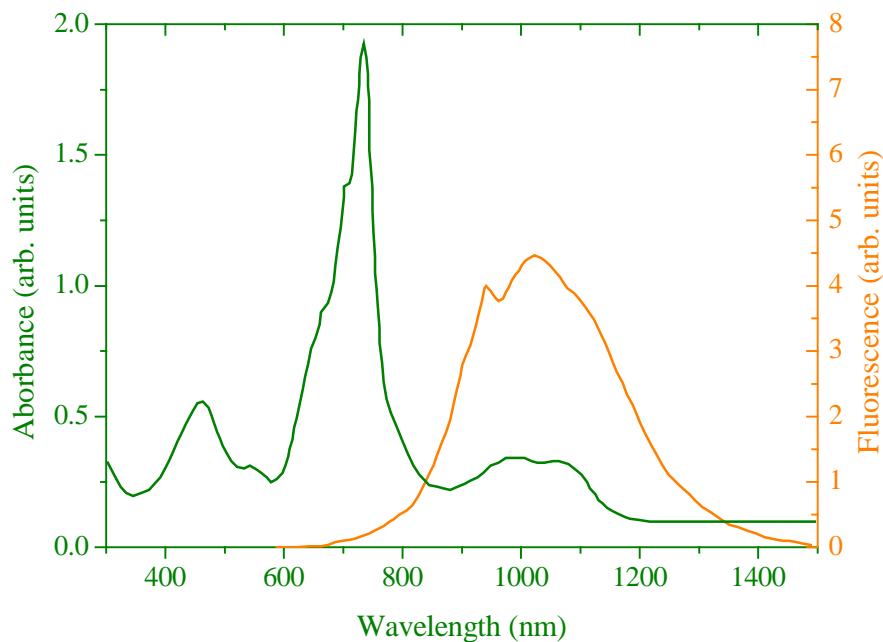
Fig. 2.2. The emission and absorption spectra for Cr^{4+}:forsterite

It can be seen that the absorption spectrum has two broad peaks, one at 780nm and one ranging from 900-1150nm ($^3A_2 \rightarrow {}^3T_1$ and $^3A_2 \rightarrow {}^3T_2$ respectively on the energy

level diagram, Fig. 2.3). This allows the crystal to be excited optically by a wide selection of commercially available lasers at 1064nm: Nd:YAG, Nd:YVO$_4$ or ytterbium fibre lasers, or high power InGaAs laser diodes at 980nm. Alternatively, Cr^{4+}:forsterite has also been pumped by a master-oscillator-power-amplifier (MOPA) at 980nm [20] and by AlGaInP laser diodes at 680nm [21].

As mentioned above, the lasing ion, Cr^{4+}, is not shielded from the surrounding lattice and so it is subjected to strong electron-phonon coupling. This acts to broaden the energy levels thereby creating what are known as vibronic energy levels, Fig. 2.3. It is this feature that facilitates the broadly tunable emission spectra between 1130nm and 1367nm (as shown in Fig. 2.2) and allows for the production of ultrashort pulses.

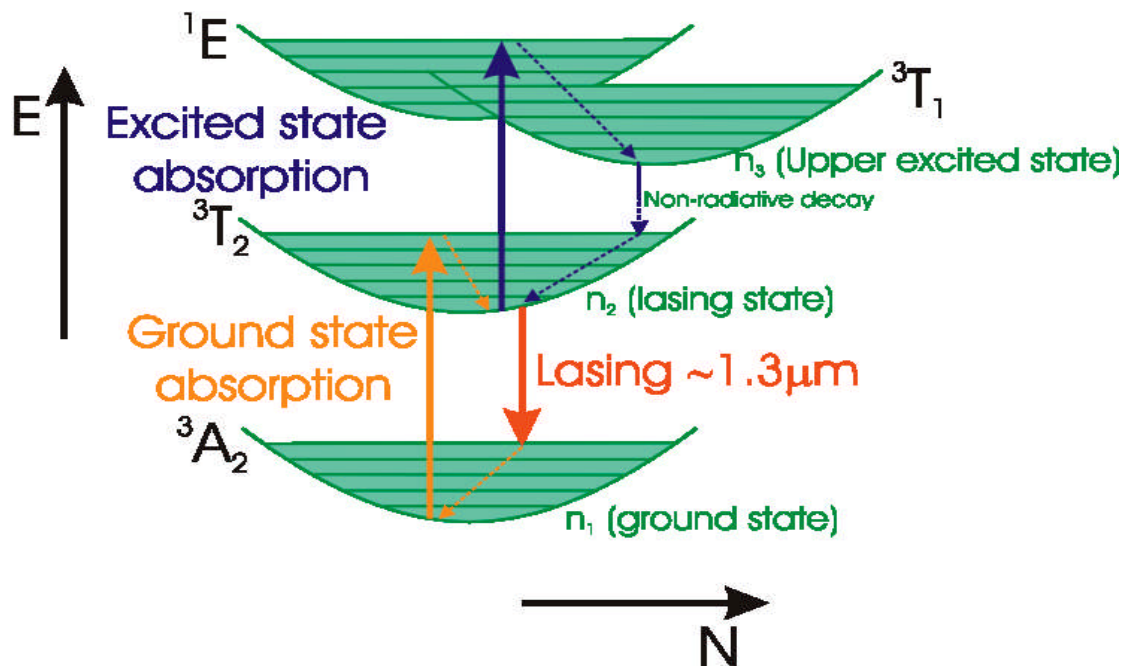The energy level scheme for Cr^{4+}:forsterite when pumped at 1064nm is shown in Fig. 2.3 [22].

Fig. 2.3 A simplified energy level diagram of Cr^{4+} in forsterite, energy vs. population density per unit volume

When pumped at 1064nm Cr^{4+} ions are excited from the ground state of ^{3}A$_2$ to the upper laser state of ^{3}T$_2$. Due to excited state absorption of the pump radiation, Cr^{4+}

ions can also be excited into the ^{1}E level from ^{3}T$_2$. These then relax into the upper excited state of ^{3}T$_1$ and return through nonradiative relaxation to the lasing state, ^{3}T$_2$.

The ^{1}E state overlaps the ^{3}T$_1$ state as shown in Fig. 2.3 causing an electronic bottleneck trap. Effectively this delays the nonradiative decay of the upper excited electron level for ~10ps. Normally the lifetime of the ^{3}T$_1$ state is a few hundred nanoseconds before decaying again through nonradiative decay into the upper lasing level ^{3}T$_2$. Lasing occurs between ^{3}T$_2 \rightarrow ^3$A$_2$ states of the 3d electrons and provides the output spectrum for the laser centred near 1250nm. At room temperature Cr^{4+}:forsterite has a upper state lifetime of 2.7μs. This upper-state lifetime is sensitive to temperature and by cooling to liquid nitrogen temperatures (77K) the upper-state lifetime can be increased to ~20μs. The thermal load from the pump beam inside the crystal can have a detrimental effect on this duration, through a local increase of the crystal temperature decreasing the upper-state lifetime. This necessitates a heat removal mechanism to keep the crystal at a constant temperature. In these experiments the heat was removed from the crystal by water-cooling.

2.4 The Cr^{4+}:forsterite laser cavity

In designing a laser cavity there are many aspects that must be considered prior to its construction. These include the stability of the cavity, the pump source and geometry, the mirrors that are to be used and the gain medium itself. The Cr^{4+}:forsterite crystal has already been discussed together with its suitability for the generation of femtosecond pulses around the 1300nm spectral region, this section will describe the design of the continuous wave cavity around this crystal and the details this entails.

2.4.1 Cavity design

A major consideration in building a Cr^{4+}:forsterite laser is the low gain nature of the crystal. This dictates that there must be extremely good mode matching of the pump and laser beams. Also, due to the short upper-state lifetime of Cr^{4+}:forsterite (~2.7μm), a high intensity pump beam is required to provide and sustain a sufficient population inversion for lasing. To achieve this intensity a tightly focused pump beam size is essential, which can be achieved with appropriate focusing of a near-diffraction-limited pump beam (M^2~1). There are a number of possible laser cavities that can be constructed, but for the future use as a test bed for potential saturable absorber devices a four-mirror cavity was adopted as the most suitable option. The large stability regions of this laser cavity design allowed for the simple insertion of intracavity elements such as prisms or saturable absorbers. A schematic of a four-element cavity is shown in Fig. 2.4. Other cavity designs such as a two-mirror resonator or a three-mirror resonator are not asymmetric, therefore it is difficult to incorporate the saturable absorber device inside the cavity with the required spot size incident upon it and still maintain the appropriate spot size within the laser crystal. By contrast, the asymmetric nature of the four-mirror cavity allows the spot size upon the saturable absorber and inside the crystal to be chosen.
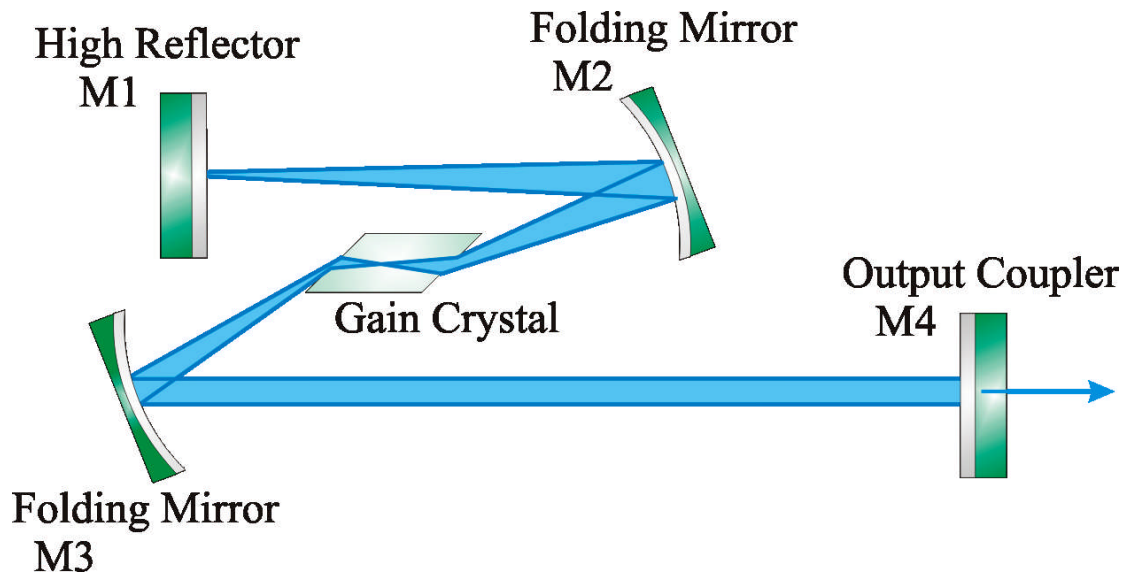
Fig. 2.4 A representative schematic of a typical four-mirror, astigmatically compensated cavity showing the beam mode size.

The added advantage of using this form of asymmetric laser cavity is that a tight focus exists at mirror M1. This enables saturable absorber devices placed at M1 to become optically bleached, allowing mode locking to be initiated. The spot size can be slightly altered on the saturable absorber by translating the device, changing the distance between M1 and M2, allowing for a range of incident fluences. For the laser cavity used in this project to investigate saturable absorber devices this is shown in Fig. 2.5. It is common for the ends of gain crystals to be cut at Brewster's angle, and this is the case with the Cr^{4+}:forsterite crystal used here. Although this acts to minimise the Fresnel losses at the surface of the crystal, the presence of a Brewster-cut introduces an associated astigmatism. This can be compensated for by carefully choosing the angles of the two folding mirrors M2 and M3 that are placed at either side of the crystal. These also keep the intracavity beam focused inside the crystal for mode matching. A well-collimated beam is formed between M3 to M4. This is where intracavity prisms for dispersion compensation can be inserted. Finally, mirror M4 is an output coupler, a partially reflecting mirror which allows a small percentage

of intracavity power to escape the cavity. This is dictated by the coupling efficiency of the output coupler.
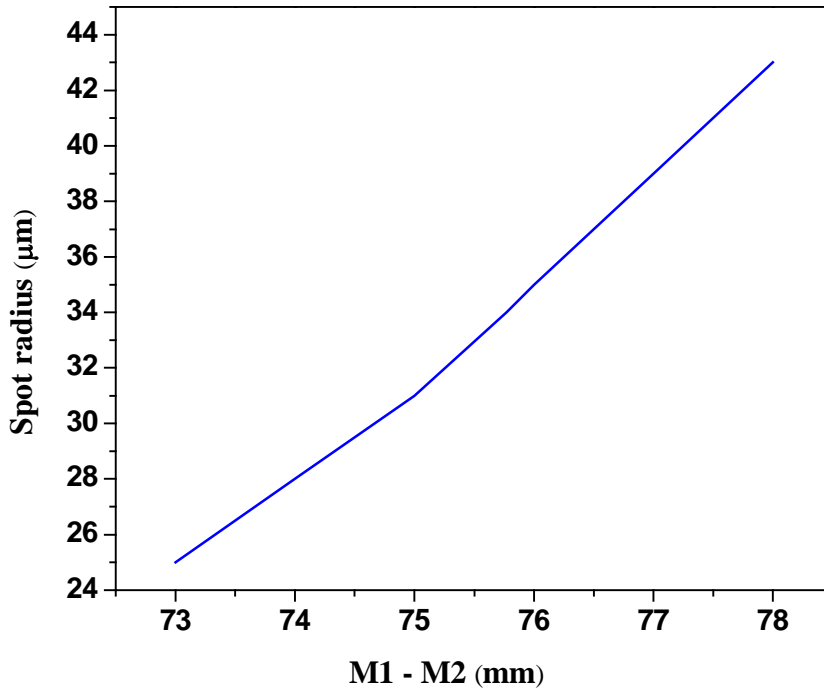

Fig. 2.5 The variation of the spot size on M1 with increasing distance M1-M2

Throughout this project the laser cavities described were designed using a laser cavity design package called LCAV. This used ABCD matrix multiplication to calculate the mirror and crystal positions and orientations [23]. The associated stability and mode size information for each cavity were supplied by the programme, allowing for an appropriate spot size within the crystal, and upon the saturable absorber device at M1 to be chosen.

2.4.2 Mirrors and the Cr^{4+}:forsterite crystal

As mentioned in the previous section, the Cr^{4+}:forsterite crystal was cut along the a-axis and Brewster-cut to minimise the Fresnel losses. It had a small-signal pump absorption coefficient of 1.3cm^{-1} and the dimensions 3x3x11.6mm. The crystal was

wrapped in indium foil and clamped into a copper mount that allowed for water-cooling to 15°C and also provided the mechanism for heat removal when pumped at high powers.

The mirrors used in this project were designed specifically for use around 1300nm and were coated for broadband high reflection with R>99.96% between 1250nm and 1550nm and with high transmission at 1064nm (the wavelength of the pump light). A selection of mirrors was purchased from *LaserOptik GmbH*, enabling a number of cavity options to be configured. The choice of cavity depended on the laser mode size required, inside the crystal and upon the saturable absorber, and the output coupling required for stable operation of the laser. The set of mirrors consisted of four folding mirrors, of which two were -100mm radii of curvature and two were -75mm radii of curvature, plus two plane-wedged high reflectors. The set was completed with three broadband plane-wedged output couplers with nominal transmissions of 0.5%, 1% and 2%. Representative transmission curves are included as Fig. 2.6. It should be noted that the mirror characteristic in Fig. 2.6(b) implies a 2% transmission.
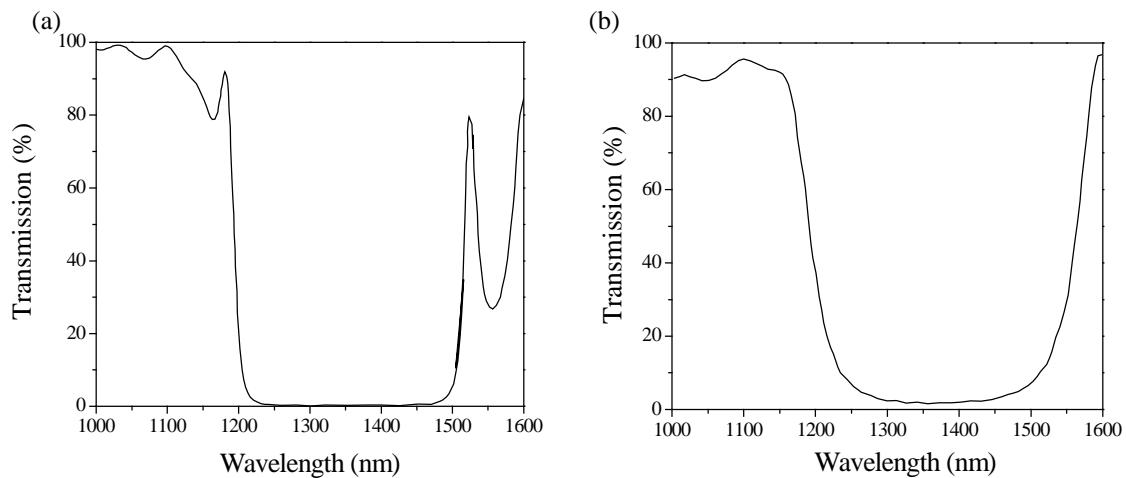

Fig. 2.6 Transmission curves for (a) a high reflector and (b) a 2% output coupler .

2.4.3 Pump source and geometry

The final aspects of the design of the laser cavity that need to be considered are the pump source and the geometry of the optics needed to couple the pump beam most effectively into the gain crystal to create the population inversion. The pump source used was a Nd:YVO$_4$ laser from *Spectra Physics Inc*. This produced up to ten Watts of linearly polarised, near-diffraction-limited light at 1064nm. A schematic of the pump geometry is included as Fig. 2.7.

As can be seen, the pump beam first passes through a half-wave plate. This allowed the linearly polarised light to be rotated to minimise the pump reflection at the Brewster-angled face of the Cr^{4+}:forsterite crystal, enabling the maximum absorption of the pump light. The telescope system and focusing lens allowed control over the pump spot size within the crystal to provide the maximum mode matching of the pump and intracavity beams. An assortment of lenses for the telescope system and focusing lens were investigated before the final version (Fig. 2.7) was selected. A computerised beam profiler was used to measure the spot size and investigate different combinations of lenses to provide a tight focus of the pump beam inside the crystal. (More details will be provided about the choice of these lenses in the following section).
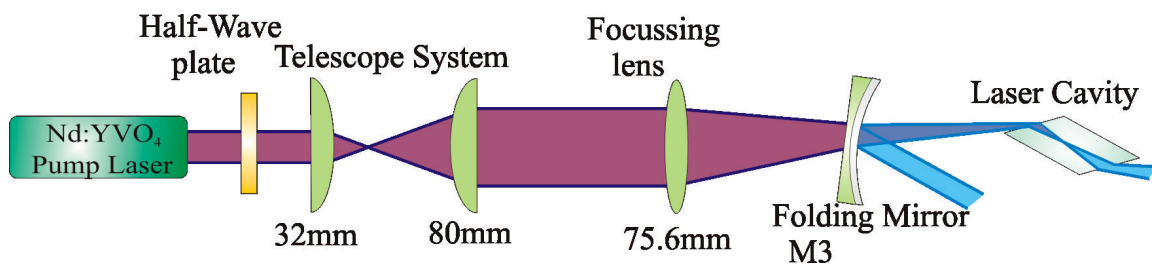

Fig. 2.7 The pump geometry for the laser cavity showing the focal lengths of the lens used throughout this thesis.

2.5 Continuous wave operation of the Cr^{4+}:forsterite laser

Originally the Cr^{4+}:forsterite laser was designed and built with a different pump geometry to that shown in Fig. 2.7. Lenses were used to provide a spot size of ~80μm in diameter inside the crystal. The corresponding cavity was designed so that the laser mode was of comparable size inside the crystal for mode matching purposes. With this arrangement, continuous wave (CW) operation was realised but with a lasing threshold of 3.7W. This value was higher than expected for the laser system and raised concern over the quality of the optical components, the mirrors and the Cr^{4+}:forsterite crystal. Based on Equation 2.1 we can see that the pump power at threshold is related to the pump beam mode size inside the crystal[24].

$$P_{th} = \left(\frac{\delta - \ln R}{2} \right) \frac{Ah\nu_L}{\eta \sigma \tau_f} \qquad (2.1)$$

In Equation 2.1 δ is the resonator losses, R the reflectivity of the output coupler, A the cross sectional area of the gain, h Planck's constant, ν_L the wavelength of the laser, σ the stimulated emission cross section, τ_f the fluorescence lifetime and η combines the various efficiency terms for the laser. These include the absorption efficiency, quantum efficiency and the temperature dependence.

From Equation 2.1, for a small cross-sectional area of gain, A, a lower lasing threshold should be accessible. This can be achieved by decreasing the pump mode size within the crystal. However, in decreasing the pump mode size the efficiency, η, will be changed due to the extra thermal load in the crystal. An optimum spot size therefore exists for a given laser configuration that will provide a low threshold before thermal lens effects begins to effect detrimentally the operation of the laser.

It was decided to decrease the spot size within the crystal by varying the telescope system and focusing lens until an optimum spot size was found (Fig. 2.7).

The pump spot size was decreased from ~80μm to ~45μm in diameter. This was observed to provide sufficient population inversion and a dramatically improved cw laser performance. The laser cavity dimensions that were required to provide a laser mode size of ~45μm in diameter inside the crystal for mode matching are shown in Fig. 2.8.

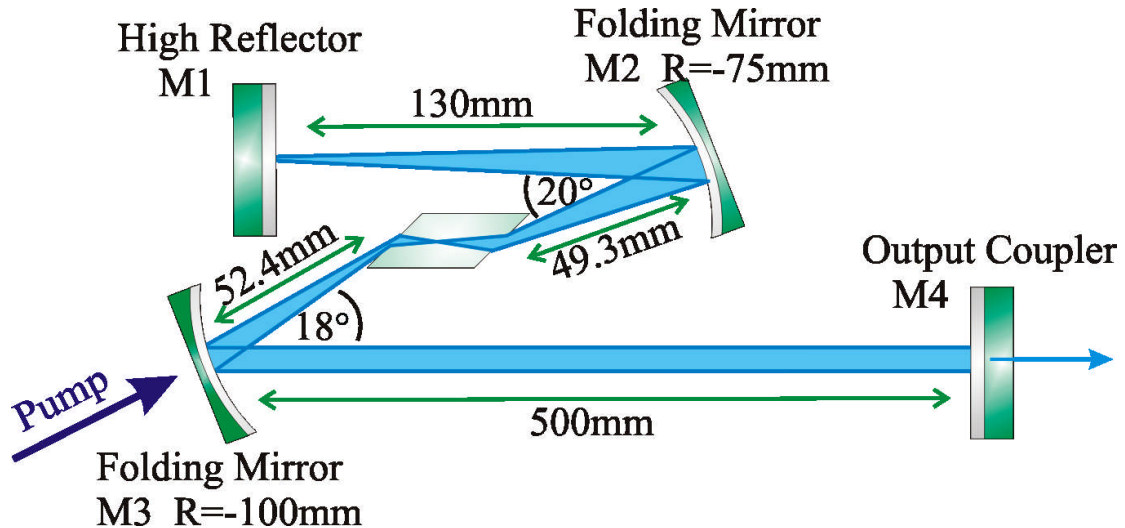Fig. 2.8 Cr^{4+}:forsterite laser cavity for continuous wave operation.

This laser provided a continuous wave output in the 1300nm spectral region with a minimum lasing threshold of 1.4W, which is comparable to other reported Cr^{4+}:forsterite lasers [25].

The continuous wave performance of the laser was then characterised. Firstly, the performance of the laser with the three available output couplers was evaluated, as shown in Fig. 2.9. From Fig. 2.9 the slope efficiency of the laser with the available output couplers was calculated. For the 0.5%, 1% and 2% output couplers the slope efficiencies were calculated to be 2.6%, 3.3% and 4.4%, respectively. From Fig. 2.9 it can be seen that a threshold of 1.4W was realised with the 0.5% output coupler.

With the 2% output coupler, an output power of 351mW was realised with a pump power of 6W.
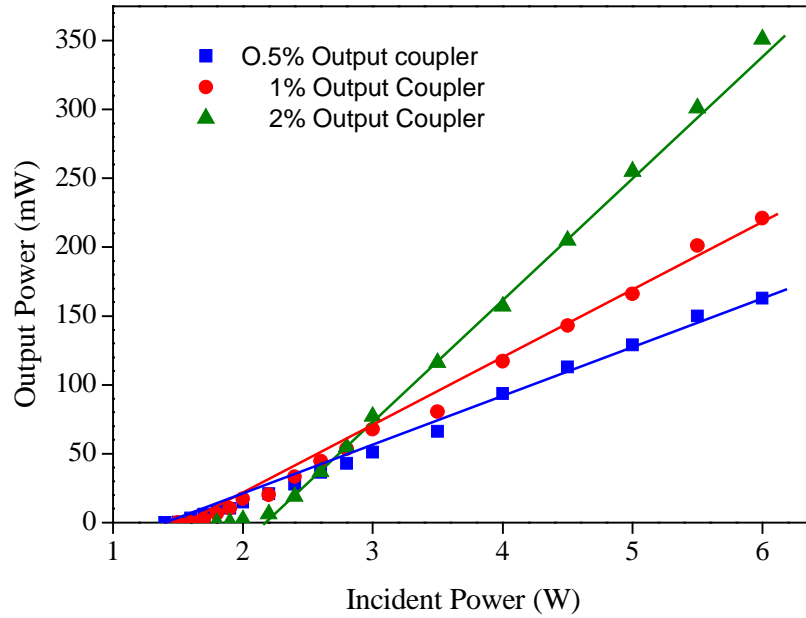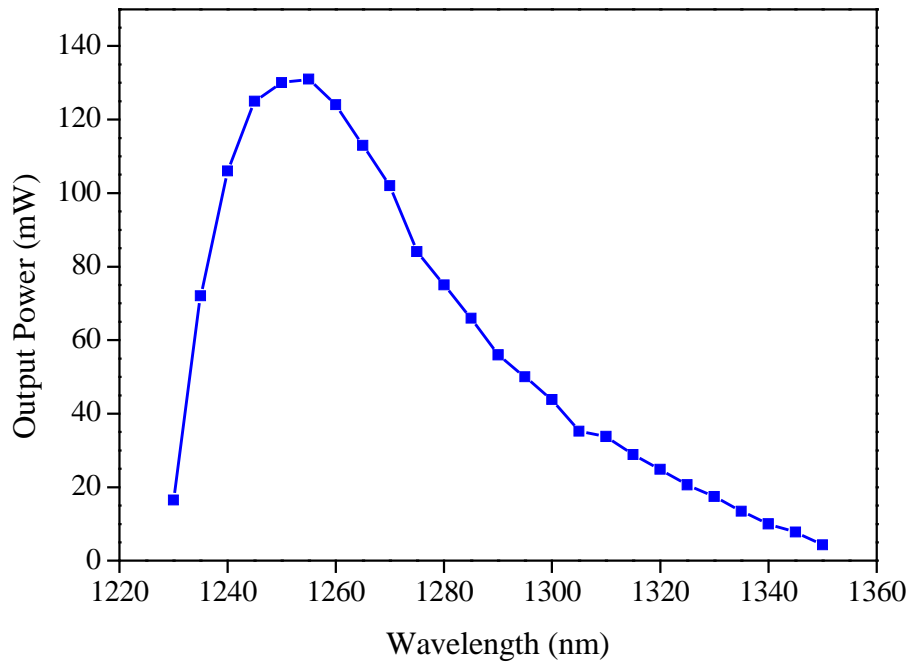

Fig. 2.9 Continuous wave performance characteristics

Fig. 2.10 The tunability of the Cr^{4+}:forsterite laser.

Due to the small pump spot size inside the Cr^{4+}:forsterite crystal at high pump powers, the high intensity would heat the gain medium and leading to a thermal lens being created above 6W of incident pump power. This caused the laser performance to become unstable and introduced a significant decrease in output power.

The second feature of the laser to be characterised was its frequency tunability. This was achieved by placing a single prism in the long arm of the cavity. This acted to disperse the intracavity modes enabling discrete wavelengths to be selected by changing the angle of the output coupler. The tunability of the laser with the 0.5% output coupler in place is shown in Fig. 2.10. It can be seen that the laser was tunable between 1230nm and 1350nm. The lower cut off point was due to the reflectivity of the mirrors (Fig. 2.6) and the upper cut off at 1350nm was attributable to the crystal itself (Fig. 2.2). For these measurements the spectrum was monitored with a REES spectrometer with measurements taken every 5nm.

2.6 Conclusion

In this chapter the properties of the Cr^{4+}:forsterite crystal as a suitable gain material for a solid-state laser have been described. Its potential to be pumped by widely available commercial laser sources and the broad emission spectrum that makes it suitable for mode locked operation have been highlighted. A brief history of Cr^{4+}:forsterite lasers was given to put the research presented in this thesis into context with previously reported work. The components of the laser cavity and the reasoning behind the use of a four-element cavity were put forward, before details of the cavity design itself and the continuous wave performance characteristics were described.

It is this basic laser configuration that was used in the project to test saturable absorber devices (see Chapters 3 and 4). These include a novel GaInNAs device (Chapter 3) and a new quantum-dot saturable absorber (Chapter 4). Finally, this laser was used for biophotonics experiments relating to assessments of tissue penetration and chromosome cutting with coherent radiation in the 1300nm region (Chapter 5).

2.7 References

1.   Geusic, J.E., H.M. Marcos, and L.G. Van Uitert, "*Laser oscillations in Nd-doped Yttrium Aluminum, Yttrium gallium and Gadolinium Garnets",* Applied Physics Letters, 1964. **4**(10): p. 182-184.

2.   Sorokin, P.P. and M.J. Stevenson, "*Stimulated emmission from trivalent uranium",* Physical Review Letters, 1960. **5**(12): p. 557-559.

3.   Snitzer, E., "*Optical Maser Action of Nd3+ in a Barium Crown Glass",* Physical Review Letters, 1961. **7**(12): p. 444-446.

4.   Spence, D.E., P.N. Kean, and W. Sibbett, "*60-fsec pulse generation from a self-mode-locked Ti-sapphire laser",* Optics Letters, 1991. **16**(1): p. 42-44.

5.   Sennaroglu, A., "*Broadly tunable Cr4+ doped solid-state lasers in the near infrared and visible",* Progress in Quantum Electronics, 2002. **26**(6): p. 287-352.

6.   Verdun, H.R., L.M. Thomas, D.M. Andrauskas, T. McCollum, and A. Pinto, "*Chromium-doped forsterite laser pumped with 1.06 μm radiation",* Applied Physics Letters, 1988. **53**(26): p. 2593-2595.

7.   Petricevic, V., S.K. Gayen, R.R. Alfano, K. Yamagishi, H. Anzai, and Y. Yamaguchi, "*Laser action in chromium-doped forsterite",* Applied Physics Letters, 1988. **52**(13): p. 1040-1042.

8.   Petricevic, V., A. Seas, and R.R. Alfano, "*Forsterite laser tunes in near-IR",* in *Laser Focus World.* 1990. p. 109-116.

9.   Petricevic, V., S.K. Gayen, and R.R. Alfano, "*Laser action in chromium-activated forsterite for near-infrared excitation: Is Cr^{4+} the lasing ion?"* Applied Physics Letters, 1988. **53**(26): p. 2590-2592.

10.   Jai, W., H. Liu, S. Jaffe, and W.M. Yen, "*Spectroscopy of Cr^{3+} and Cr^{4+} ions in forsterite",* Physical Review B (Condensed Matter), 1991. **43**(7): p. 5234-5242.

11.   Baryshevskii, V.G., M.V. Korzhik, A.E. Kimaev, M.G. Livshits, V.B. Pavlenko, M.L. Meil'man, and B.I. Minkov, "*Tunable Chromium Forsterite Laser in the Near IR Region",* Journal of Applied Spectroscopy, 1990. **53**(1): p. 675-676.

12.   Seas, A., V. Petricevic, and R.R. Alfano, "*Continuous-Wave Mode-Locked Operation of a Chromium-Doped Forsterite Laser",* Optics Letters, 1991. **16**(21): p. 1668-1670.

13.   Sennaroglu, A., T.J. Carrig, and C.R. Pollock, "*Femtosecond Pulse Generation by Using an Additive-Pulse Mode-Locked Chromium-Doped Forsterite Laser Operated at 77-K",* Optics Letters, 1992. **17**(17): p. 1216-1218.

14.   Seas, A., V. Petricevic, and R.R. Alfano, "*Generation of sub-100-fs pulses from a cw mode-locked chromium-doped forsterite laser",* Optics Letters, 1992. **17**(13): p. 937-939.

15.   Seas, A., V. Petricevic, and R.R. Alfano, "*Self-Mode-Locked Chromium-Doped Forsterite Laser Generates 50-Fs Pulses",* Optics Letters, 1993. **18**(11): p. 891-893.

16.   Chudoba, C., J.G. Fujimoto, E.P. Ippen, H.A. Haus, U. Morgner, F.X. Kartner, V. Scheuer, G. Angelow, and T. Tschudi, "*All-solid-state Cr:forsterite laser generating 14-fs pulses at 1.3µm",* Optics Letters, 2001. **26**(5): p. 292-294.

17.   Guerreiro, P.T., S. Ten, E. Slobodchikov, Y.M. Kim, J.C. Woo, and N. Peyghambarian, "*Self-starting mode-locked Cr:forsterite laser with semiconductor saturable Bragg reflector",* Optics Communications, 1997. **136**: p. 27-30.

18.   Zhang, Z., T. K., T. Itatani, K. Kobayashi, T. Sugaya, T. Nakagawa, and H. Takahashi, "*Broadband semiconductor saturable-absorber mirror for a self-starting mode-locked Cr:forsterite laser",* Optics Letters, 1998. **23**(18): p. 1465-1467.

19.   Zhang, Z., K. Torizuka, T. Itatani, K. Kobayashi, T. Sugaya, and T. Nakagawa, "*Self-starting mode-locked femtosecond forsterite laser with a semiconductor saturable-absorber mirror",* Optics Letters, 1997. **22**(13): p. 1006-1008.

20.   Evans, J.M., V. Petricevic, A.B. Bykov, A. Delgado, and R.R. Alfano, "*Direct diode-pumped continuous-wave near-infrared tunable laser operation of Cr^{4+}:forsterite and Cr^{4+}:Ca$_2$GeO$_4$",* Optics Letters, 1997. **22**(15): p. 1171-1173.

21.   Quan, L., X. Liu, and F. Wise, "*Cr:forsterite laser pumped by broad-area laser diodes",* Optics Letters, 1997. **22**(22): p. 1707-1709.

22.   Togashi, T., Y. Nabekawa, T. Sekikawa, and S. Watanabe, "*High-peak-power femtosecond Cr:forsterite laser system",* Applied Physics B: Lasers and Optics, 1999. **68**(2): p. 169-175.

23.   Siegman, A.E., "*Lasers".* 1986, California: University Science Books.

24.   Koechner, W. and B. Bass, "*Solid-State Lasers".* 2003: Springer.

25.   Zhavoronkov, N., A. Avtukh, and V. Mikhailov, "*Chromium-doped forsterite laser with 1.1W of continuous-wave output power at room temperature",* Applied Optics, 1997. **36**(33): p. 8601-8605.

Chapter 3 – The GaInNAs saturable absorber

3.1 Introduction

The quantum-well devices that had previously been grown for the 1300nm spectral region were discussed in Chapter 2. Specifically, these devices were based on GaAs-based Bragg mirrors with InGaAs quantum wells [1, 2] or InP-based Bragg mirrors with InGaAsP quantum wells [3]. Both of these device types when grown for operation at 1300nm have acknowledged shortcomings. Firstly, the indium concentration required for operation around 1300nm results in a lattice constant differential that exceeds the acceptable level of strain in the InGaAs:AlAs/GaAs mirror structure. Strain relaxations then arise leading inevitably to strain-induced high non-saturable losses together with a low damage threshold. Secondly, the scheme involving InGaAsP quantum-wells on an InP Bragg mirror structure results in a narrow reflectivity bandwidth for the Bragg mirror. This arises from the small refractive index contrast achievable from the materials that can be lattice matched to the InP substrate for reflectivity at 1300nm. This small reflective bandwidth imposes a limit on the minimum pulse duration produced from the laser, as explained in Chapter 1.

The poor performance of saturable absorbers at 1300nm provided the incentive for the design and development of new quantum-well-based saturable absorbers for this spectral region, such as the GaInNAs-based device discussed in this chapter. It is important to state at the outset that the inclusion of nitrogen in the quantum well serves to reduce the strain (Fig. 3.1[4]) and acts to shift the absorption edge into the 1200-1400nm region, thereby reducing the non-saturated losses in the device [5].
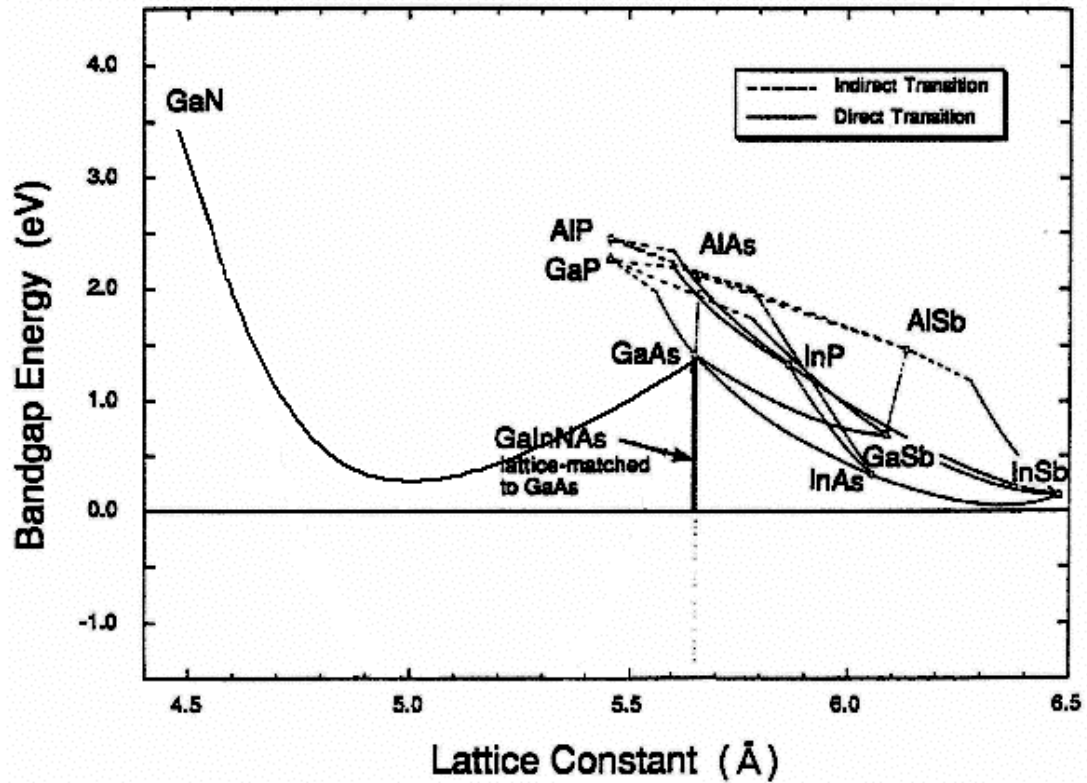
Fig. 3.1 The bandgap energy versus the lattice constant for various semiconductors. Note that the lattice constants for GaAs and GaInNAs can be matched.

The laser cavity described in Chapter 2 was used to evaluate a novel GaInNAs saturabe Bragg reflector (SBR) and the suitability of this material for the generation of femtosecond pulses from a solid-state laser was assessed [6]. The structure of the GaInNAs devices will be discussed here, together with a review of its advantages over previous devices grown for this spectral region. The most salient properties of the GaInNAs SBR will be discussed and then the mode locked performance of a laser that incorporates this device will be described.

3.2 The GaInNAs SBR

GaInNAs as a material system was first proposed theoretically and then experimentally verified by the growth of laser diodes in the 1300-1500nm region by Kondow et al. in 1995/6 [7]. More recently high quality vertical-cavity-surface-emitting lasers (VCSELs) have been grown and some are now on the road to commercialisation [8, 9]. Lately, progress has been made in the use of this material for diode-pumped high-power VECSELs [10], vertical external-cavity surface-emitting lasers (VECSELs) [11], diode-pumped vertical-cavity semiconductor optical amplifiers (VCSOAs) [12] and semiconductor saturable absorber mirrors (SESAMs) for use in laser mode locking. It is this latter application that is most relevant to the research outlined here.

The device used in these investigations was based on material grown at the Optoelectonics Research Centre in Tampere, Finland and subsequently processed in suitable device configurations by collaborating researchers at the Institute of Photonics in Strathclyde. The basic device design is shown in Fig. 3.2 where the material structure was grown by solid source molecular beam epitaxy with a nitrogen plasma source. The structure consisted of a GaAs substrate upon which was grown a 21-layer-pair AlAs (115nm)/GaAs (97nm) Bragg stack designed for high reflectivity around 1300nm. The final quarter-wave layer of this Bragg stack contained a single 7nm thick $Ga_{0.65}In_{0.35}N_{0.019}As_{0.981}$ quantum-well, which was grown at 430°C midway within the layer. No annealing, either *in situ* or *ex situ* was performed on the sample used in this investigation.

21 pair AlAs/GaAs Bragg mirror

7nm thick single $Ga_{0.65}In_{0.35}N_{0.019}As_{0.961}$ quantum well
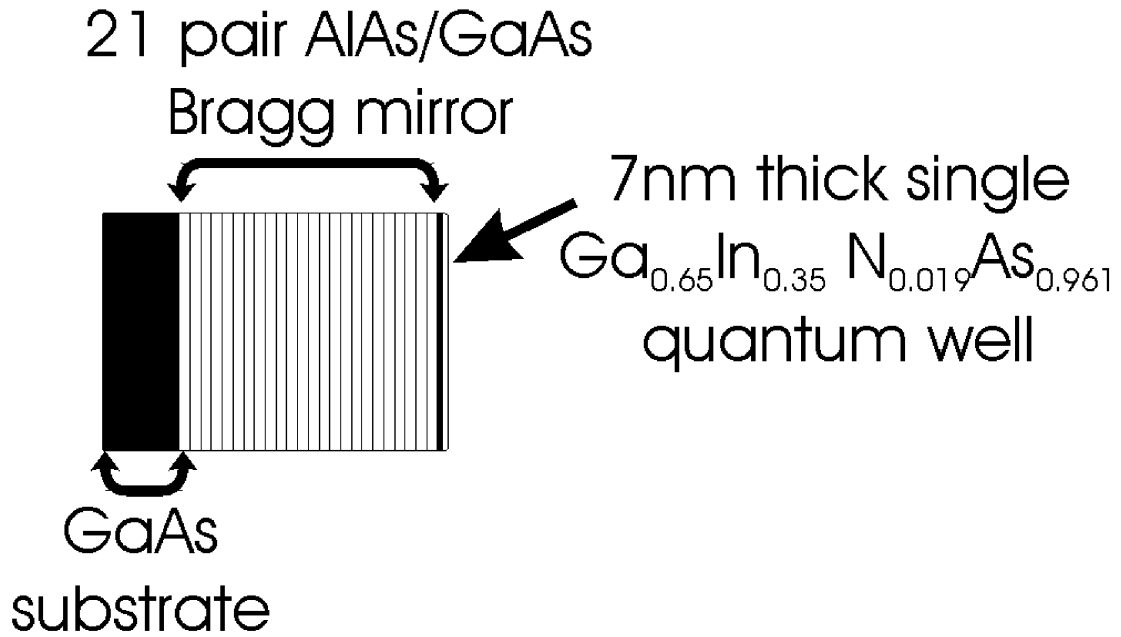
GaAs substrate

Fig. 3.2 A schematic of the GaInNAs SBR

The reflectivity and photoluminescence characteristics for this device (Fig. 3.3) show that the stop band of the Bragg stack was >110nm in width, centred on 1320nm, and that the quantum-well luminescence peaked at 1340nm at room temperature.
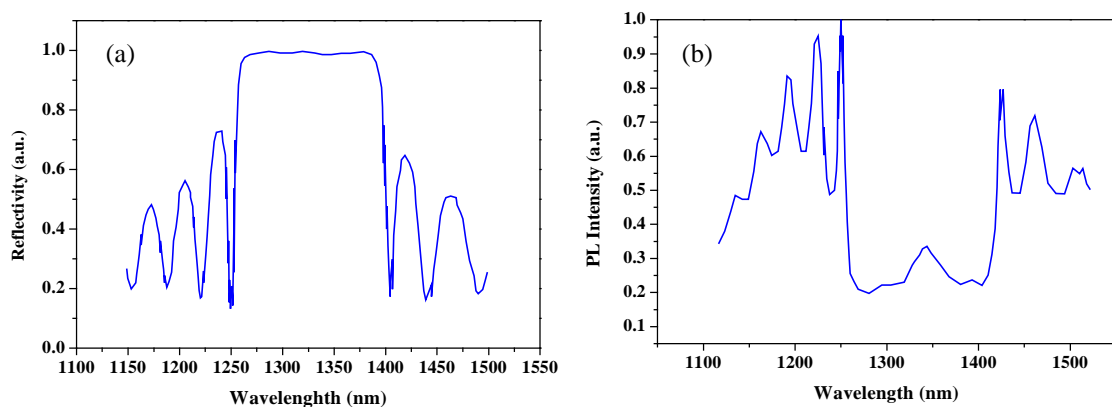
Fig. 3.3 (a) The reflectivity spectrum of the Bragg stack and (b) the photoluminescence intensity of the GaInNAs SBR.

The excitonic luminescence decay was studied by time-gated frequency up-conversion at the University of Iowa and was found to be mono-exponential with a time constant of 69ps, as indicated in Fig. 3.4. (The technique used to obtain this result is described in references [13, 14]).
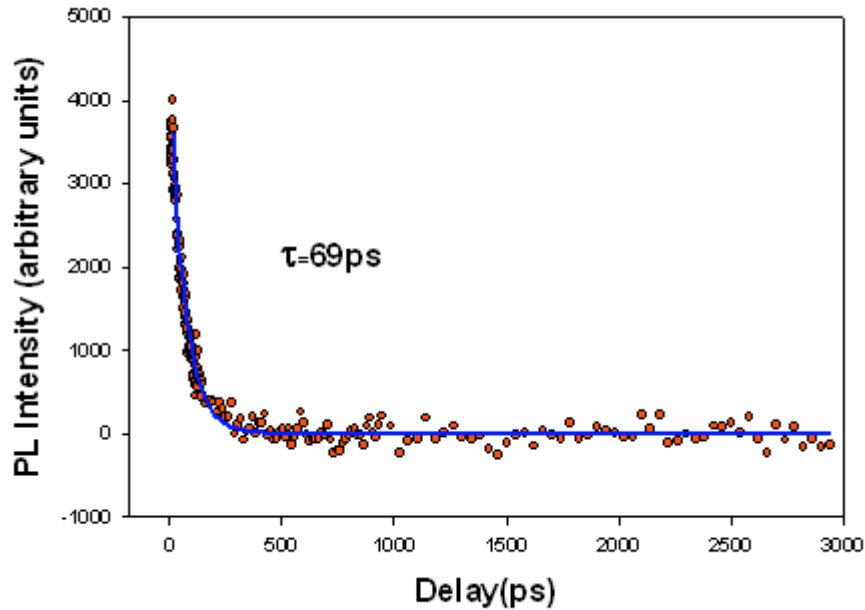

Fig. 3.4 The excitonic luminescence decay of the GaInNAs SBR sample.

The GaInNAs saturable Bragg reflector used in these experiments was tested initially in a low-loss high-power picosecond neodymium laser [5, 15]. This showed for the first time that a GaInNAs based saturable absorber could be used to passively mode lock a solid-state laser in the 1300nm spectral region. By comparing the reflectivity of the SBR with that of a high-reflecting dielectric mirror (with 99.9% reflectivity), the SBR was found to be superior with a residual loss of less than 0.1%. To date, it has not been possible to measure this loss more accurately but it is clear that the GaInNAs device had significantly less loss than the previous devices that had been produced for operation at 1300nm. To test the damage threshold of the device the

laser was allowed to Q-switch, thereby causing higher power levels (estimated to be ~50W) to be incident upon the SBR. Under these conditions no observable damage was suffered by the device, confirming the existence of a high damage threshold. The GaInNAs SBR enabled pulse durations of 22ps to be produced at an average output power of 20W during the 200µs of on-time that the eight bar diode stack was pumping the neodymium laser. During this on-time the eight bar stack produced 360W of average output power at 804nm. A mode locked tuning range of 46nm (1305-1351nm) was found, showing the potential for this material to cover a wide selection of wavelengths in the 1300nm spectral region. It should be noted that femtosecond pulses had not, prior to the work reported here, yet been produced from a solid-state laser incorporating a GaInNAs based saturable absorber.

3.3 Laser cavity

Initially the GaInNAs SBR was incorporated into the experimental laser cavity described in Chapter 2 (Fig. 3.4).
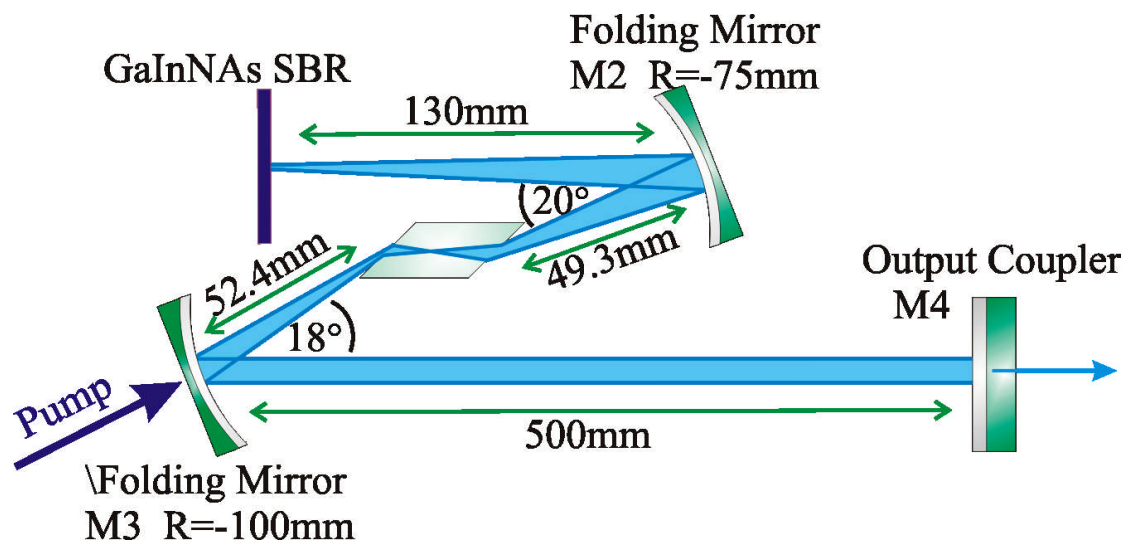

Fig. 3.4 The initial cavity design for testing the GaInNAs SBR providing a spot size of 80µm on the device.

In this configuration the spot size on the SBR was ~80μm in diameter. Before the prism pair was placed into the long arm of the cavity, picosecond operation was observed as the output from this laser. This demonstrated that the device could support mode locked operation in this particular cavity configuration. Fig. 3.5 shows the autocorrelation profile for the picosecond pulse sequences produced by the laser in this configuration.
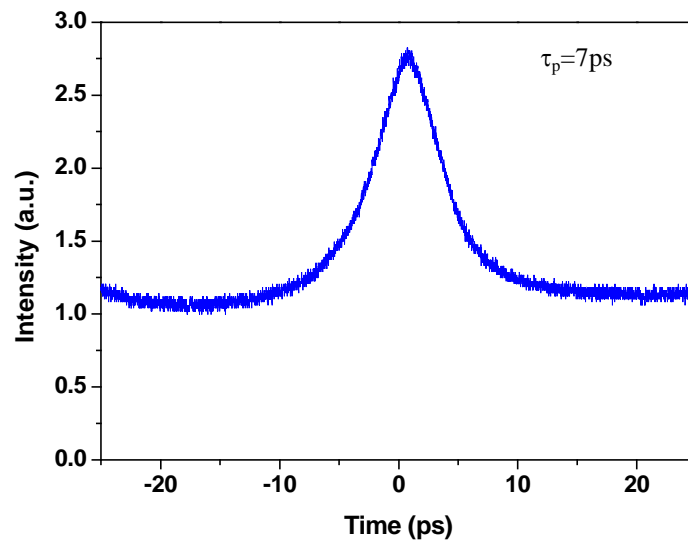

Fig. 3.5 The autocorrelation trace for the laser operating in the picosecond regime.

Fig. 3.5 shows that pulses of 7ps were produced from the laser, assuming a sech^2 pulse shape. Lasing occurred at 1277nm, with an average output power of 48mW measured at a pulse repetition frequency of 184MHz for a pump power of 6W.

Two fused silica prisms were then inserted into the long arm of the cavity (Fig. 3.4) to provide the necessary compensation for the positive group dispersion in the cavity. The separation needed between the prism pair to provide the appropriate amount of negative dispersion was calculated using the following formula [16]:

$$\frac{d^2P}{d\lambda^2} = 4l \left\{ \left[\frac{d^2n}{d\lambda^2} + \left(2n - \frac{1}{n^3}\right)\left(\frac{dn}{d\lambda}\right)^2 \right] \sin\beta - 2\left(\frac{dn}{d\lambda}\right)^2 \cos\beta \right\} \qquad (3.1)$$

Here P is the optical path length, l the prism separation in millimetres, n the refractive index and β is the angle between the red and blue incoming rays to the prism. The derivatives, $dn/d\lambda$ and $d^2n/d\lambda^2$, are the first and second derivatives of the Sellmeier equation and are included below.

$$n^2 - 1 = \sum_{j=1}^{N} \frac{\lambda^2 B_j}{\lambda^2 - C_j^2} \qquad (3.2)$$

$$\frac{dn}{d\lambda} = -\frac{\lambda}{n} \sum_{j=1}^{N} \frac{C_j^2 B_j}{\left(\lambda^2 - C_j^2\right)^2} \qquad (3.3)$$

$$\frac{d^2n}{d\lambda^2} = \frac{1}{n} \sum_{j=1}^{N} \frac{C_j^2 \left(3\lambda^2 + C_j^2\right) B_j}{\left(\lambda^2 - C_j^2\right)^3} - \frac{1}{n}\left(\frac{dn}{d\lambda}\right)^2 \qquad (3.4)$$

Finally, to relate $d^2P/d\lambda^2$ to $d^2\phi/d\lambda^2$ the more commonly quoted parameter with units fs^2/mm is given by Equation 3.5:

$$\frac{d^2\phi}{d\lambda^2} = \frac{\lambda^3}{2\pi l^2} \frac{d^2P}{d\lambda^2} \qquad (3.5)$$

Using published results for dispersion in Cr^{4+}:forsterite crystals [17] the positive group dispersion from the 11.6mm long crystal can be readily deduced from the equations above. The required separation of the fused silica prism pair to introduce an equal amount of negative group dispersion to the cavity was calculated to be 350mm.

When the prism pair as included with a separation as described above, mode locking into the femtosecond regime was realised. A tuning range of 15nm from 1269nm to 1284nm was found with the 0.5% transmission output coupler in place. Transform limited pulses of 170fs were produced in the central region of the range

centred around 1274nm. Output powers of 40mW were found for these pulses, at a pulse repetition frequency of 180MHz.

With a 1% output coupling the tuning range decreased to 10nm, but the available mode locked output powers in the centre of this range (1274nm) increased to 70mW. Transform-limited pulses with a time-bandwidth product of 0.32 were produced with typical durations of 120fs (see fig. 3.6 (a) for a autocorrelation trace of 123fs pulses for which a sech^2 pulse shape was assumed). The associated spectral trace with a FWHM of 14nm is included as Fig. 3.6 (b).
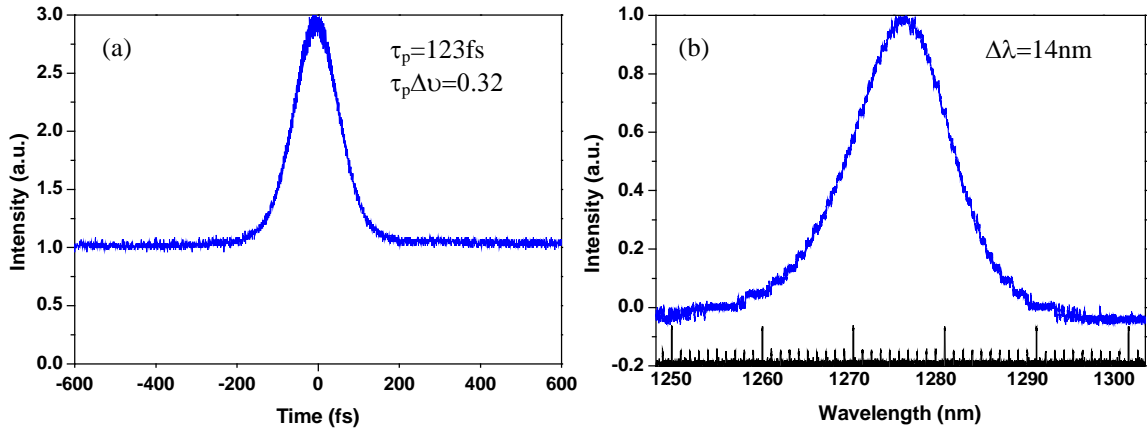

Fig. 3.6 (a) The measured intensity autocorrelation (b) the optical output spectrum from the Cr^{4+}:forsterite laser in the initial configuration.

The observation of these mode-locked pulses demonstrated, for the first time, the ability for a GaAs-based saturable absorber with GaInNAs quantum-well to successfully enable the production of femtosecond pulses [18]. The substantial reduction in output power from over 200mW when used with the 1% output coupler and the high reflector in place for continuous wave operation, to 70mW while mode locked did, however, imply that the cavity had not yet been optimised for use with this SBR. It was hypothesised that the 80μm diameter spot size was insufficient to fully saturate the saturable absorber and therefore the output power from the mode-

locked laser suffered as a consequence. The mode locking in this configuration was also somewhat unstable because thermal lensing effects became serious at pump powers above 6 Watts. For these reasons a redesign of the cavity was undertaken, again using LCAV, to provide a smaller spot size incident upon the SBR and thereby producing a higher incident fluence that would fully saturate the device.
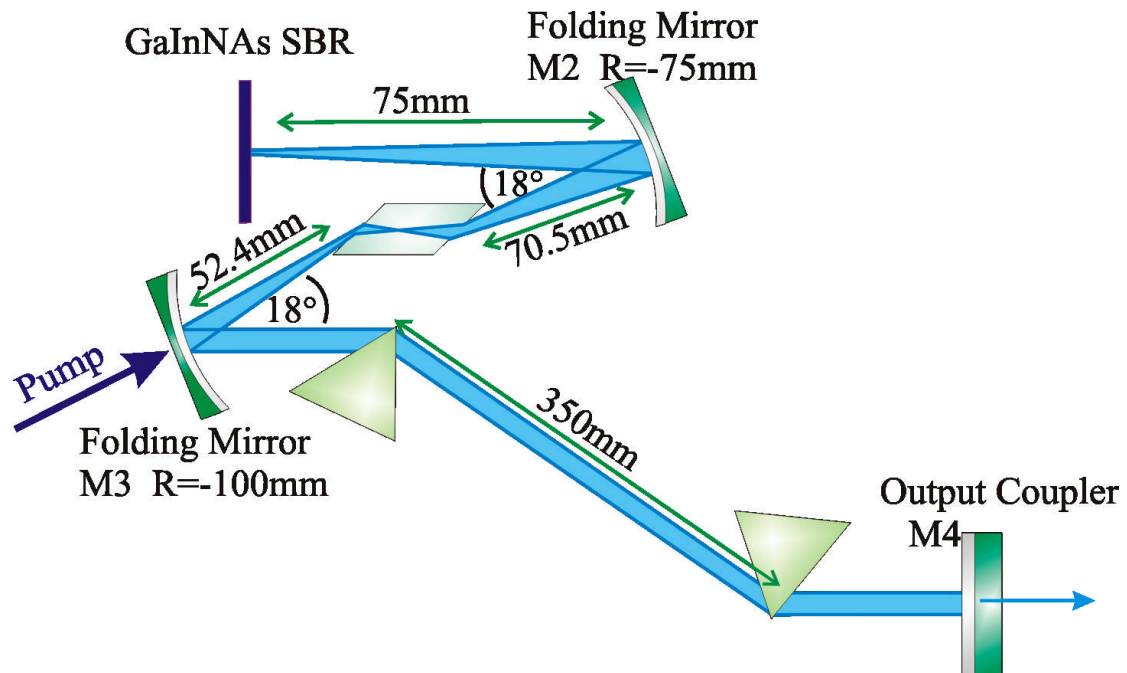

Fig. 3.7 The schematic of the cavity used with the GaInNAs SBR - note the difference in the short arm of the cavity in comparison to Fig. 3.3

This cavity has been altered from that shown in Fig. 3.4 by increasing the total distance in the short arm and decreasing the angle of the second folding mirror. This acted to decrease the spot diameter on the SBR from 80μm to 30μm. It was with this spot size and short arm configuration that the following results were obtained.

With the new cavity configuration the continuous wave performance was similar to that described in Chapter 2. The output powers from the laser were slightly lower, with a maximum of 240mW achievable with the 2% output coupler compared

to the 350mW power level obtained previously. This configuration acted to minimise the thermal lens effect in the cavity and pump powers of 7-8 Watts could readily be used. It was also found that the smaller spot size on the GaInNAs SBR fully saturated the device allowing for stable mode-locked operation with dramatically reduced pulse durations as described later.

3.4 Improved mode-locked operation with the GaInNAs SBR

There are two aspects to the results presented in this section. These relate to the laser output (pulse durations, output powers, tuning ranges) and the device characteristics of the SBR (saturation fluence, the non-saturable losses and modulation depth). The output characteristics of the laser are presented first.

3.4.1 Laser output

Again, a pair of fused silica prisms was inserted into the long arm of the cavity (Fig. 3.7) to compensate for the positive group velocity dispersion. The tip-to-tip separation was 350mm. This allowed the production of femtosecond pulses from the laser cavity and, with the 0.5% output coupler in place, the shortest pulses from the laser were observed.
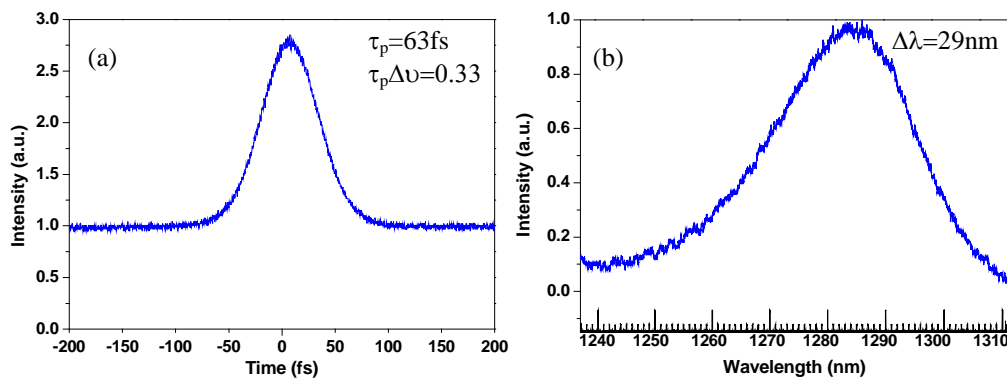

Fig. 3.8 (a) The measured intensity autocorrelation (b), the optical output spectrum from the Cr^{4+}:forsterite laser for the shortest, 63fs, pulses.

Fig. 3.8 (a) shows the two-photon absorption autocorrelation trace for these pulses and implies a pulse duration of 63fs for an assumed sech^2 pulse shape. Fig. 3.8 (b) is the output spectrum of the laser and has a FWHM of 29nm that, when combined with the pulse duration, gave a time-bandwidth of 0.33 indicating that these pulses were close to the transform limit. The pulse repetition frequency was 178MHz, and with the 0.5% output coupler mode locked output powers of 85mW were reached.

With the alternative 1% and 2% output couplers, respective mode-locked laser output powers of 130mW and 215mW were obtained respectively. The transform-limited pulse durations with these output couplers were 77fs for the 1% output coupler and 98fs with the 2%. The autocorrelation trace and spectrum for the system with the 2% output coupler in place are included as Fig. 3.9.
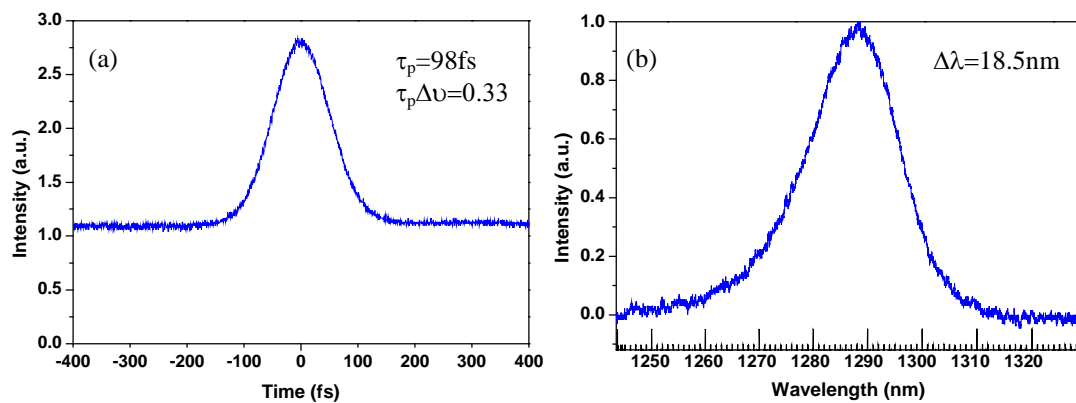
Fig. 3.9 (a) The measured intensity autocorrelation (b), the optical output spectrum from the Cr^{4+}:forsterite laser with the 2% output coupler in place.

When the available mode-locked output powers from the second cavity are compared with those from the previous cavity configuration, the improvement is obvious. This enhancement is due to the GaInNAs device being fully saturated. To highlight the effect of this the output powers from the laser with and without the SBR in place can be contrasted. With the initial cavity and a 2% output coupler in place

continuous wave output powers of 350mW were achievable, but when mode locked

with the GaInNAs SBR only ~70mW was obtained. In the new configuration, with a

spot size of 30μm in the short arm, the continuous wave power with the 2% output

coupler had been reduced to 240mW but the mode locked output power was now

215mW.

A further novelty of the Bragg stack in the GaInNAs SBR was that it had been

grown with a 15nm variation in thickness across the wafer.   Therefore, just by

translating the SBR across the intracavity beam, different mode locked centre-

wavelengths were accessible. Using this method the mode locked tuning range shown

in Fig. 3.10 was found. The 15nm variation is in the total thickness of the Bragg stack

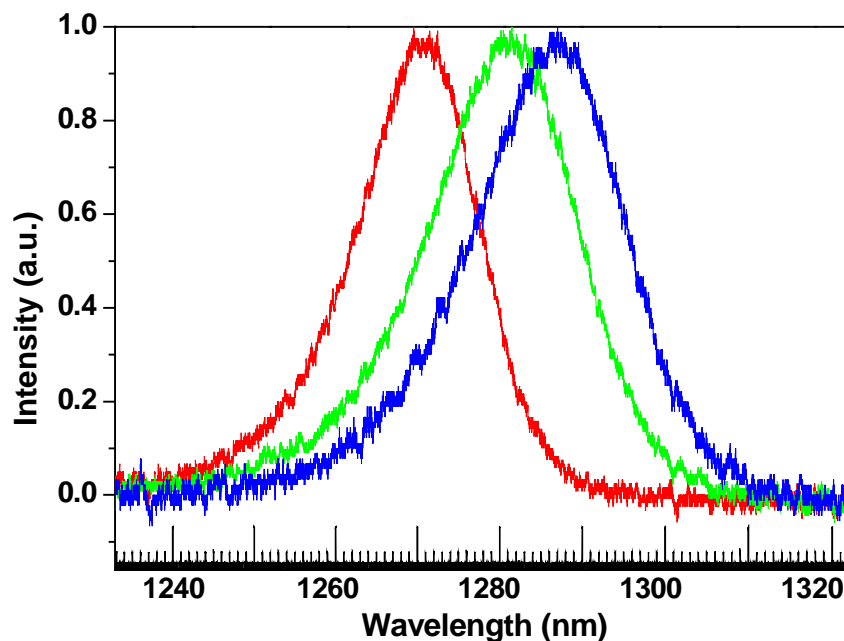across the wafer and is directly attributable to the growth process of the device.

Fig. 3.10 The tuning range of the mode locked output from the laser solely by translating the SBR
across the laser cavity.

This shows that mode locking was achievable across a 16nm range from 1270nm to 1286nm. With the additional inclusion of an intracavity slit between the second prism and the output coupler, this tuning range was increased to range over 25nm from 1268nm to 1293nm as indicated in Fig. 3.11.
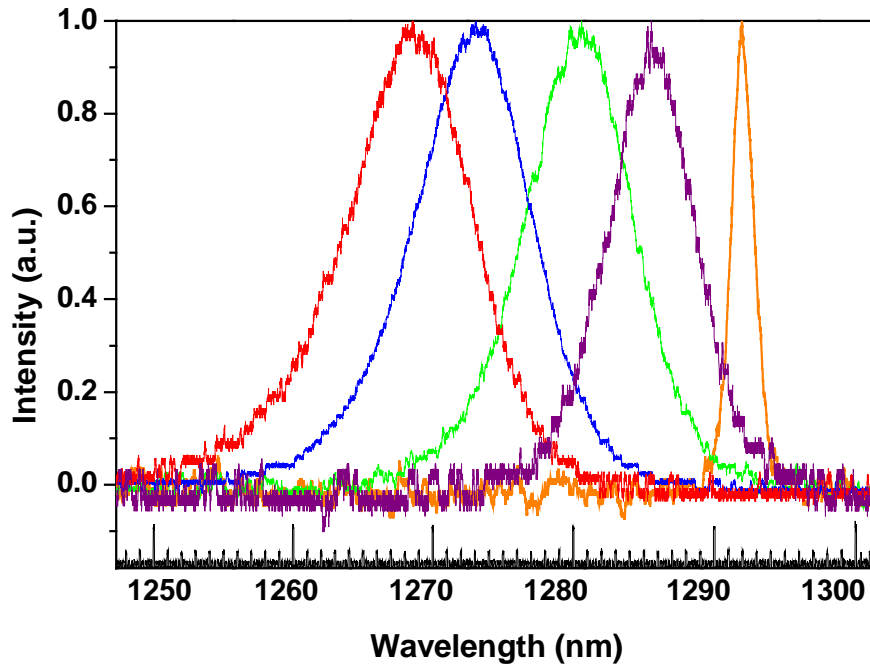

Fig. 3.11. The tuning range of the mode locked laser with the inclusion of a slit.

These measurements for the tuning range of the mode-locked laser were taken with a 0.5% output coupler and at a pump power at 7W. Transform-limited pulses having durations of approximately 100fs were monitored in the centre of the tuning ranges, with the pulse durations increasing to 300-400fs at either edge of the range.

With the 1% and 2% output couplers in place, similar tuning ranges were obtained but with the slightly smaller ranges of 19nm with the 1% and 18nm with the 2% output coupler. With higher value output couplers the intracavity power was reduced and therefore the fluence incident upon the device was decreased. When mode locking occurred at the edges of these tuning ranges, the losses in the cavity

increased to the point that mode locking was no longer sustainable. As expected, the 0.5% output coupler with the highest intracavity powers allowed access to the widest range of mode locked centre wavelengths.

3.4.2 The GaInNAs device characteristics

The performance of the GaInNAs SBR was investigated in detail. Mode locking of the Cr^{4+}:forsterite laser was self-starting for output powers above 25mW with the 0.5% output coupler. This allowed the intracavity power to be calculated as 5W, which, along with pulse repetition frequency, allowed the circulating intracavity energy incident upon the SBR per pulse to be estimated as 27nJ. From this, and using Equation 3.6, the estimate of the saturation fluence on the SBR was calculated to be $980\mu J/cm^2$.

$$\zeta = \frac{E_{pulse}}{\pi r^2} \qquad (3.6)$$

E_{pulse} is the energy of a pulse incident upon the SBR and r is the radius of the spot size on the SBR. This value of $980\mu J/cm^2$ compares well with other saturation fluences for saturable absorbers.

An important feature to ascertain for the SBR was a measure of the non-saturable losses. This would show if a GaInNAs SBR was compatible for mode locking a low-gain material and if it is superior to the devices grown previously for this spectral region. To determine this, the power transfer curves from the laser were investigated and compared with either a high reflectivity mirror or the SBR in place. The power transfer curve is the amount of output power emitted from the laser compared to the amount of pump power incident upon the laser crystal. The SBR was

first placed in the cavity, and as the pump power was increased, the laser would begin its self-starting mode locked operation whenever the intracavity power was sufficient to saturate the SBR absorption. The exact orientation of the SBR and distance from the folding mirror was noted so that the HR-mirror could be placed in that position and the experiment repeated. The results are shown in Fig. 3.12.
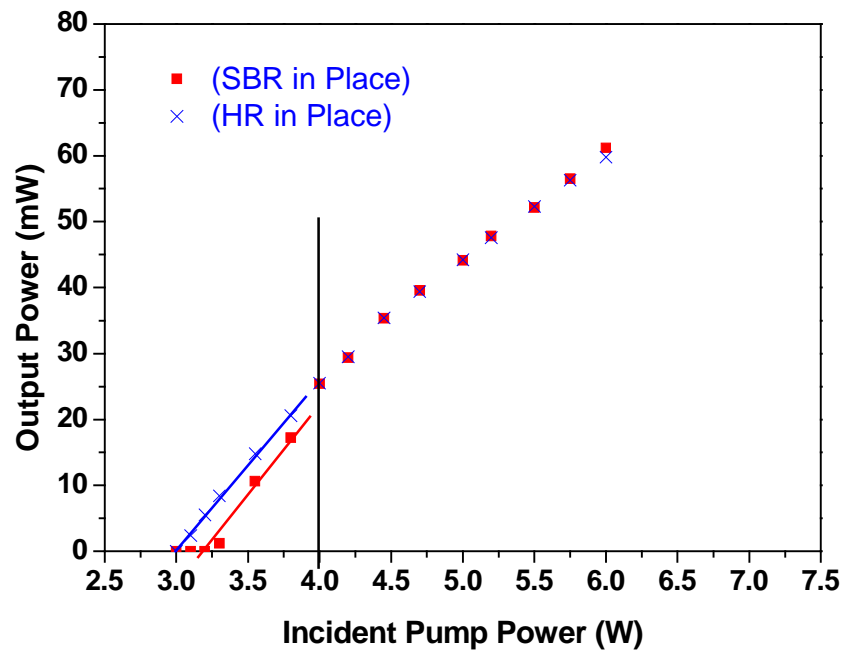

Fig. 3.12 The power transfer characteristics of the laser with a 0.5% output coupler with and without the SBR in place.

As can be seen in Fig. 3.12, the output power from the laser with the SBR in place above the threshold for mode locked operation is comparable to that with the mirror in place. This shows that there are negligible non-saturable losses present in the GaInNAs SBR making this an ideal device for use with low-gain media. Similar results were also obtained for the cavities with the 1% and 2% output couplers.

Finally, an estimate of the modulation depth of the SBR device was deduced by performing a Findlay-Clay analysis [19]. This is a method of calculating the internal losses from a laser cavity while the laser is operating. The lasing threshold of the laser had to be investigated for a number of output couplers, and in this case the 0.5%, 1% and 2% options were used. This investigation was undertaken with either the HR-mirror or the SBR in place and the relevant thresholds are shown in Fig. 3.13.
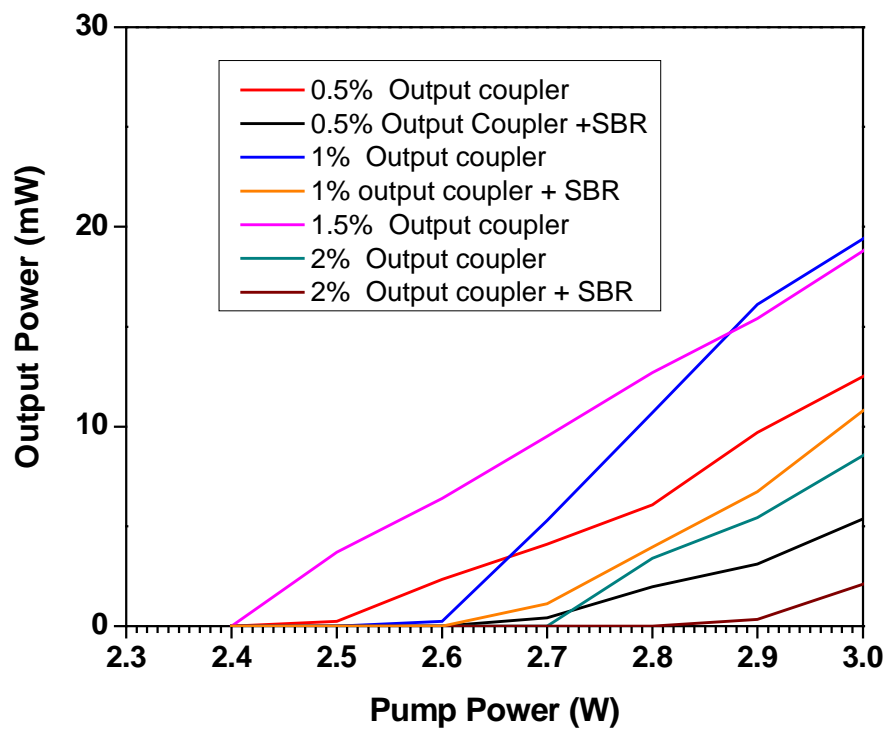

Fig. 3.13 The thresholds for lasing with and without the SBR and for the various output couplers available.

For a four-level system the power from a laser can be described by the following equation,

$$P_{out} = A \left(\frac{1-R}{1+R} \right) I_s \left(\frac{2g_o l}{\delta - \ln R} - 1 \right)$$

(3.7)

Here A is the cross-sectional area of the gain, R is the reflectivity of the output coupler, l is the length of the laser rod, δ is the resonator losses. I_s is a material property of the gain material and can be expressed as,

$$I_s = \frac{hv}{\sigma\tau} \tag{3.8}$$

where v is the wavelength of operation, σ is the emission cross-section, h Plancks constant and τ is the upperstate lifetime. Also from equation 3.7, g_o is the small signal gain and is expressed as,

$$g_o = \frac{\sigma\tau\eta P_{in}}{hvV} \tag{3.9}$$

with η the efficiency of the laser, P_{in} the input pump power and V the gain volume. Equation 3.8 can then be substituted into 3.9 to become,

$$g_o = \frac{\eta P_{in}}{VI_s} \tag{3.10}$$

At lasing threshold the output power from the laser is zero and so Equation 3.7 can be rearranged to become,

$$\frac{2g_o l}{\delta - \ln R} - 1 = 0 \tag{3.11}$$

or,

$$2g_o l = \delta - \ln R \tag{3.12}$$

Substituting equation 3.10 into equation 3.12 and rearranging, the following expression emerges.

$$-\ln R = \frac{2\eta}{AI_s} P_{in} - \delta \tag{3.13}$$

It can be seen that this equation takes the generic form of $y = mx + c$, where m is the gradient of the line and c the y-axis intercept. By plotting a graph of $-lnR$ vs. P_{in} (the pump power at threshold), a line with gradient $2\eta/AI_s$ will be found and a y-axis

intercept of δ, the losses in the resonator. As was shown in Fig. 3.12, the GaInNAs SBR had negliable non-saturable losses, therefore any increase in the resonator losses on insertion of the SBR were due to the presence of the quantum-well in the device alone. As such the difference in the *y*-intercept between the two lines gives a direct measurement of the modulation depth of the device. This graph is included as Fig. 3.14 using the values plotted in Fig. 3.13.
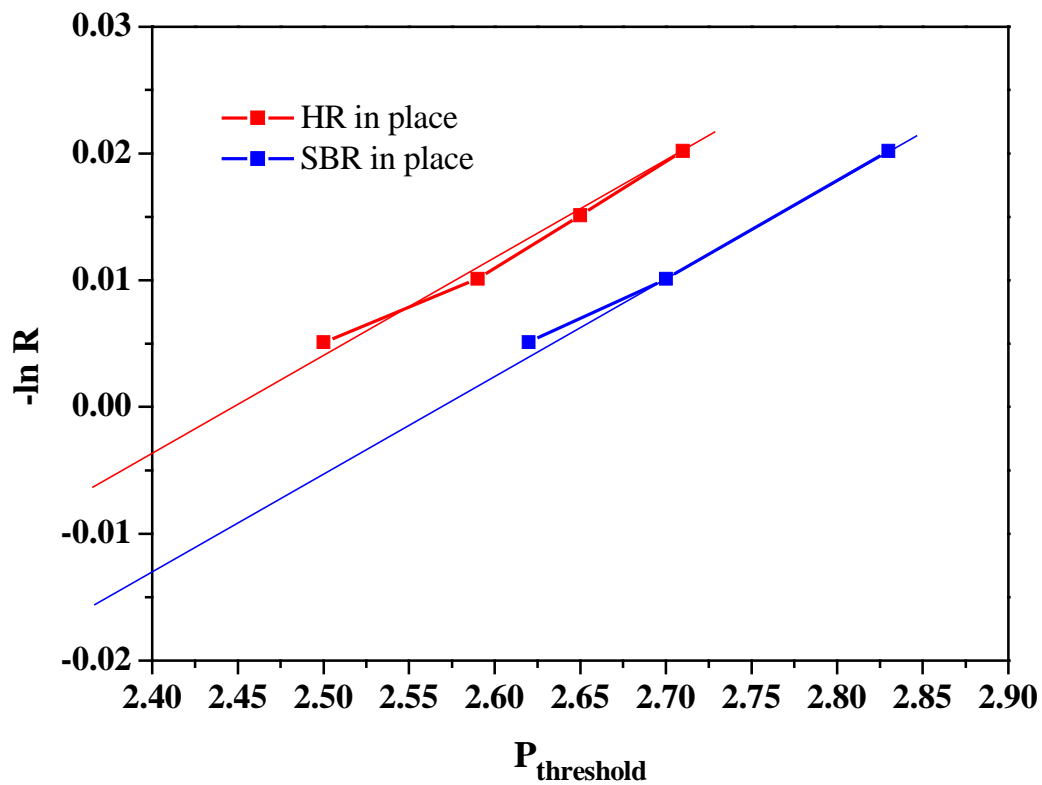

Fig. 3.14. *–lnR vs. $P_{threshold}$*

By extrapolating the parallel lines to intercept the *x*-axis the difference between the laser cavity with and without the SBR can be found. This allows the modulation depth of the GaInNAs device to be found to be ~1%

3.5 Conclusion

The research outlined in this chapter shows for the first time that a GaInNAs based saturable Bragg reflector can be used to mode lock a solid-state laser in the femtosecond regime at 1300nm [6, 20]. The main benefit of a GaInNAs SBR over previously investigated devices is the negligible non-saturable losses inherent in the device. This arises from the ability to pseudomorphically match the GaInNAs quantum-well with the AlAs/GaAs Bragg mirror structure. The SBR used in this project enabled transform-limited mode locked pulses of 63fs to be produced at a pulse repetition frequency of 180MHz and with an output power of 85mW. With a 2% output coupler, the pulse duration increased to 98fs but the mode-locked output power increased to 215mW. This level of mode locked output power allows the laser to be considered for a wide variety of applications, including those described in Chapter 5.

The continued development of this type of saturable absorber device could and should be pursued on a number of fronts. In the context of the *Ultrafast Photonics Collaboration* and using this laser as a suitable ultrafast source for a femtosecond network, the cavity size has to be decreased to increase the pulse repetition frequency. This could be accomplished by replacing the prisms with chirped mirrors, such that a pulse repetition frequency of 1GHz is probably practicable. The laser could also be used with frequency doubling crystals to provide a femtosecond source around 650nm or, as has already been shown, with the technique of sum frequency mixing with a Nd:YVO$_4$ laser to produce a tunable source of yellow light [21]. To date, this has only been attempted in continuous wave operation but a mode-locked source would be possible. A yellow light source is particularly attractive for applications in dermatology.

In terms of the GaInNAs device itself, a greater understanding has been gained in how it performed and how future devices could be adapted for longer wavelengths. This has already been shown in an erbium fibre laser where a GaInNAs SBR was used to generate pulses of 1.2ps at 1.55μm [22].   Recently a GaInNAs device designed for low-loss operation at 1500nm (the second telecommunications window) has been demonstrated with a Cr:YAG laser cavity to produce femtosecond pulses [23].

3.6 References

1. Guerreiro, P.T., S. Ten, E. Slobodchikov, Y.M. Kim, J.C. Woo, and N. Peyghambarian, "*Self-starting mode-locked Cr:forsterite laser with semiconductor saturable Bragg reflector",* Optics Communications, 1997. **136**: p. 27-30.

2. Zhang, Z., K. Torizuka, T. Itatani, K. Kobayashi, T. Sugaya, and T. Nakagawa, "*Self-starting mode-locked femtosecond forsterite laser with a semiconductor saturable-absorber mirror",* Optics Letters, 1997. **22**(13): p. 1006-1008.

3. Zhang, Z., T. K., T. Itatani, K. Kobayashi, T. Sugaya, T. Nakagawa, and H. Takahashi, "*Broadband semiconductor saturable-absorber mirror for a self-starting mode-locked Cr:forsterite laser",* Optics Letters, 1998. **23**(18): p. 1465-1467.

4. "www.nccr-qp.epfl.ch"

5. Calvez, S., J.-M. Hopkins, S.A. Smith, A.H. Clark, R. Macaluso, H.D. Sun, M.D. Dawson, T. Jouhti, M. Pessa, K. Gundogdu, K.C. Hall, and T.F. Boggess, "*GaInNAs/GaAs Bragg-mirror-based structures for novel 1.3μm device applications",* Journal of Crystal Growth, 2004. **268**: p. 457-465.

6. McWilliam, A., A.A. Lagatsky, C.G. Lebum, P. Fischer, C.T.A. Brown, G.J. Valentine, A.J. Kemp, S. Calvez, D. Burns, M.D. Dawson, M. Pessa, and W. Sibbett, "*Low-loss GaInNAs saturable Bragg reflector for mode-locking of a femtosecond Cr4+: Forsterite-laser",* IEEE Photonics Technology Letters, 2005. **17**(11): p. 2292-2294.

7. Kondow, M., K. Uomi, A. Niwa, T. Kitatani, S. Watahiki, and Y. Yazawa, "*GaInNAs: A novel material for long-wavelength-range laser diodes with excellent high-temperature performance",* Japanese Journal of Applied Physics Part 1-Regular Papers Short Notes & Review Papers, 1996. **35**(2B): p. 1273-1275.

8. Sato, S., N. Nishiyama, T. Miyamoto, T. Takahashi, N. Jikutani, M. Arai, A. Matsutani, F. Koyama, and K. Iga, "*Continuous wave operation of 1.26 mu m GaInNAs/GaAs vertical-cavity surface-emitting lasers grown by metalorganic chemical vapour deposition",* Electronics Letters, 2000. **36**(24): p. 2018-2019.

9. Knowles, G., R. Fehse, S. Tomic, S.J. Sweeney, T.E. Sale, A.R. Adams, P. O'Reilly, G. Steinle, and H. Riechert, "*Investigation of 1.3-mu m GaInNAs vertical-cavity surface-emitting lasers (VCSELs) using temperature, high-pressure, and modelling techniques",* IEEE Journal of Selected Topics in Quantum Electronics, 2003. **9**(5): p. 1202-1208.

10.   Kuznetsov, M., F. Hakimi, R. Sprague, and A. Mooradian, "*Design and characteristics of high-power (> 0.5-W CW) diode-pumped vertical-external-cavity surface-emitting semiconductor lasers with circular TEM00 beams*", IEEE Journal of Selected Topics in Quantum Electronics, 1999. **5**(3): p. 561-573.

11.   Calvez, S., N. Laurand, S.A. Smith, A.H. Clark, J.M. Hopkins, H.D. Sun, M.D. Dawson, T. Jouhti, J. Kontinnen, and M. Pessa, "*1.3-mu m GaInNAs surface-normal devices*", IEEE Proceedings-Optoelectronics, 2004. **151**(5): p. 442-446.

12.   Calvez, S., D. Burns, and M.D. Dawson, "*Optimization of an optically pumped 1.3-mu m GaInNAs vertical-cavity surface-emitting laser*", IEEE Photonics Technology Letters, 2002. **14**(2): p. 131-133.

13.   Zhang, L., T.F. Boggess, D.G. Deppe, D.L. Huffaker, O.B. Shchekin, and C. Cao, "*Dynamic response of 1.3-mu m-wavelength InGaAs/GaAs quantum dots*", Applied Physics Letters, 2000. **76**(10): p. 1222-1224.

14.   Zhang, L., T.F. Boggess, K. Gundogdu, M.E. Flatte, D.G. Deppe, C. Cao, and O.B. Shchekin, "*Excited-state dynamics and carrier capture in InGaAs/GaAs quantum dots*", Applied Physics Letters, 2001. **79**(20): p. 3320-3322.

15.   Sun, H.D., G.J. Valentine, R. Macaluso, S. Calvez, D. Burns, M.D. Dawson, T. Jouhti, and M. Pessa, "*Low-loss 1.3-μm GaInNAs saturable Bragg reflector for high- power picosecond neodymium lasers*", Optics Letters, 2002. **27**(23): p. 2124-2126.

16.   Fork, R.L., O.E. Martinez, and J.P. Gordon, "*Negative dispersion using pairs of prisms*", Optics Letters, 1984. **9**(5): p. 150-152.

17.   Thomann, I., L. Hollberg, S.A. Diddams, and R. Equall, "*Chromium-doped forsterite: dispersion measurement with white light interferometry*", Applied Optics, 2003. **42**(9): p. 1661-1666.

18.   McWilliam, A., C.G. Leburn, A.A. Lagatsky, C.T.A. Brown, W. Sibbett, G.J. Valentine, A.J. Kemp, S. Calvez, D. Burns, M.D. Dawson, J. Kontinnen, T. Jouhti, and M. Pessa. "*Femtosecond Cr:forsterite laser modelocked with a GaInNAs saturable Bragg reflector*". in *Advanced Solid State Photonics*. 2005. Vienna.

19.   Findlay, D. and R.A. Clay, "*Measurement of Internal Losses in 4-Level Lasers*", Physics Letters, 1966. **20**: p. 277.

20.   McWilliam, A., A.A. Lagatsky, C.G. Lebum, P. Fischer, C.T.A. Brown, G.J. Valentine, A.J. Kemp, S. Calvez, D. Burns, M.D. Dawson, M. Pessa, and W. Sibbett. "*Low-loss GaInNAs saturable Bragg reflector for femtosecond modelocking of a Cr4+:forsterite laser*". in *European Conference on Lasers and Electro-Optics*. 2005. Munich.

21. Mortensen, J.L., A. McWilliam, C.G. Leburn, P. Tidemand-Lichtenberg, M. Thorhauge, J. Janousek, C.T.A. Brown, A.A. Lagatsky, P. Buchhave, and W. Sibbett, "*Up to 30 mW of broadly tunable CW green-to-orange light, based on sum-frequency mixing of Cr4+ : forsterite and Nd : YVO4 lasers",* Optics Communications, 2006. **260**(2): p. 637-640.

22. Okhotnikov, O.G., T. Jouhti, J. Konttinen, S. Karirinne, and M. Pessa, "*1.5-mu m monolithic GaInNAs semiconductor saturable-absorber mode locking of an erbium fiber laser",* Optics Letters, 2003. **28**(5): p. 364-366.

23. Leburn, C.G., A.D. McRobbie, A.A. Lagatsky, B. C.T.A., W. Sibbett, S. Calvez, D. Burns, M.D. Dawson, J.A. Gupta, and G.C. Aers. "*Self-starting femtosecond Cr:YAG laser mode locked with a GaInNAs saturable Bragg reflector".* in *QEP-17*. 2006. Manchester.

Chapter 4 – Quantum-dot-based saturable absorbers

4.1 Introduction

Quantum-dot (QD) based saturable absorbers are attractive devices for mode locking solid-state lasers because the inhomogeneous broadening associated with the distribution of dot sizes enhances the spectral bandwidth and thus provides broadband absorption and emission spectra [1]. This makes these devices particularly attractive in the context of the generation and amplification of ultrashort pulses. In the previous chapter I discussed some of the drawbacks of the currently available saturable absorbers based on quantum-wells [2-4] as well as one material, GaInNAs, that could possibly circumnavigate these problems [5] for the 1300nm spectral region. The incorporation of a QD saturable absorber into a laser resonator could provide a valuable alternative pathway for the generation of pulses in the femtosecond regime for the 1300nm spectral region, and indeed for any wavelength.

Recent progress in molecular beam epitaxy (MBE) has led to a wide range of QD structures becoming available [1]. In fact, the ongoing development of semiconductor saturable absorbers has fuelled some significant recent progress in new areas of ultrafast science and technology. Existing devices are based predominantly on quantum-well designs, such as the GaInNAs device described in Chapter 3. Within this context, the potential of quantum-dot based semiconductors, when incorporated into ultrashort-pulse lasers, has yet to be fully exploited. For instance femtosecond pulses have not been produced from a solid-state laser mode locked using a QD saturable absorber.

Bulk	*Quantum Well*	*Quantum Dot*

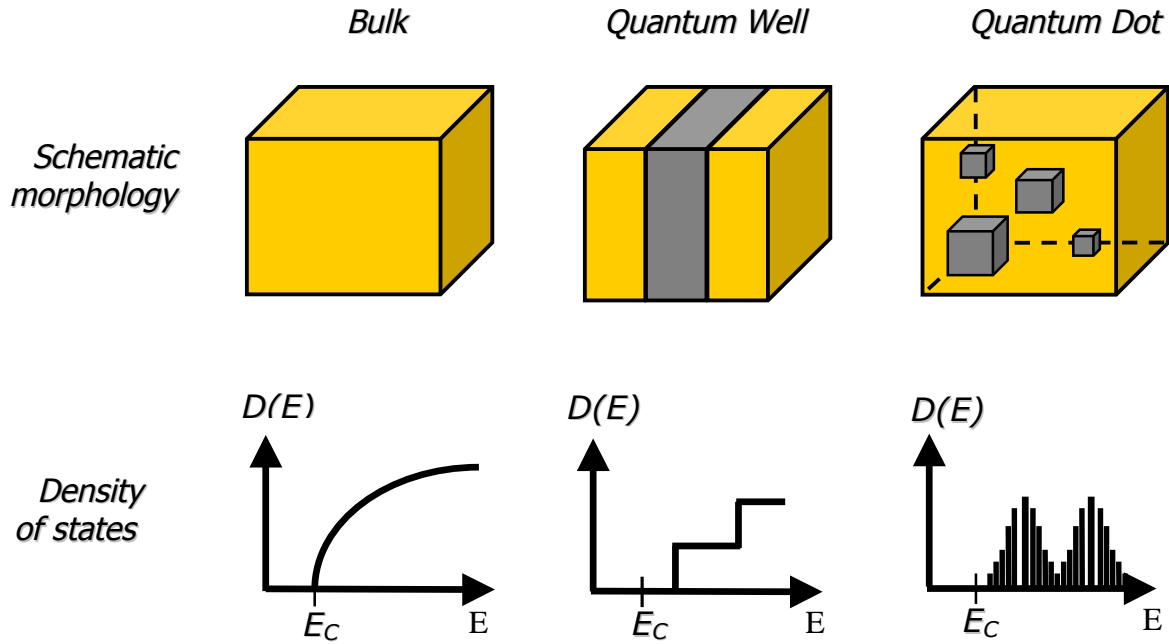*Schematic morphology*

Density of states

Fig 4.1 Schematic diagram comparing the density of states of a bulk material, a quantum-well and quantum-dots.

Fig 4.1 shows a comparison of the density of states between different morphologies. Note how the different sizes of quantum-dots each contribute a discrete energy level. These discrete energy levels arise from the 3-dimensional nature of the confinement of the individual QDs. The dispersion of the QDs size arises from their self-organised growth within the device and causes the inhomogeneous broadening in the lineshape. It is this property of the QDs that provides the broadband emission and absorption spectra that is so desirable for the mode locking of lasers.

In this chapter, I will describe the performance of a Cr^{4+}:forsterite laser that incorporates a quantum-dot-based saturable absorber. To put this work into a suitable context, an overview of QD based saturable absorbers used in solid-state lasers for mode locking into the picosecond regime is included. Until now, QD based saturable absorbers have been unsuccessful in mode locking solid-state lasers in the femtosecond regime. However, using a novel cavity design incorporating the QD

sample at an angle, a Cr^{4+}:forsterite solid-state laser achieved precisely this. Interestingly, this also provided a method for tuning the output pulse duration that could be produced from the laser. After an investigation into this pulse tuning effect a second QD device was grown and tested for the production of femtosecond pulses in the more conventional normal-incidence arrangement, as described in the previous chapter for the GaInNAs saturable Bragg reflector.

4.2 Quantum-dot based saturable absorbers

Mode locking of solid-state lasers with QD saturable absorbers has produced pulses as short as 4ps [6]. These were generated by a Yb:KYW laser that was mode locked using an InGaAs QD saturable absorber. A similar device that incorporated a p-n junction was also investigated [7]. By altering the reverse bias across this device more stable mode locked operation was found without affecting the output power from the laser. The difference between unbiased and biased pulse durations ranged from 10.5ps to 6ps. Lasing occurred at 1040nm with output powers of 90mW and the time-bandwidth product was 0.78. These experiments indicated some potential for QD devices as saturable absorber elements in the mode locking of solid-state lasers. Recently, the shortest pulses from a laser system mode locked with a QD saturable absorber were produced by a ytterbium-doped fibre laser. This produced 2.8ps pulse durations with an average output power of 5mW generated at 1042nm [8].

Work undertaken in the spectral region around 1300nm, where the Cr^{4+}:forsterite laser operates, has also shown performance improvements in the last few years [9]. Most notably, picosecond operation from a Nd:YVO$_4$ laser using a QD saturable absorber has been realised. The saturable absorber consisted of 3 InAs QD layers and also served as the output coupler. The spot size of the incident focussed

laser beam on the QD saturable absorber was 42μm in diameter. The duration of the mode locked pulses from this laser was 26ps at 1342nm. With a spectral bandwidth of 0.101nm a time-bandwidth product of 0.44 was calculated and average output powers of 0.85W were attained for input pump powers of 12.6W. These were the shortest pulses produced in the 1300nm spectral region from a solid-state laser mode locked with a QD based saturable absorber before the work reported here was undertaken.

It is worth pointing out here that the generation of femtosecond pulses from a two-section QD semiconductor device had been reported [10]. Pulses of 400fs at 1260nm were generated with output powers of 45mW at a pulse repetition frequency of 21GHz. This two-section device was grown on a GaAs substrate and had an active region of five InGaAs QD layers. By altering the drive current conditions to the device, the pulses from the laser could be tuned directly from 2ps to 400fs.

The potential for reaching the femtosecond regime with QD saturable absorbers will be discussed further in this chapter. Two devices were used in this work, one with 20 layers of QDs and a second with 35 layers. The results obtained from the first device then led to the redesign of the sample and the use of the second 35-layer QD-device.
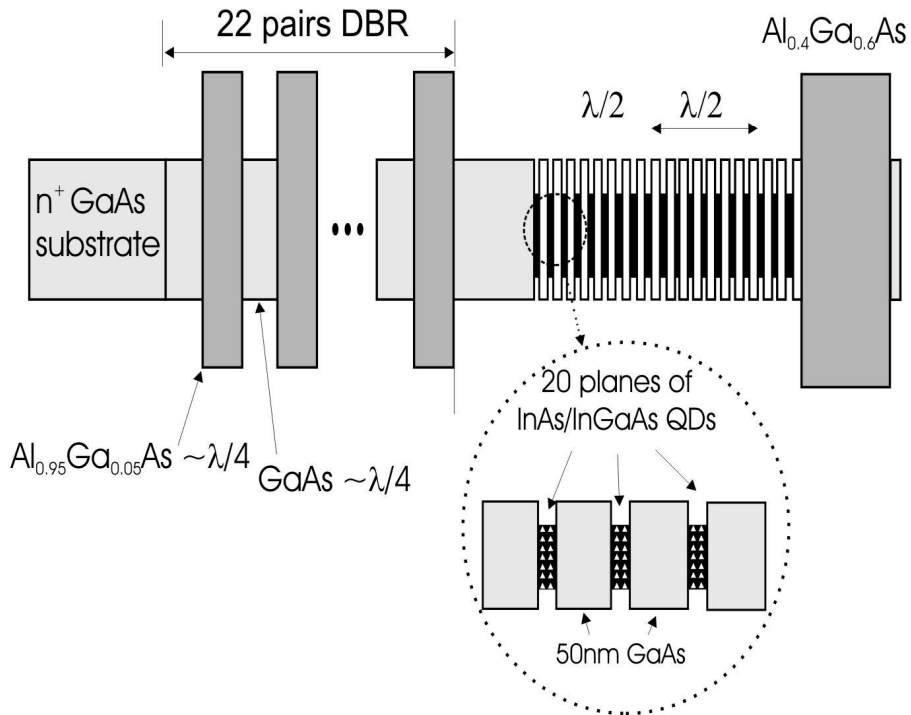
Fig. 4.2 A schematic of the QD saturable absorber used in the initial QD assessments

The QD saturable absorber was grown in the Ioffe Institute in St Petersburg by molecular beam epitaxy, in a Riber 32P machine equipped with In, Al and two Ga sources and an As valved-cracker cell. The structure, included as Fig. 4.2 [11], was grown on a GaAs substrate. A distributed Bragg reflector with 22-period quarter-wave $Al_{0.95}Ga_{0.05}As$/GaAs layers provided high reflectivity between 1250nm to 1400nm with 20 layers of InAs QDs grown on top to provide the saturable absorption. The second device used in the later assessments had the same structure and growth process as described here but had 35 layers of InAs QDs instead of the 20 layers shown in Fig. 4.2.

4.3 Mode locking with the quantum-dot saturable absorber

At the outset of this part of the research project, the QD saturable absorber with 20 layers of InAs QDs was placed into the cavity used previously to test the GaInNAs saturable Bragg reflector (Fig. 4.3).
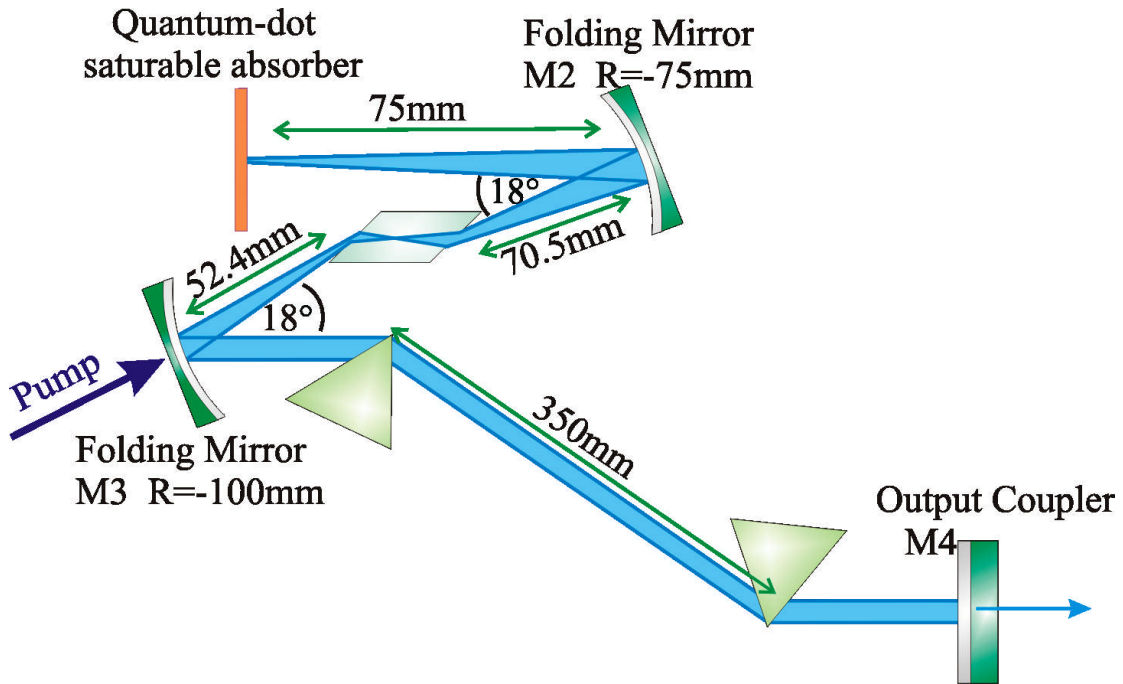

Fig. 4.3 The laser cavity used to test the quantum-dot-based saturable absorber.

In this configuration the pump geometry and optical components were as described in Chapter 2. The fused silica prisms had a tip-to-tip separation of 350mm in the long arm of the cavity to compensate for positive group dispersion. During these experiments a 0.5% output coupler was used and pulses of 58ps were produced (Fig. 4.4). These pulses had a bandwidth of 0.5nm at 1278nm with output powers of 85mW and a pulse repetition rate of 180MHz during mode locked operation. Fig. 4.4 shows the real time trace from a fast oscilloscope with the pulse duration measured directly. (This oscilloscope has a temporal resolution of 20ps).
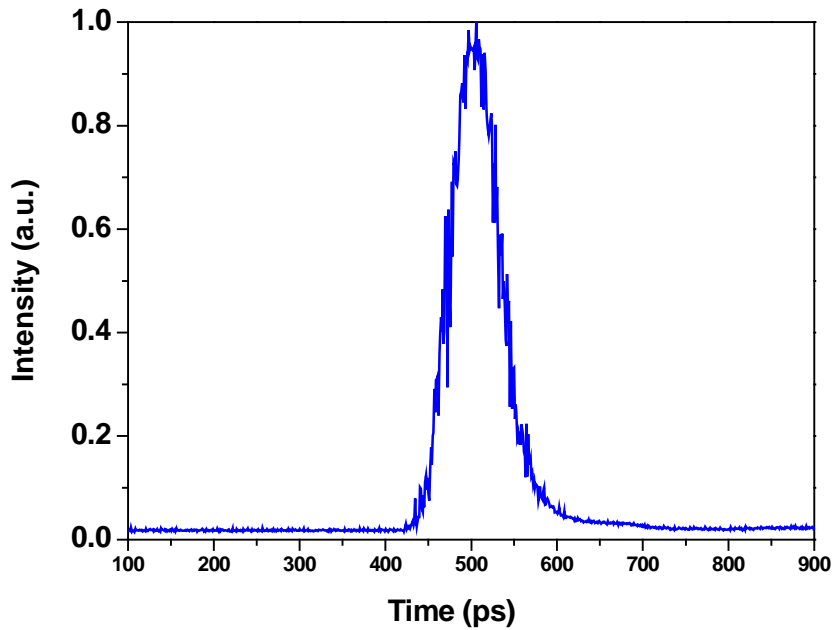
Fig. 4.4 Picosecond pulses from the Cr^{4+}:forsterite laser with the first QD saturable absorber sample in a perpendicular orientation.

Previous work indicated that the expected pulses should be shorter than the 58ps that were generated. This led to a redesign of the cavity configuration to incorporate the QD sample at an angle. This required an additional mirror to terminate the short arm of the cavity as depicted in Fig. 4.5. A second 75mm radius of curvature mirror was chosen to terminate the short arm of the cavity so that the spot size upon the QD saturable absorber could be kept at ~30μm in diameter. This spot size was kept constant throughout the range of angles used. The longer arm of the cavity, the prisms, the pump geometry and therefore the spot size within the Cr^{4+}:forsterite crystal were unaltered in the cavity. The 0.5% output coupler was in place for all of these assessments.
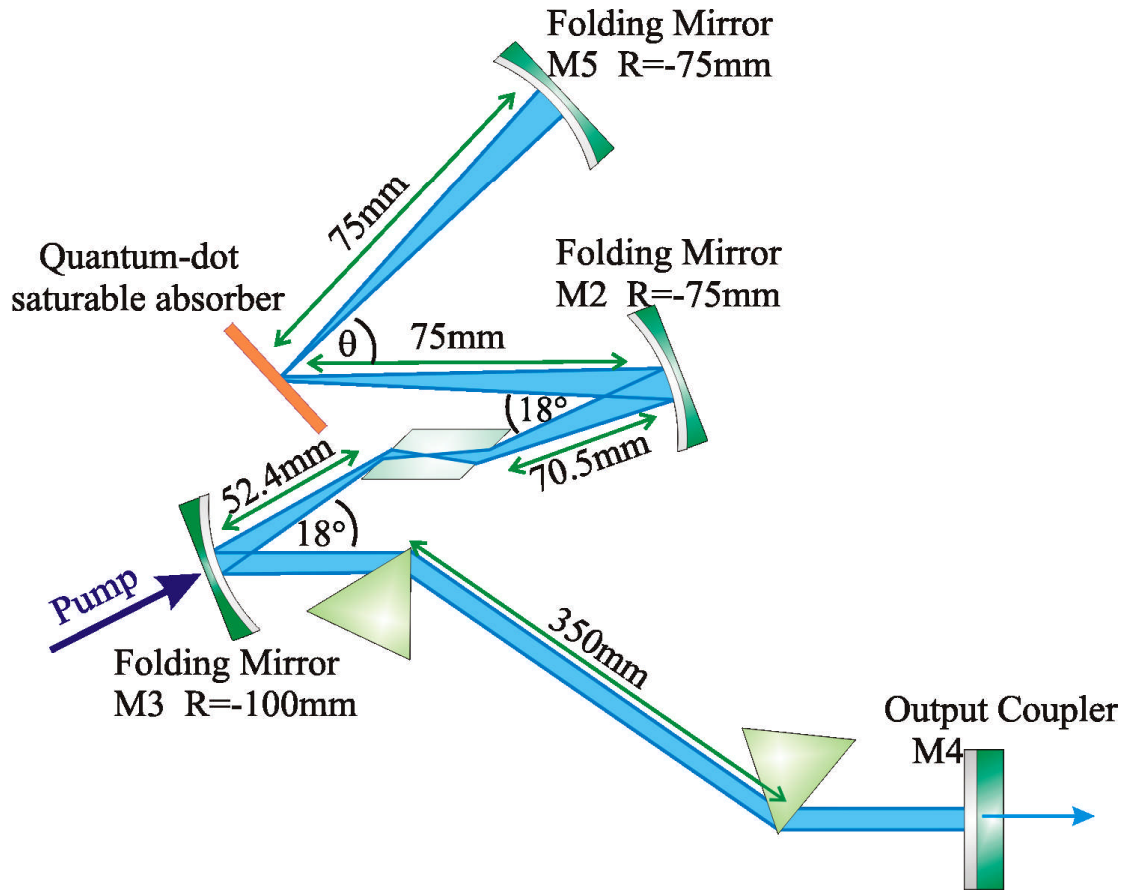
Fig. 4.5 The cavity configuration for incorporating the QD saturable absorber at an angle inside the laser cavity.

The angle θ shown in Fig. 4.5 was varied over the range 30°<θ<60° with the shortest

pulses being measured at an angle of 45° (see Fig. 4.6).
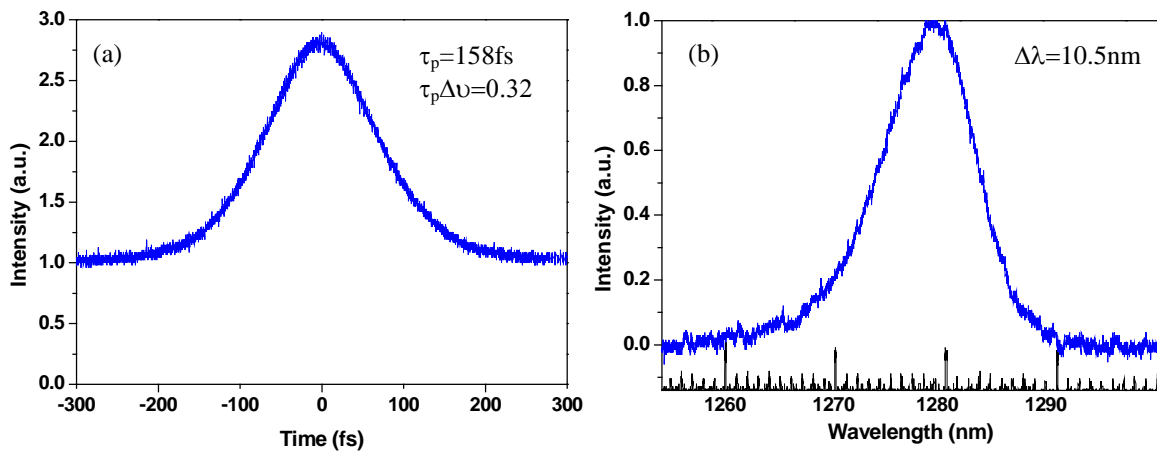

Fig .4.6 (a) Measured intensity autocorrelation and (b) spectral trace of the pulses from the Cr^{4+}:forsterite laser with the QD saturable absorber at 45°

Fig. 4.6 (a) shows the intensity autocorrelation of the pulses, which, for an assumed sech^2 pulse profile, implied a duration of 158fs. By combining this with the spectrum shown in Fig. 4.6 (b) for the mode-locked pulses (FWHM of 10.5nm), we inferred that the pulses, with a time-bandwidth product of 0.32, were transform limited. With the saturable absorber at this angle, the output power from the laser was 64mW with a pulse repetition frequency of 194MHz. Significantly, this was the first time that femtosecond pulses were obtained from a solid-state laser mode locked with a QD saturable absorber![11].

By way of representative performance features it is interesting to consider some of the results obtained under the different operating conditions. For instance, by increasing the angle of the absorber element from 45° to 60° and decreasing the angle from 45° to 30° longer pulse durations were generated. Fig. 4.7 shows the autocorrelation and spectral trace for 30°, whilst Fig. 4.8 shows the autocorrelation and spectral trace for an angle of 60°.
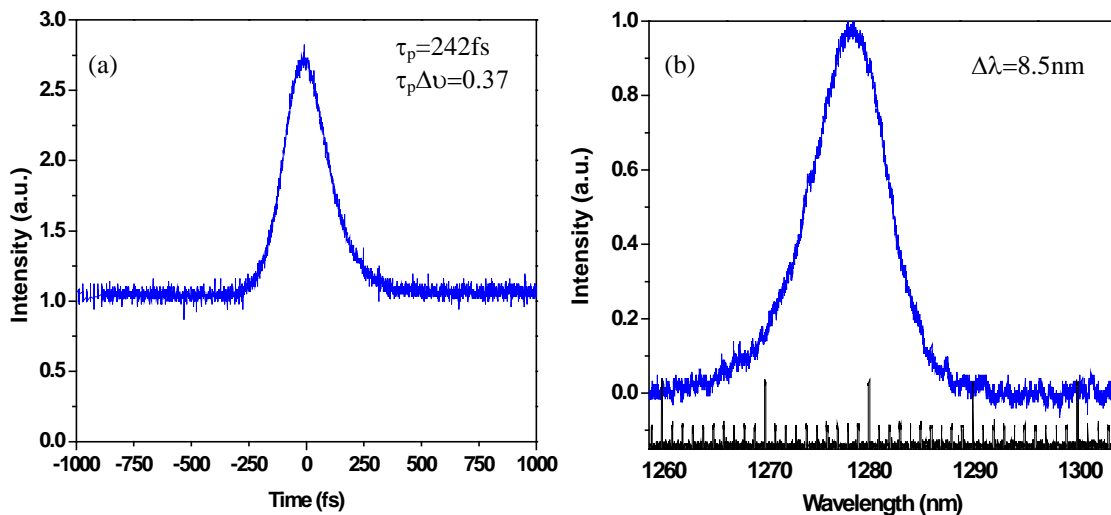

Fig. 4.7. (a) Measured intensity autocorrelation and (b) the spectral trace for the pulses from the Cr^{4+}:forsterite laser with the QD saturable absorber oriented at 30°

At 30°, transform limited pulses of 242fs in duration were produced where the average output power was 70mW (as shown in Fig. 4.7).
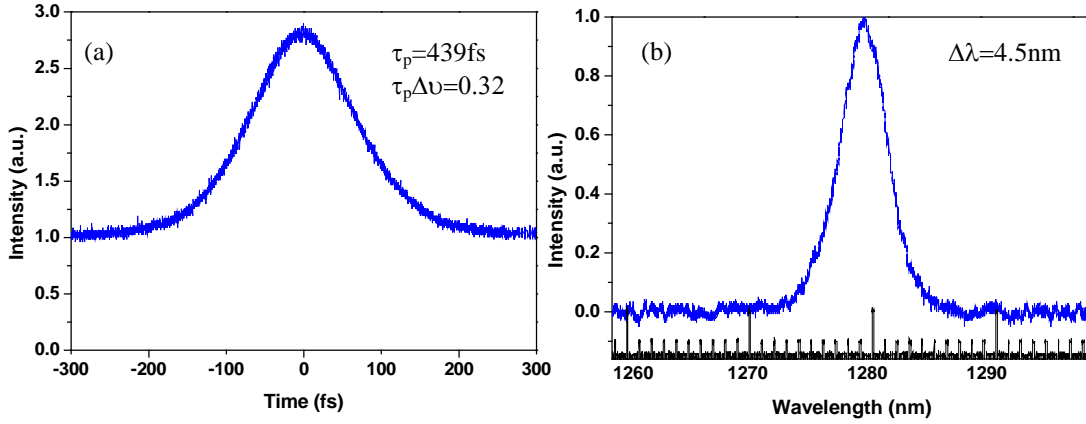

Fig. 4.8 (a) Measured intensity autocorrelation and (b) the spectral trace of the pulses from the Cr^{4+}:forsterite laser with the QD saturable absorber oriented at 60°

At 60°, which was the other extreme of the range of angles, the pulses increased to 439fs with a spectral bandwidth of 4.5nm, indicating transform limited pulses. At this angle the output power from the laser was 46mW. A summary of the results obtained for the various angles investigated across this range is included as Fig. 4.9. It can be seen that as the angle is increased the output power falls off steadily and that the pulse duration reaches a minimum for a 45° angle of orientation of the absorber. The results in Fig. 4.9 are summarised in Table 4.1, which also shows the near transform-limited nature of the pulses produced. During these evaluations the maximum intracavity fluence incident upon the device was estimated to be 2.3mJ/cm^2.
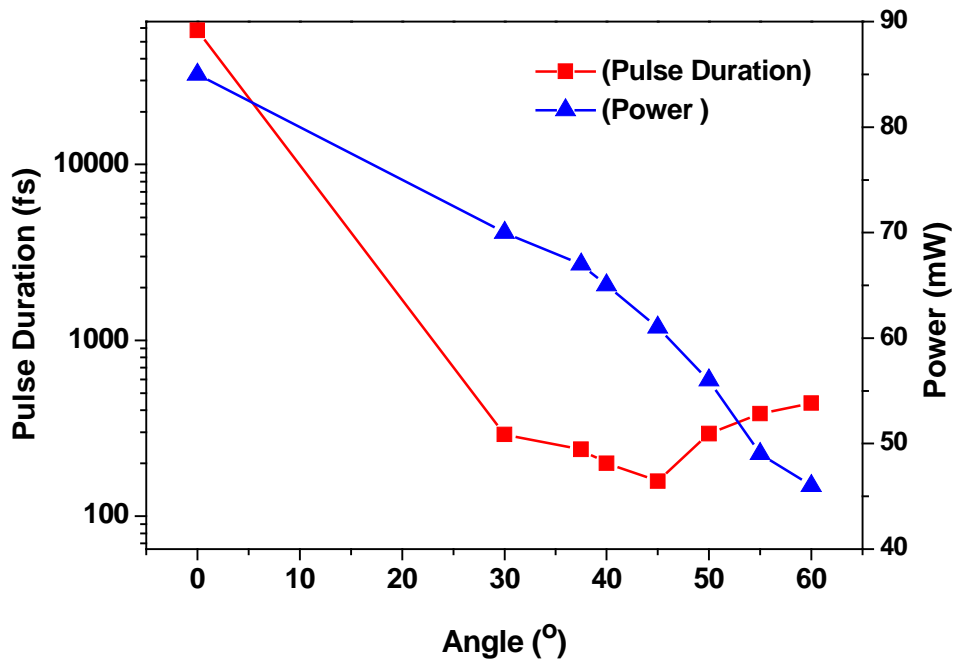
Fig. 4.9 Pulse duration and output power from the Cr^{4+}:forsterite laser versus angle at which the QD saturable absorber was incorporated into the cavity, θ

Angle (°)	Pulse Duration (fs)	$\Delta\upsilon\Delta\tau$	Power (mW)
30	240	0.33	70
40	200	0.33	65
45	158	0.32	61
50	295	0.35	56
55	383	0.32	49
60	439	0.32	46

Table 4.1 A summary of the results obtained with the QD saturable absorber at the various angles of orientation.

The lack of results between 0° and 30° is due to positional constraints on the mirror mounts used. At small angles the position of the second folding mirror required to maintain stability began to overlap with the position of first folding mirror. This positional constraint meant that small angles could not be accessed with this

laser cavity. Also, due to the lack of results in this range it cannot be said if the transition from 58ps when at normal incidence to 240fs when at 30° is a smooth transition or whether there is a certain angle at which the pulse duration jumps into the femtosecond domain. If this pulse tuning behaviour is to be further investigated and exploited then results in this range will be needed, necessitating a redesign of the laser cavity.

At angles in excess of 60° mode locking was no longer possible due to the increased losses in the cavity. For angles in excess of 70° continuous wave operation could no longer be achieved. At 60° the losses from the QD device were 13% increasing to 18% for an angle of 70° (see Fig.4.12). For a low gain material such as Cr^{4+}:forsterite this was sufficient to inhibit lasing. These losses were expected as the Bragg stack in the device was designed for operation at normal incidence and not when included into the cavity at an angle.

These experimental assessments were also repeated using 1% and 2% output coupling. Similar results to those presented above were obtained but the range of useful orientation angles was reduced. For the higher percentage output couplers the intracavity power was significantly reduced and insufficient to fully saturate the QD-based absorber to initiate mode locking.

For the 1% output coupler the angles over which lasing was achieved ranged from 0° to 55° with the shortest pulses still found at 45°. These had a pulse duration of 200fs, as shown in Fig. 4.10.
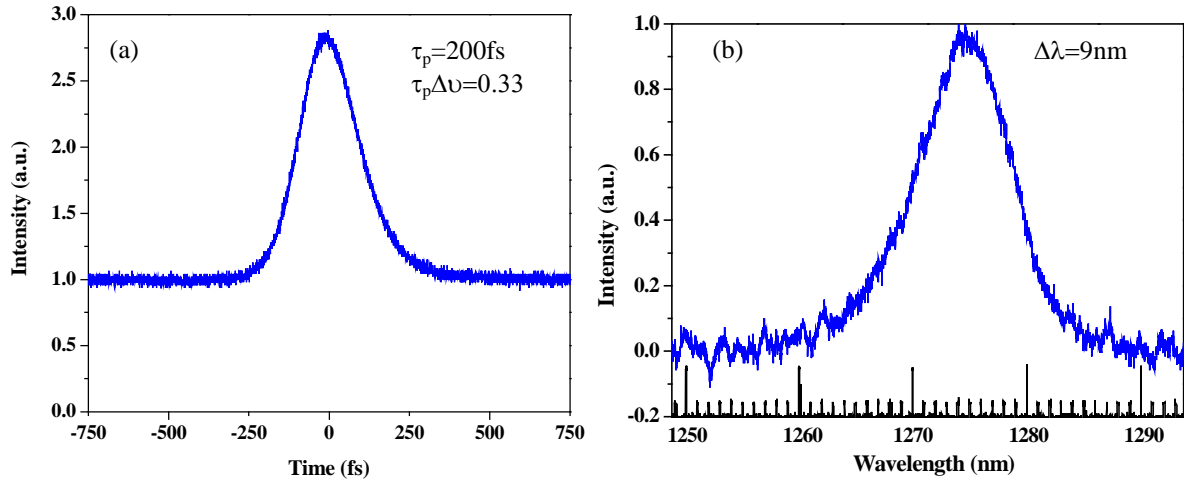
Fig, 4.10 (a) Measured intensity autocorrelation and (b) the spectral trace for the pulses from the Cr^{4+}:forsterite laser with the QD saturable absorber oriented at 45° and the 1% output coupler.

Nearly transform limited pulses of 200fs were measured from the laser when a 1% output coupler was used, as shown in Fig. 4.10. This had an average output power of 75mW when mode locked at a pulse repetition frequency of 194MHz. Pulse durations across the range available with the 1% output coupler increased to nearly 300fs at 30° and 400fs for 55°.

Similarly, for the 2% output coupler the shortest pulse durations were found at 45° and were measured to be 308fs (Fig. 4.11). The output power of the laser while mode locked in this configuration was measured to be 54mW. However, as the angle was increased towards 50°, the output power rapidly fell and mode locking was no longer possible for angles of 50°.
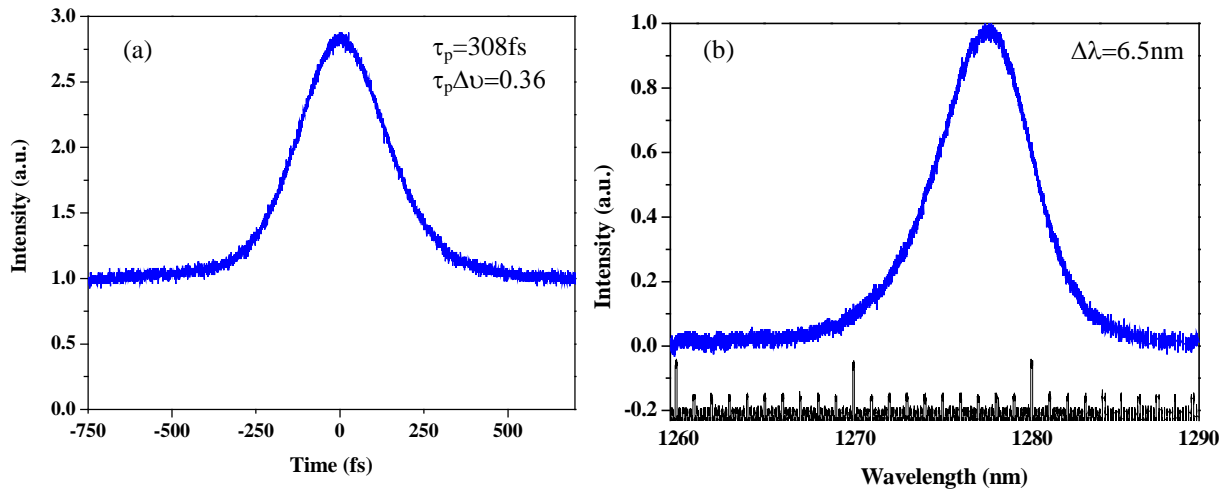
Fig, 4.11 (a) Measured intensity autocorrelation and (b) the spectral trace for the pulses from the Cr^{4+}:forsterite laser with the QD saturable absorber oriented at 45° and the 2% output coupler.

4.4 Improved QD structures for increased performance of the laser

An explanation for the behavioural features of the QD saturable absorber was required so that an optimised QD device could be designed and produced to provide mode locking in the more normal (θ=0°) orientation. For this purpose an investigation into the reflectivity characteristics of the QD device was undertaken for the different angles used, Fig. 4.12. These measurements were taken at the Ioffe institute.
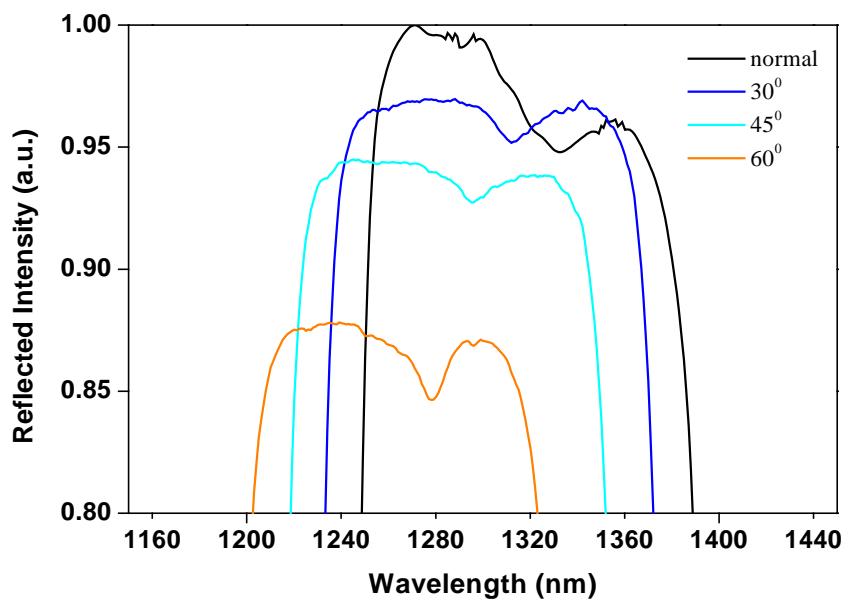

Fig. 4.12 Reflectivity spectra of the quantum-dot saturable absorber for various angles of incidence.

The information contained in Fig. 4.12 can be used to explain the phenomena represented by Fig. 4.9. Firstly, as the angle of incidence is increased the reflected intensity decreases, so the output power from the laser will decrease as observed. This was confirmed by measuring the transmitted power through the QD sample while in the cavity. As the angle was increased the power transmitted also increased, as indicated in Fig. 4.13.
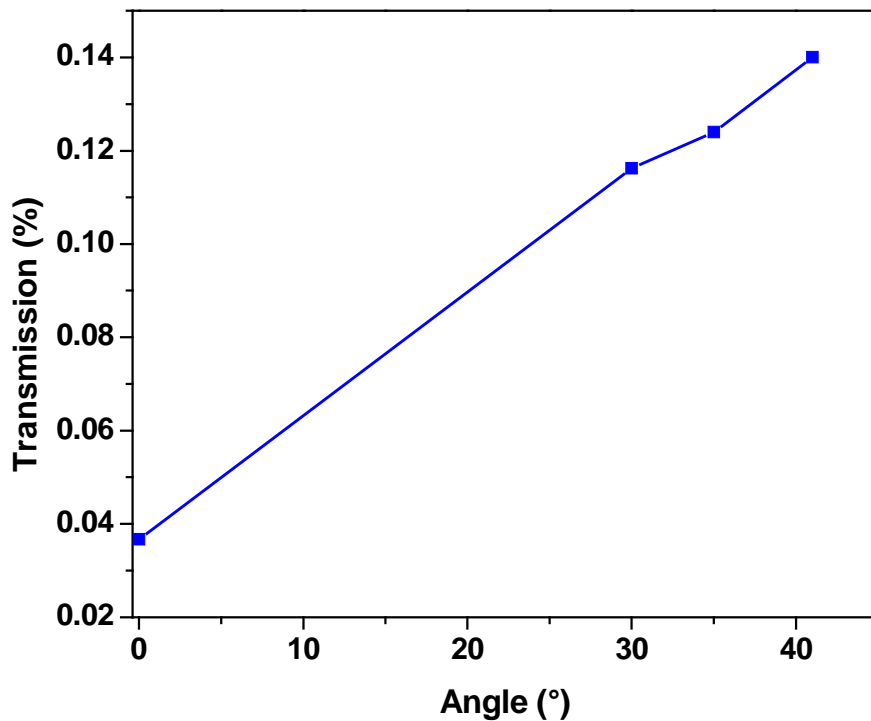
Fig. 4.13 The transmission of intracavity power through the QD device for various angles.

To explain the change in pulse duration the absorption peak of the QDs has to be studied. As can be seen from Fig. 4.12, the peak of absorption for the QD device at normal incidence lies at 1332nm but at the preferred lasing wavelength of the laser (~1278nm) the available modulation depth is negligible. As a consequence, only operation in the picosecond regime was possible. By contrast, as the angle is increased the peak of absorption moves towards and then through the lasing

wavelength region, thereby allowing larger modulation depths to become accessible. The shortest pulses were obtained for an angle of 45° where a modulation depth of 0.5% was estimated. It should be noted that the greatest overlap between the peak of absorption and the lasing wavelength occurred at 60°, where the device had a modulation depth of ~2%. In this configuration the output power of the laser was relatively low and the intracavity fluence was insufficient to fully saturate the QD device, hence the longer pulses shown in Fig. 4.8. It can also be seen in Fig. 4.11 that at normal incidence the FWHM of the peak of absorption is approximately 30nm wide. It follows, therefore, that if this device was redesigned so that this peak of absorption coincided with the lasing wavelength, the generation of shorter pulses should become feasible.

Redesigned QD devices were grown on the basis of this information, so that the peak of absorption would be coincident with the operating spectral range of the laser, allowing operation to occur with the absorber at normal incidence. These devices had 35 layers of InAs quantum-dots. The absorption spectrum is included as Fig. 4.14.

The slightly altered design of the device with the additional layers of quantum-dots arose from an effort to increase the modulation depth of the device. In order for a pulse to be able to propagate inside the laser cavity it has to have a peak power sufficient to saturate the device and be reflected from the Bragg stack. Therefore the greater the number of saturable elements grown into the device the higher the peak power of the pulse needed to satisfy this criterion. There are two possible solutions for this, either a higher average output power from the laser or a shorter pulse duration. In this case the output power is dictated by the available pump powers and the gain characteristics of the Cr^{4+}:forsterite crystal and cannot be increased

sufficiently. Therefore it was believed that the inclusion of more layers of QDs would necessitate the need for a shorter pulse duration from the laser.
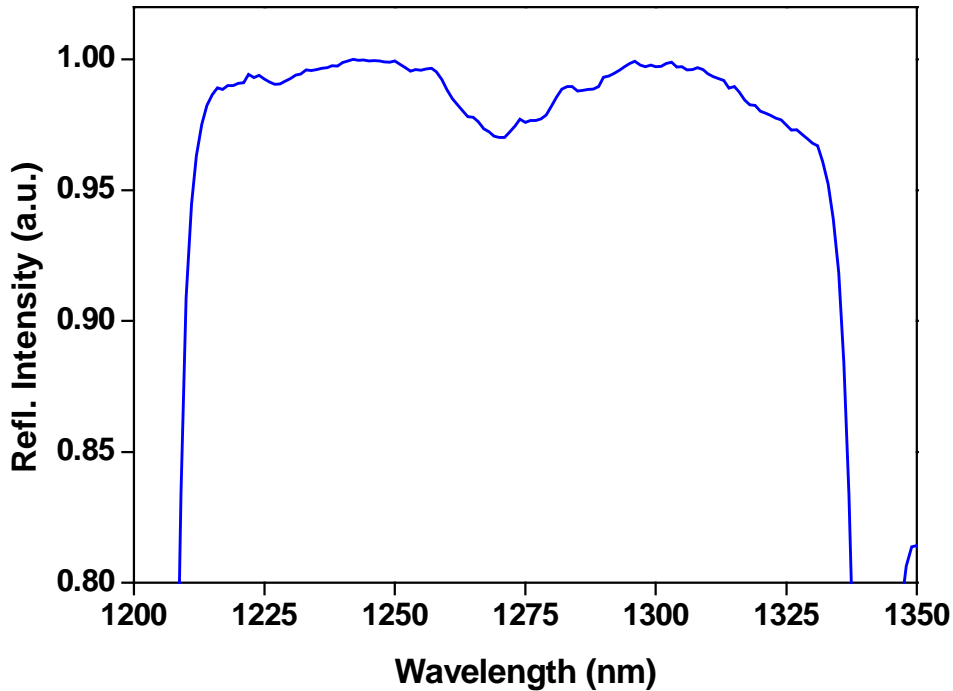

Fig. 4.14 Absorption spectrum for the 35 layer QD device at normal incidence.

As Fig. 4.14 shows, the peak of absorption for the new QD device lay at 1271nm which is much closer to the lasing wavelength of the laser at 1278nm than that of the previous QD device. This device was placed into the short arm of the cavity in normal incidence as indicated in Fig. 4.3 and an output coupler of 0.5% was again used. With this redesigned saturable absorber, femtosecond pulses were produced directly from the laser for an orientation of 0°. The shortest measured pulse durations were 160fs as shown in Fig. 4.15. Combining this with the spectral trace of the mode locked laser which has a FWHM of 11nm (shown in Fig. 4.15 (b)) near-transform-limited pulses with a time-bandwidth product of 0.33 were deduced. The output power of the laser while mode locked under these conditions was 66mW for a

pulse repetition rate of 180MHz. Interestingly, these results were comparable to the shortest pulses generated with the original QD absorber when it was oriented at 45°.
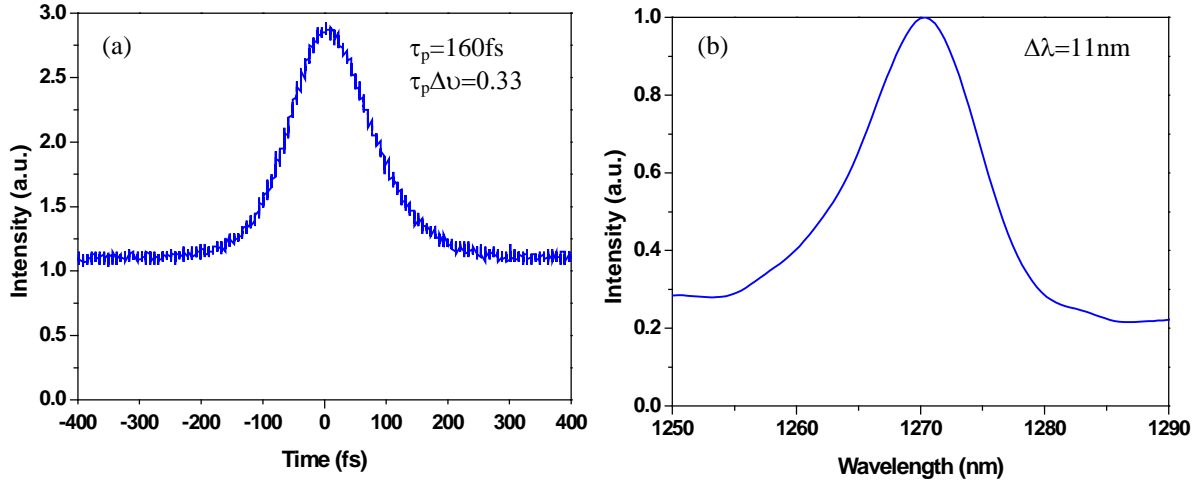

Fig. 4.15 (a) Measured Intensity autocorrelation (b) spectral trace of the pulses from the Cr^{4+}:forsterite laser with the new QD saturable absorber at normal incidence.

Due to the presence of the addition layers of QDs in the redesigned device it was hoped that shorter pulses durations would be achieved. Shorter pulse durations are indeed possible in this cavity configuration, as was demonstrated in Chapter 3. Further investigations with these devices should and will be continued in an effort to further understand and improve their performance. These are the first results in which a QD based saturable absorber has mode locked a solid-state laser into the femtosecond regime, therefore more research is necessary to discover how to fully optimise these devices.

The mode-locking threshold of the laser with this sample in place was self-starting at an output power level of 7mW from the laser. This allowed an estimation of the saturation fluence upon the device to be calculated to be $280\mu J/cm^2$. This value is ~3 times smaller than the saturation fluence calculated in the previous chapter for the GaInNAs saturable Bragg reflector ($980\mu J/cm^2$), highlighting one of the potential

advantages of quantum-doted based devices over their quantum well counterparts [12]. The recovery time of these devices was not measured, but similar devices grown at the Ioffe Institute displayed recovery times between 1-50ps. It is therefore believed that the recovery time of these experimental devices was less than 50ps, which is shorter than the 69ps measured for the GaInNAs device.

The tuning range of the sample was also investigated by placing an intracavity slit between the second intracavity prism and the output coupler. By translating this slit across the intracavity beam, a tuning range of 10nm (from 1269nm to 1279nm) was measured, as shown in Fig. 4.16. It should be noted that this tuning range matches well with the position of the absorption peak of the QD absorber (see Fig. 4.14). The corresponding mode locked output powers across this range are shown in Fig. 4.17.
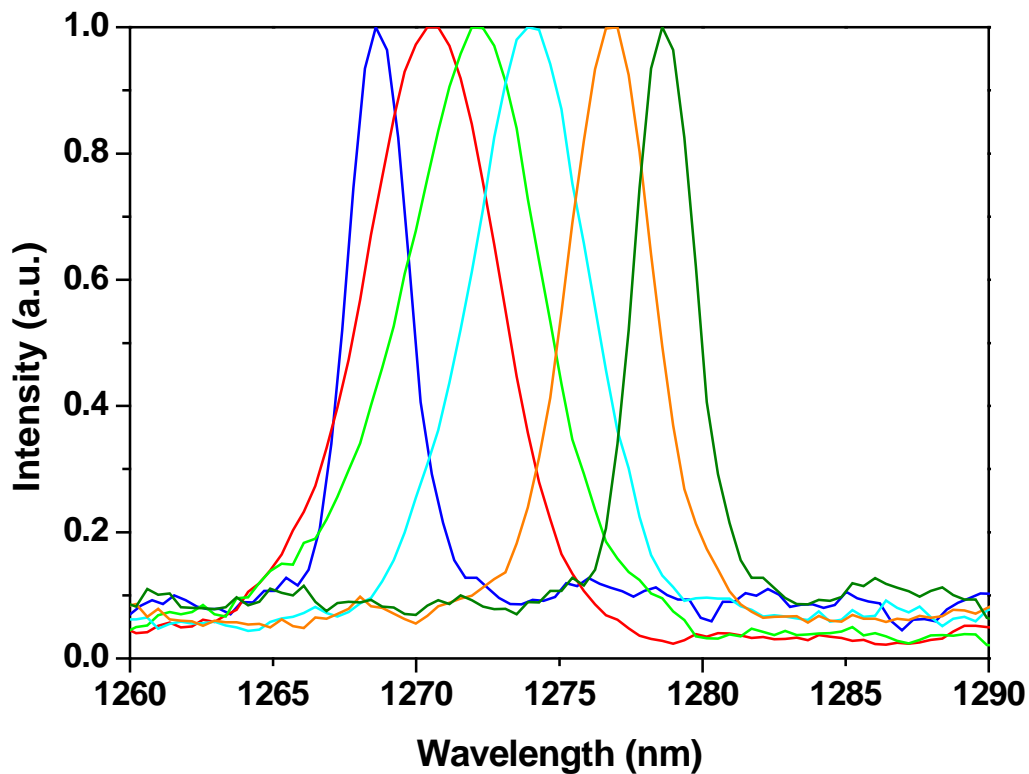

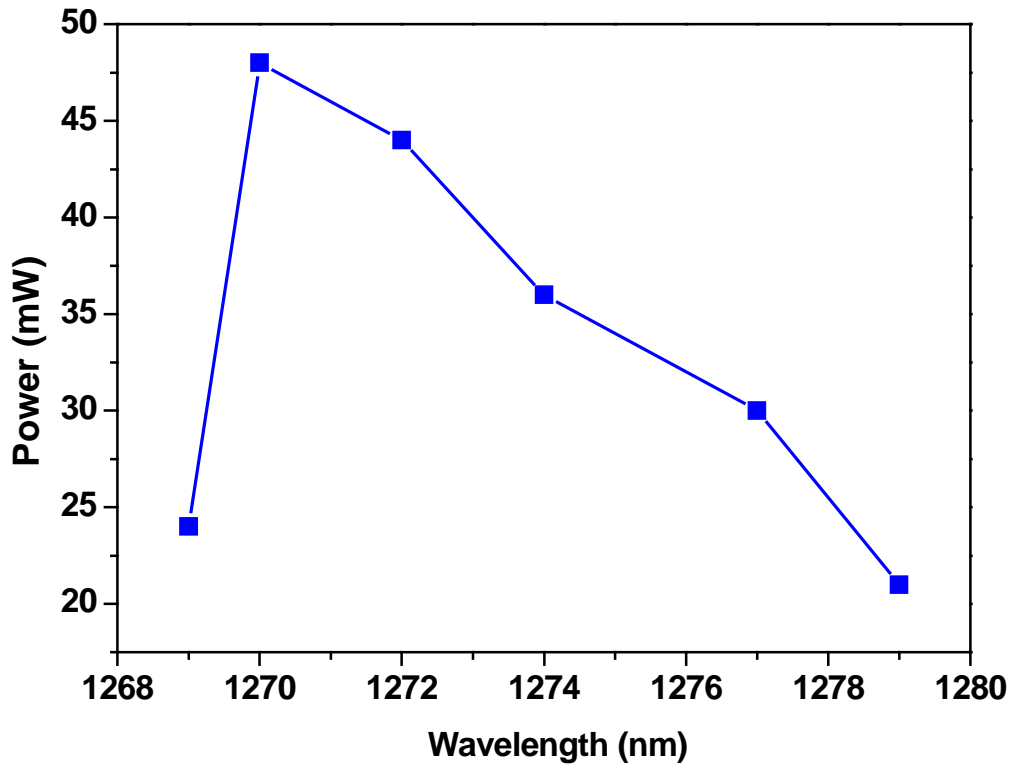Fig. 4.16 The tuning range of the QD sample with an intracavity slit.

Fig. 4.17 The output power from the laser across the tuning range of the QD saturable absorber.

4.5 Conclusions

The work described in this chapter has shown for the first time that quantum-dot based saturable absorbers can be used to mode lock solid-state lasers into the femtosecond regime. This provides a further practical route into this highly desirable ultrashort pulse region.

This was demonstrated with a broadband Cr^{4+}:forsterite laser. Initially a QD device with 20 layers of QDs was incorporated inside the laser cavity at an angle to achieve femtosecond mode locking. Changing the angle at which the QD absorber element was placed gave access to a range of pulse durations, from picosecond when at normal incidence to 158fs when at 45°. In this latter case, a mode locked output power of 65mW was attained. This observation opened up the possibility of redesigning the QD based saturable absorber device to have an absorption peak that was better matched to the lasing wavelength of the laser.

Whether this is a product of a Fabry etalon effect inside the quantum-dot structure or possibly a manifestation of strong coupling remains to be investigated and promises to provide some interesting results from these devices in the future.

Easy access to a range of pulse durations is desirable for applications such as imaging, where shorter pulse durations broaden the bandwidth, creating a greater resolution. Therefore, with a tunable pulse duration, the resolution of the image could be selected. In addition, the shorter the pulse duration the greater the peak power of the pulse and therefore nonlinear effects in materials could be controlled. A quantum-dot saturable absorber has shown the potential to provide access to such a range of pulse durations.

The lower saturation fluence for quantum-dot saturable absorbers in comparison to the GaInNAs saturable Bragg reflector is a significant advantage for

the QD devices. Also, the enhanced spectral bandwidth due to the size distribution of the quantum dots together with the fast recovery time of these devices mean that QD based saturable absorbers have the potential to compete against the more commonly used quantum-well devices. I believe that the research presented in this chapter represents the first step for quantum-dot devices mode-locking solid-state lasers. The benefits of quantum-dot devices highlighted above will ensure that they are here to stay, and with appropriate research and development, have the capabilities to compete against and in some aspects to outperform quantum-well devices.

4.6 References

1. Ustinov, V.M., A.E. Zhukov, A.Y. Egorov, and N.A. Maleev, "*Quantum dot lasers*", in *Series on Semiconductor Science and Technology*, O.S. publications, Editor. 2003.

2. Guerreiro, P.T., S. Ten, E. Slobodchikov, Y.M. Kim, J.C. Woo, and N. Peyghambarian, "*Self-starting mode-locked Cr:forsterite laser with semiconductor saturable Bragg reflector*", Optics Communications, 1997. **136**: p. 27-30.

3. Zhang, Z., T. K., T. Itatani, K. Kobayashi, T. Sugaya, T. Nakagawa, and H. Takahashi, "*Broadband semiconductor saturable-absorber mirror for a self-starting mode-locked Cr:forsterite laser*", Optics Letters, 1998. **23**(18): p. 1465-1467.

4. Zhang, Z., K. Torizuka, T. Itatani, K. Kobayashi, T. Sugaya, and T. Nakagawa, "*Self-starting mode-locked femtosecond forsterite laser with a semiconductor saturable-absorber mirror*", Optics Letters, 1997. **22**(13): p. 1006-1008.

5. McWilliam, A., A.A. Lagatsky, C.G. Lebum, P. Fischer, C.T.A. Brown, G.J. Valentine, A.J. Kemp, S. Calvez, D. Burns, M.D. Dawson, M. Pessa, and W. Sibbett, "*Low-loss GaInNAs saturable Bragg reflector for mode-locking of a femtosecond Cr4+: Forsterite-laser*", IEEE Photonics Technology Letters, 2005. **17**(11): p. 2292-2294.

6. Rafailov, E.U., S.J. White, A.A. Lagatsky, A. Miller, W. Sibbett, D.A. Livshits, A.E. Zhukov, and V.M. Ustinov, "*Fast quantum-dot saturable absorber for passive mode-locking of solid-state lasers*", IEEE Photonics Technology Letters, 2004. **16**(11): p. 2439-2441.

7. Lagatsky, A.A., E.U. Rafailov, W. Sibbett, D.A. Livshits, A.E. Zhukov, and V.M. Ustinov, "*Quantum-dot-based saturable absorber with p-n junction for mode-locking of solid-state lasers*", Ieee Photonics Technology Letters, 2005. **17**(2): p. 294-296.

8. Herda, R., O.G. Okhotnikov, E.U. Rafailov, W. Sibbett, P. Crittenden, and A. Starodumov, "*Semiconductor quantum-dot saturable absorber mode-locked fiber laser*", Ieee Photonics Technology Letters, 2006. **18**(1-4): p. 157-159.

9. Su, K.W., H.C. Lai, A. Li, Y.F. Chen, and K.E. Huang, "*InAs/GaAs quantum-dot saturable absorber for a diode-pumped passively mode-locked Nd : YVO4 laser at 1342 nm*", Optics Letters, 2005. **30**(12): p. 1482-1484.

10. Rafailov, E.U., M.A. Cataluna, W. Sibbett, N.D. Il'inskaya, Y.M. Zadiranov, A.E. Zhukov, V.M. Ustinov, D.A. Livshits, A.R. Kovsh, and N.N. Ledentsov, "*High-power picosecond and femtosecond pulse generation from a two-section mode-locked quantum-dot laser*", Applied Physics Letters, 2005. **87**(8).

11.   McWilliam, A., A.A. Lagatsky, B. C.T.A., W. Sibbett, A.E. Zhukov, V.M. Ustinov, A.P. Vasil'ev, and E.U. Rafailov, "*Quantum-dot-based saturable absorber for femtosecond mode-locked operation of a solid-state laser*", Optics Letters, 2006. **31**(10): p. 1444-1446.

12.   Unold, H.J., D. Lorenser, D.J.H.C. Mass, A. Rudin, R. Bellancourt, U. Keller, E. Gini, and D. Ebling. "*50-GHz mode-locked VESCELs:an integrable alternative to high-repetition-rate solid-state lasers*". in *Advanced Solid-State Photonics*. 2006. Lake Tahhoe, California.

Chapter 5 – Some applications in biophotonics

5.1 Introduction

Given that there is a relatively low absorption in biological tissue in the 1300nm spectral region, the output characteristics of the Cr^{4+}:forsterite laser, described in the previous chapters, are quite well suited to applications in biophotonics. Two such applications will be described in this chapter. By way of preliminary work, a comparison of the propagation of light through biological tissue in four laser wavelength regions (including ~1300nm) was undertaken to show that the penetration depth was the greatest around 1300nm. Several tissue samples, including poultry and mammalian, were tested with both Gaussian and Bessel beam geometries. These results were then compared with the results from a 3-D Monte Carlo simulation that modelled the path of light through such turbid media. It follows that using 1300nm laser light in photodynamic therapy it is possible to access deeper tissue without the need for invasive techniques. Also, because of the low dispersion in optical fibres around 1300nm, femtosecond pulses at this wavelength can be sent down optical fibres without significant temporal broadening. Thus ultrashort pulses could be delivered to the inside of the body through an optical fibre and with the available peak powers from femtosecond lasers this would allow two-photon processes to be exploited.

Within this chapter a two-photon technique is described as an exemplar application where the laser was used for an assessment of the two-photon cutting of chromosomes. This work illustrated the suitability of the Cr^{4+}:forsterite laser to provide features of low single-photon absorption and negligible group velocity dispersion that would not readily be made available by alternative light sources, while

successfully exploiting a two-photon cutting procedure. These initial demonstrations with this laser source represent just a few examples of many possible applications of a femtosecond Cr^{4+}:forsterite laser .

5.2 Deep tissue penetration

Deep penetration of radiation into biological tissue is important for a number of applications in biophotonics such as optical biopsy [1] and photodynamic therapy [2]. To maximise the penetration depth, the correct choice of wavelength range has to made with due consideration of the absorption characteristics of the main constituents in the tissue involved. In Fig. 5.1 the absorption is shown for water, melanin and oxygenated haemoglobin (HbO_2). It can be seen that a minimum in absorption for all three of these components lies around 1300nm. Thus, the greatest penetration depth coincided with the spectral region over which the Cr^{4+}:forsterite laser operates.
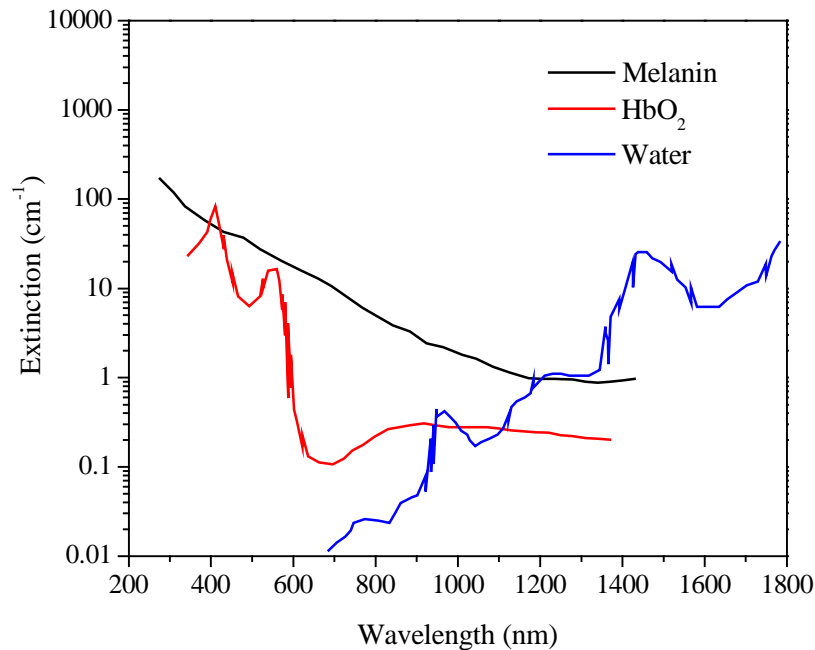

Fig. 5.1 Absorption features of biological tissue constituents as a function of wavelength.

5.2.1 Experimental set-up

To make a quantitative comparison of penetration depths, four distinctive spectral regions were chosen for the optical sources. The lasers used were all available in the St. Andrews laboratory. These were (i) a frequency-doubled Nd:YVO$_4$ laser at 532nm, (ii) a Ti:sapphire laser at 800nm, (iii) a Nd:YVO$_4$ laser operating at 1064nm and (iv) a Cr^{4+}:forsterite laser with an output tuned to 1278nm. All were operated in a continuous wave regime. For each of these wavelength bands the transmission through tissue was assessed for both Gaussian and Bessel beams. The set-up for the assessments is as shown in Fig. 5.2. The decision to deploy a Bessel beam geometry in this work was taken because previously observed self-reconstructing properties offered the possibility of enhancing the depth of focus through an extended central maximum [3, 4].
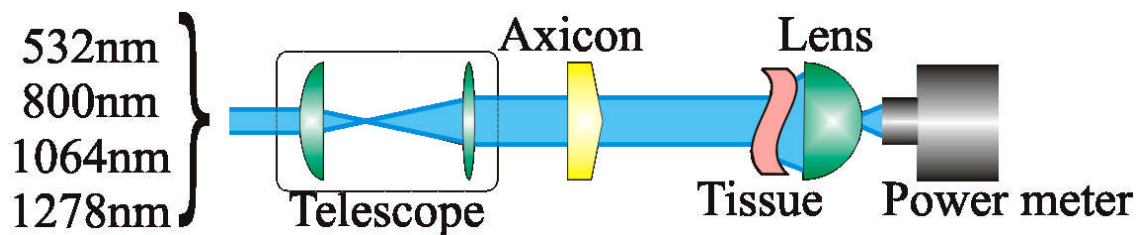
Fig. 5.2 The experimental set-up for the deep tissue penetration assessments.

A telescope system was used to produce similarly sized Gaussian and Bessel beams for each source used. These beam geometries were then incident upon the sample of tissue, the thickness of which was easily varied by the addition of further thinly sliced strips. The radiation propagating through the tissue was strongly scattered and so a short focal length (25mm) lens was used to collect this light and focus it into the power meter for measurement.

An axicon (or conical lens) was used to create the Bessel beam that can be regarded simply as an interference pattern due to a conical wavefront. There exist solutions to the Helmholtz wave equations that describe beams that do not diffract as they propagate. One such solution is a Bessel beam that can be represented mathematically as a Bessel function, J_o [5]. In reality, such beams cannot be generated as they would require infinite energy, but approximations do exist that do not diffract over modest propagation distances (typically a few mm). These are sometimes referred to as pseudo-Bessel beams. These Bessel beams consist of a central maximum spot surrounded by concentric rings. A representative picture of such a beam with its associated characteristic intensity profile is included as Fig. 5.3.
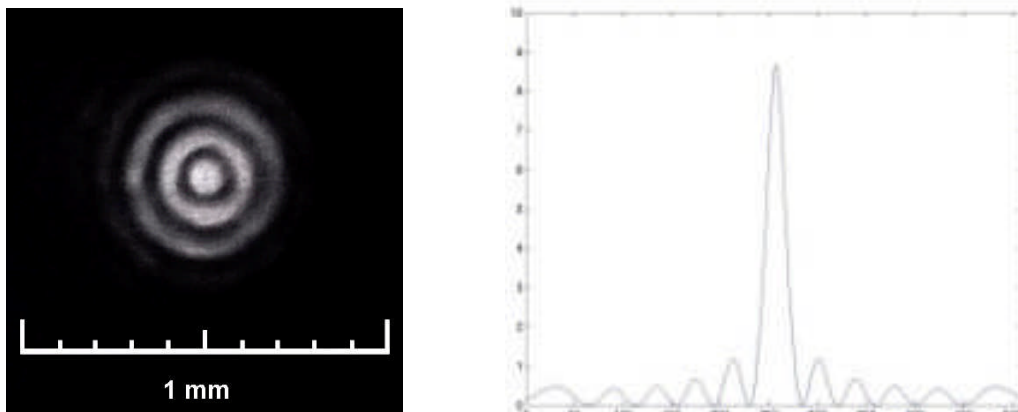
Fig. 5.3. A Bessel beam with its associated intensity profile.

As mentioned above, an attractive feature of the Bessel beam is its self-reconstructing nature. This property is not present with a Gaussian beam, and within the context of this part of my work it was felt that it might allow penetration through greater thicknesses of tissue. A Bessel beam can be thought of as light waves arranged in a cone. Thus the bright central spot seen in Fig. 5.3 that lies along the axis of the cone is created from light that arrives from the cone at an angle. Any small obstruction in the path of the beam would be expected to destroy the beam

geometry at that particular point along the propagation direction. By travelling further along the path of the beam, the light that makes up the beam pattern (Fig. 5.3) will have arisen from outside the obstruction and as such the beam geometry will be restored. The beam has thus reformed or self-healed after passing such an obstruction [6,7]. Significantly, this self-healing is a distinctive and exploitable characteristic of Bessel light beams.

5.2.2 Poultry flesh

To make a valid comparison between the propagation features of Gaussian and Bessel light beams, the telescope system of Fig. 5.2 was used to control the extent of the beam profiles. The Gaussian beam size was adjusted to match that of the central bright region of the Bessel beam. The axial region of the Bessel beam was chosen rather than the entire ring structure because the peak power of the central spot is much greater than that of the surrounding rings (Fig. 5.3). Therefore, to reach a similar intensity with the Gaussian beam, a spot size similar to that of the central ring had to be created. Optical filters were used to reduce the incident power on the tissue to the same level for both beam geometries to validate this comparison. In Table 5.1 the details of the beam size of the Gaussian and the central spot size of the Bessel beam are presented together with the power levels used. Finally, the choice of tissue had to be made carefully. Initial assessments were carried out on bacon that had been purchased from the local supermarket. However, due to the process of reforming, (where the product is has been chopped, processed and formed to take a certain appearance sometimes with the addition of other non-biological ingredients), any results that were returned proved to be invalid. Related experimentation involving

chicken slices also proved inconclusive and confirmed the necessity to use fresh, uncooked, and unprocessed meat.

Chicken breast was chosen for a subsequent set of evaluations. The chicken breast was carved into thin slices (3-4mm) to allow for a variation in thickness by layering multiple slices. Assessments were then undertaken with the four laser sources, the results of which are displayed in Fig. 5.4.

λ	532nm		800nm		1064nm		1278nm	
Type	**Gaussian**	**Bessel**	**Gaussian**	**Bessel**	**Gaussian**	**Bessel**	**Gaussian**	**Bessel**
Waist (mm)	1.2	1.2	1	1	1.4	1.4	1.1	1.1
Power (mW)	15.9	16.1	16.2	16	15.7	15.8	15.7	15.4

Table 5.1. Comparison of the beam sizes and powers for the four source wavelengths.
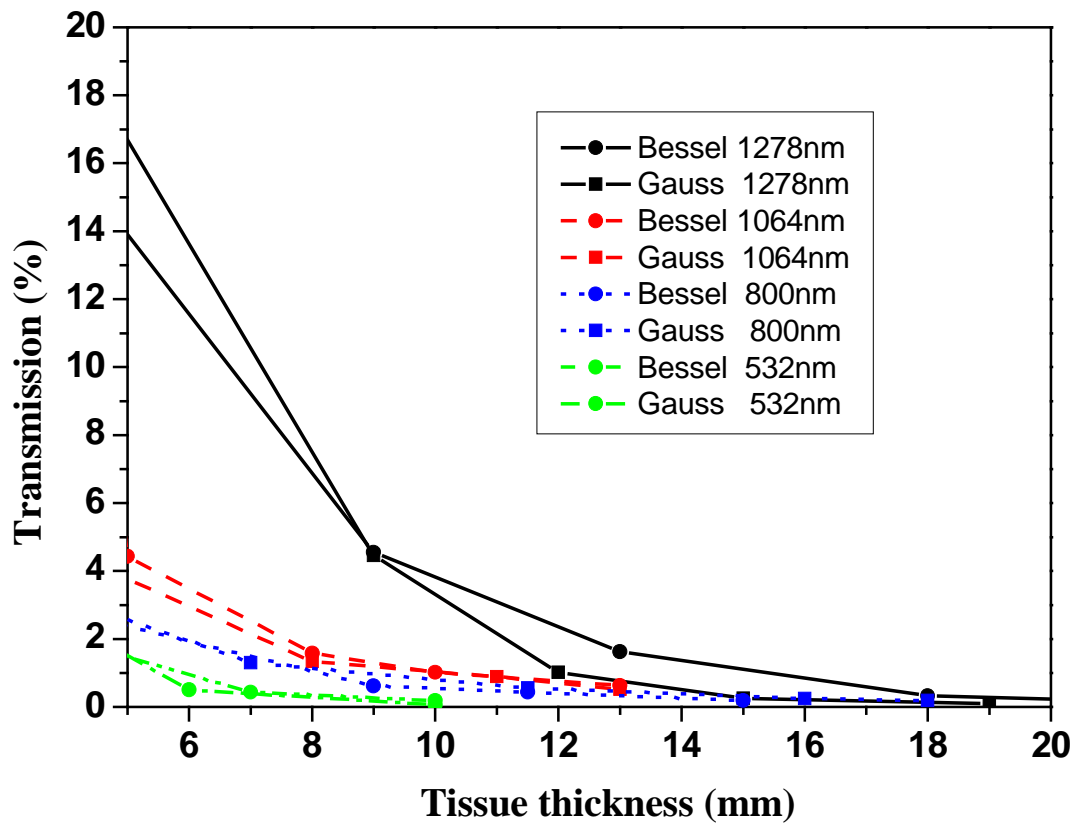

Fig. 5.4 Transmission of the four spectral bands through a range of tissue thicknesses.

105

It can be seen that the data reproduced in figure 5.4 indicate that the output beam at 1278nm from the Cr^{4+}:forsterite laser penetrates best through the tissue sample. This was the expected result and, significantly, radiation was still detectable after 15mm of tissue and the transmission at this wavelength region was approximately 2-3 times higher than that measured with the other sources. Fig. 5.4 also shows that there is no discernible difference between propagation depths for the Gaussian and Bessel beams. These experiments thus showed that there was no added benefit of using a Bessel beam over a Gaussian beam with respect to the total amount of power transmitted through biological tissue. Fig. 5.5 illustrates the experimental set-up with the 532nm (green) source.
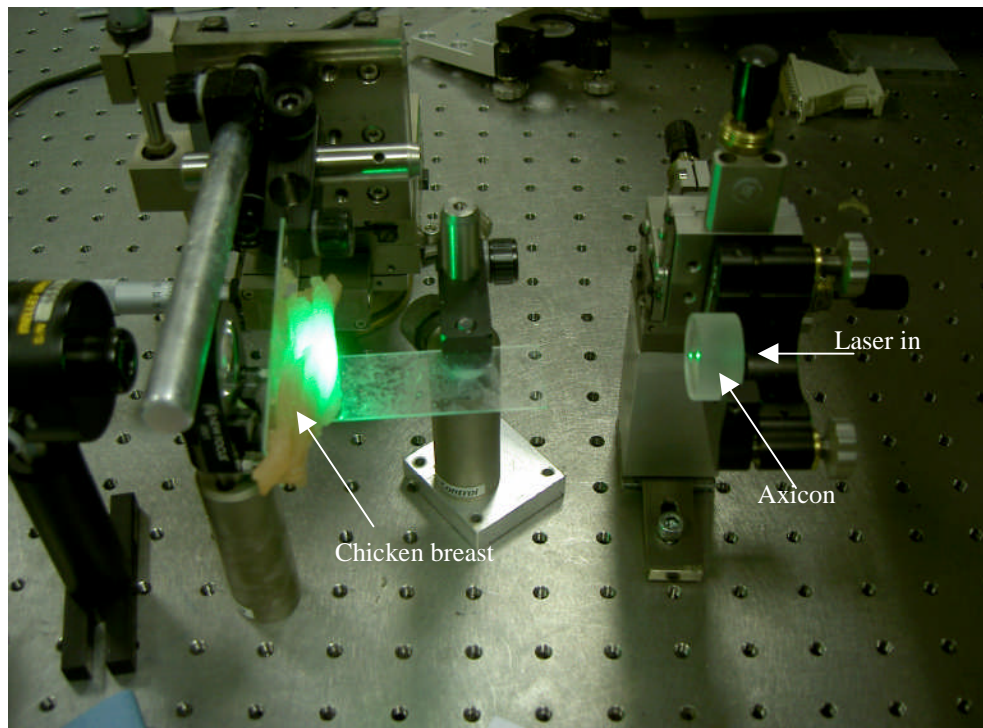

Fig. 5.5 The experimental set-up with the 532nm laser source. The axicon (seen on the right) produced the Bessel beam incident on the chicken breast, which was then collected by the lens and focused into the power meter.

Additionally, a brief experiment was undertaken with the Cr^{4+}:forsterite laser when mode locked. This ultrashort-pulse regime was achieved through the use of a GaInNAs saturable Bragg reflector [8] as described in Chapter 3. The output power from the laser while mode locked was 44mW. The associated spectrum of the mode locked laser output was monitored before and after the beam propagated through a 4mm slice of chicken breast and the data are reproduced in figure 5.6. Without any tissue in place, 136fs pulses were measured (Fig. 5.6, blue trace). These had a spectral width of 12nm centred on 1278.5nm. This corresponded to transform-limited pulses having a time-bandwidth product of 0.32. The pulse was then passed through 4mm of chicken breast tissue and the spectrum was measured again (Fig. 5.6, red trace). Unfortunately the scattered radiation could not be sufficiently collimated for an autocorrelation to be taken so the pulse duration could not be measured.
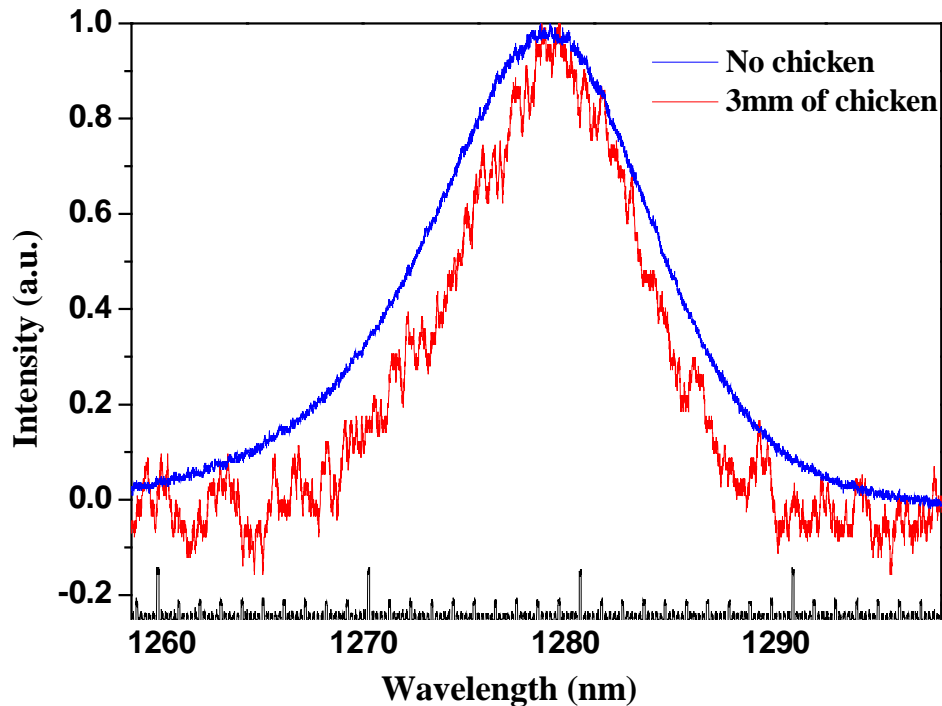

Fig. 5.6 The mode locked traces before and after a 4mm slice of chicken breast.

However, by comparing the FWHM of both spectral traces, an estimate of how much the pulse had been affected by propagation through the tissue could be deduced. The FWHM has decreased from 12nm before the tissue, to 8nm after 4mm of tissue. This implies that the pulse duration has increased (see Chapter 1). Assuming the pulses were to stay transform limited, this would correspond to a pulse of 220fs, but this assumption cannot be made on the basis of the data presented here. What this does show is that a femtosecond pulse could be delivered through a significant tissue thickness and that there is the potential to possibly exploit two-photon processes within tissue.

5.2.3 Modelling

The propagation of the radiation through chicken breast was modelled using a 3-D Monte Carlo radiation transfer code [9-11] that treats accurately the multiple, anisotropic scattering of light through a medium. This modelling was undertaken using a similar programme to that used to model the passage of starlight through interstellar dust clouds [12]. Fig. 5.7 below shows the experimentally measured scattered radiation from the chicken breast tissue (a) compared to the modelled radiation. Two modelled pictures are shown: (b) applies to a smooth model where a uniform density is assumed for the chicken breast, and (c) a clumpy model where a fractal structure is assumed. To capture this photographic result, a camera sensitive to 1300nm radiation was substituted for the power meter in the experimental set-up detailed in Fig. 5.2.
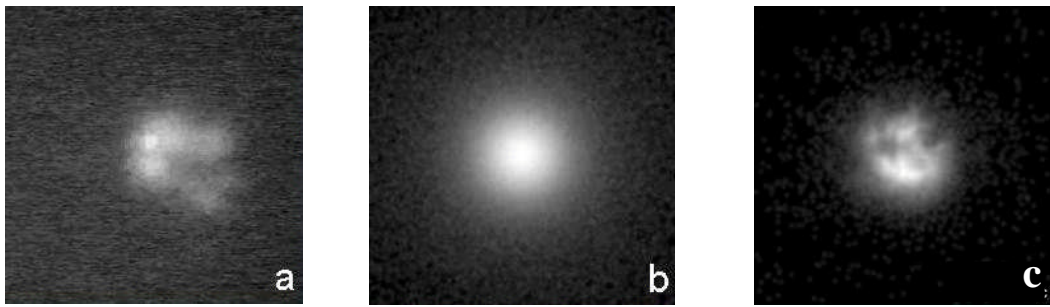
Fig. 5.7 The measured scattered radiation taken (a) experimentally, and modelled using either (b) a uniform density for the chicken breast or (c) a clumpy density.

It was hoped that by modelling the total intensity received and its scattered light pattern, the scattering properties of chicken breast (or general tissue) could be determined for these test wavelength regions. By comparing the experimental result (Fig. 5.7(a)) with the fractal model (Fig. 5.7(c)) it can be seen that the transmission patterns match fairly well. Further work on the modelling is underway to improve this match. Additional efforts to model the light transmitted from the tissue at an angle from the normal and reflected from the front of the tissue, as well as the light passing directly along the beam path, have also begun.

5.2.4 Mammalian tissues

Some propagation studies were also carried out with mammalian tissues: rat brain and pork. The rat brain samples were mounted between two cover-slides that compressed the tissue, forming 1mm thick slices. Again, transmission assessments were performed with both Gaussian and Bessel beam geometries. In this case, the light sources were the Cr^{4+}:forsterite laser at 1278nm, a He-Ne laser at 632.8nm and the frequency-doubled $Nd:YVO_4$ laser at 532nm. As before, the Gaussian beams were altered to be the same size as the Bessel beam central spot for comparison purposes

(~1.2mm in diameter) and the transmission through 1mm of rat brain was calculated

(Fig. 5.8). In agreement with the earlier observations, this graph shows the superior

penetration characteristics of the Cr^{4+}:forsterite laser radiation over the other test

sources. Again, these data did not imply any appreciable difference between the

transmission of beams that had been configured to have Gaussian or Bessel profiles.

Transmission through Rat Brain
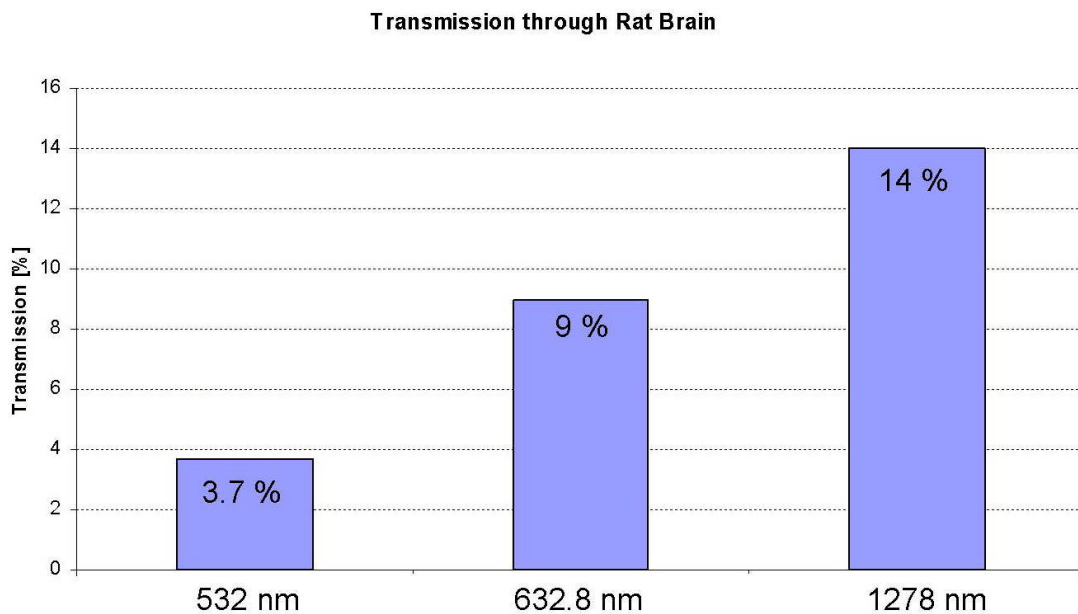
Fig. 5.8 Transmission through 1mm of rat brain tissue for three different wavelengths.

Additional experiments were undertaken with pork tissue, because it is

understood that pork tissue closely resembles human tissue. This work was done

primarily to provide images for comparison with the modelling. Thus different laser

sources were not compared for this tissue. The propagation of the Cr^{4+}:forsterite laser

through the pork tissue was measured for both Gaussian and Bessel beam geometries.

Through a 3mm slice of pork, the Gaussian geometry transmitted 30.4% of the

incident power, while the Bessel beam counterpart had a transmission of 30.7%. With

a 6mm thickness of pork the transmissions were 14.7% and 15.9% respectively. Once again this confirms the previous results, showing Gaussian and Bessel beams propagate with essentially the same transmissivity through tissue.

Fig. 5.9 (a), (b) illustrate the sample preparation of the rat brain and Fig. 5.9 (c) illustrates the experimental set-up with the 532nm source, where the collecting lens and power meter are located behind the sample.

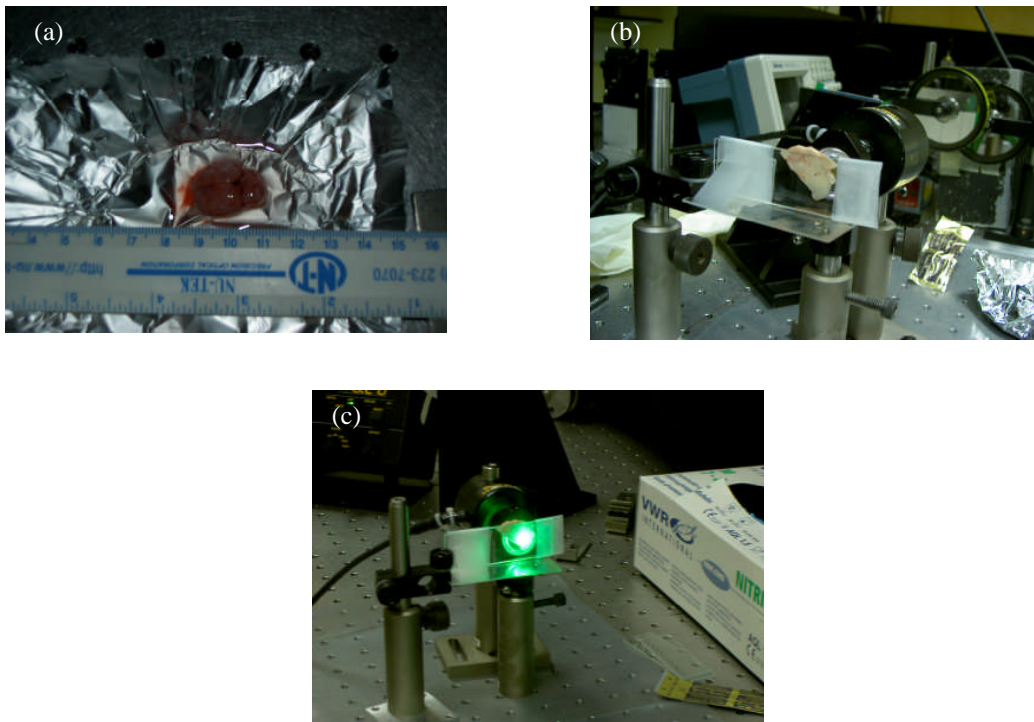Fig. 5.9 (a) and (b) the sample preparation of the rat brain, and (c) the experimental set-up undertaken with the 532nm source.

5.2.5 Conclusions

In this section some assessments of light penetration into tissue have been described. The transmission of 1300nm radiation through tissue has been shown to be ~3-4 times greater than at 532nm, 800nm and 1064nm. Gaussian and Bessel beams geometries were investigated to determine whether the Bessel beams had any advantageous qualities in respect of penetration depth but none were found. A preliminary experiment on the propagation of femtosecond pulses was also undertaken where the pulse bandwidth was found to increase, but the retention of significant pulse peak intensity implies that nonlinear processes could still be exploitable within tissue.

This represents some initial work to show the potential of the Cr^{4+}:forsterite laser for biophotonics applications. The ability to propagate further through tissue opens the possibility of photodynamic therapies at significant depths through skin [13]. With the additional uses of a femtosecond pulse, which were shown in this chapter to be deliverable through a depth of tissue, two-photon techniques afford further possibilities.

Future work to be undertaken to push towards these goals will include repeating these experiments with other wavelengths to confirm the benefit of using optical radiation in the 1300nm spectral region. Also, measurements of the pulse duration after propagation in tissue could be accomplished by collecting light into an optical fibre and delivering it to an autocorrelator. Using the femtosecond pulses, two-photon effects could be shown after passage through a thickness of tissue.

Further work on modelling the passage of light as it travels through the tissue is needed. In conjunction with this work more accurate methods of capturing the experimental image of the light as it leaves the tissue are required. Once the model

works satisfactorily, the passage of various beam geometries through tissue could be modelled for the greatest penetration depth, or the most accurate delivery to a specific area of tissue. This can then be experimentally verified with the incident beam being suitably adapted to provide a chosen "designer" beam geometry.

5.3 Two-photon chromosome cutting

As was shown in the previous section, the interaction of light with biological material is highly wavelength dependent [13]. This also applies to intracellular bodies such as organelles or as is the case here, chromosomes. To precisely target such bodies ultrashort pulses can be exploited by utilising a two-photon interaction. This allows the delivery of a dose of optical radiation to a precise 3-D localisation within tissue. Minimising the absorption outside this area requires that the single-photon absorption is kept as low as possible. This gives good reason to choose a Cr^{4+}:forsterite laser operating at 1278nm because the single-photon absorption in tissue is low in this spectral region (Section 5.2). In general, multi-photon interactions at longer wavelengths require more incident photons for ionisation, therefore the absorption cross-section is lower than that for shorter wavelengths and the localisation of the two-photon process is increased [14, 15].

Additionally, to deliver the light to a particular area of tissue it is often necessary to make use of a complex optical system. Also, in delivering an ultrashort pulse through these optics, consideration has to be given to the additional wavelength dependence from the dispersion in these components [16]. This provides the second reason for using a Cr^{4+}:forsterite laser where a low dispersion window for fused silica exists around 1300nm.

Laser cutting of chromosomes was first demonstrated in 1993 using a frequency-doubled $Nd:YVO_4$ laser that produced nanosecond pulses at a pulse repetition frequency of 10Hz [17, 18]. Two-photon cutting of chromosomes was then demonstrated in 2001 using 170fs pulses from a Ti:sapphire laser operating at 800nm. This had a pulse repetition frequency of 80MHz and the average powers employed ranged from 15mW to 100mW [19].

In this section, the two-photon ablation of Muntjac deer chromosomes using femtosecond pulses from a Cr^{4+}:forsterite laser is described. Initially an investigation into the how these pulses broaden during the passage through the relay optics was undertaken and compared against the more readily available pulses from a mode-locked Ti:sapphire laser at similar durations.

5.3.1 Delivery of the femtosecond pulses

An investigation of the pulse broadening effect of a femtosecond pulse passing through the delivery optics used to target the chromosome sample was undertaken. Most of the optical elements that the pulse had to pass through were housed inside the microscope objective used to focus on to the sample. Therefore, by examining the broadening effect resulting from pulse propagation through a microscope objective, it was possible to obtain a reliable estimation of the pulse duration that actually arrived at the sample plane. To achieve this, autocorrelations were taken before and after passage through the microscope objective. However, to provide a collimated beam to perform an autocorrelation, a second microscope objective lens with the same focal length was needed to provide a collimated beam (fig. 5.10). Therefore, the pulse durations were measured following propagation through two objectives rather than just one, and so Equations 5.1 and 5.2 were employed.
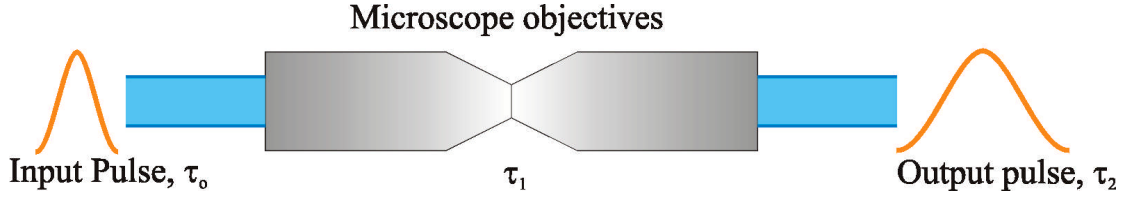
Fig. 5.10 The experimental set-up used to investigate the pulse broadening effects on femtosecond pulses passing through a microscope objective.

The initial pulse duration, τ_o, and the broadened pulse duration after two microscope objectives, τ_2, were measured directly using an autocorrelator. To calculate the pulse duration after only one objective the following formulae were used. The pulse duration after the first microscope objective, τ_1, can be described by [20],

$$\tau_1 = \tau_o \sqrt{1 + \left(\frac{4\ln(2)\phi}{\tau_o^2} \right)^2} \tag{5.1}$$

Similarly the pulse duration after the second microscope objective will be,

$$\tau_2 = \tau_1 \sqrt{1 + \left(\frac{4\ln(2)\phi}{\tau_1^2} \right)^2} \tag{5.2}$$

In these equations ϕ is the group velocity dispersion (GVD) which, because it is the same for each objective, can be treated as a constant. This allows Equations 5.1 and 5.2 to be combined and solved for τ_1 (Equation 5.3), the pulse duration at the exit of one objective, in terms of the initial and final pulse durations that can readily be measured.

$$\tau_1 = \frac{1}{8\ln 2} \sqrt{2\tau_o^2 \tau_2^2 - 6\tau_o^4 + 2\sqrt{\tau_o^4 \tau_2^4 - 2\tau_o^6 \tau_2^2 + 5\tau_o^8}} \tag{5.3}$$

The pulse broadening was measured for the Cr^{4+}:forsterite laser at 1280nm and by way of comparison, for a Ti:sapphire laser at 800nm. Both lasers were operating with an initial pulse duration, τ_o, of 100fs. The pulse durations for both these

wavelengths after X40, X60 and X100 microscope objective lenses are included as table 5.2.

Microscope Objective	Cr^{4+}:forsterite		Ti:Sapphire	
	ϕ (fs^2)	τ_1 (fs)	ϕ (fs^2)	τ_1 (fs)
X40	2193	117	8004	243
X60	2430	121	9509	282
X100	1664	110	10200	300

Table 5.2 The pulse broadening after one objective lens for a variety of microscope objectives for an incident pulse of 100fs duration.

In this experimental work, the microscope objective used was a 100X Olympus ACH with a numerical aperture of 1.25 (last entry in Table 5.2). This focused the beam at the sample plane to allow for two-photon absorption. As can be seen from Table 5.2, the pulse durations from the mode-locked Cr^{4+}:forsterite laser increased by 10% with this objective, whereas the pulses around 800nm from the Ti:sapphire laser increased by 300%. This shows clearly one immediate advantage for the deployment of light pulses around 1300nm. Furthermore, in this set-up the transmission through the microscope objective was found to depend on wavelength. With the Cr^{4+}:forsterite laser output, 71% of the incident power was transmitted, whereas the transmission was just 37% for the output of the Ti:sapphire laser. This is attributable directly to the lower attenuation of 1300nm radiation through the constituent materials of the objective lens (see Fig. 1.1).

5.3.2 Chromosome cutting

Chromosomes absorb radiation around 260nm [21], and thus to obtain absorption at half the wavelength of the Cr^{4+}:forsterite laser (~650nm), the Muntjac deer chromosomes were stained with methylene blue. This stain has a strong absorption in the region around 650nm but has 100% transmission at 1300nm, so the presence of

the stain did not increase the single-photon absorption in the sample. The relevant spectral profiles are included as Fig. 5.11 (a) and (b) respectively.
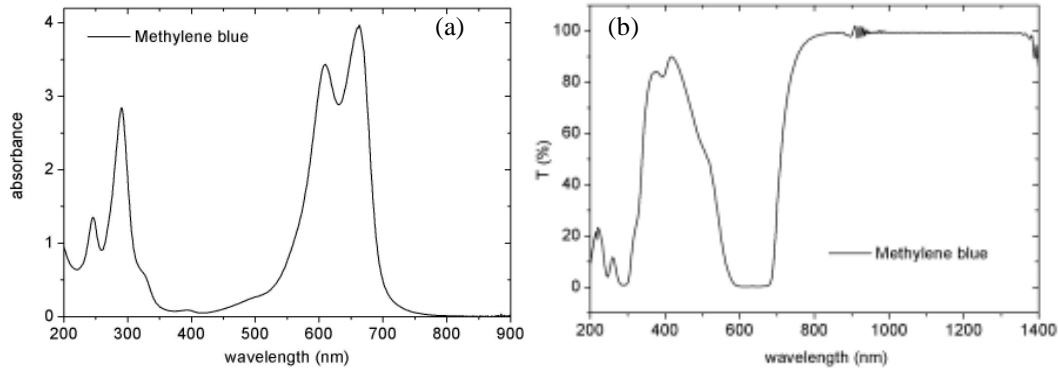

Fig. 5.11 The absorption (a) and transmission (b) curves for methylene blue. Note that the noise around 900nm was due to a change of lamp.

The absorption curve was taken with a spectrometer that included corrections for the water absorption that was used as the solvent in the dye. The transmission curve was measured with an ellipsometer.

Lyn Paterson prepared metaphase spreads of Muntjac chromosomes as follows. (Metaphase is a stage during mitosis where the pairs of chromosomes align in the middle of the cell before separating into the two daughter cells.) Muntjac cells were grown in T125 flasks (in minimal essential medium (MEM) supplemented with 10% foetal calf serum) until approximately 80% confluent (merge, run together to form a mass). Colcemid (a chemical that inhibits mitotic spindle formation halting cells at the at the metaphase stage of the cell cycle) was added to the medium at a final concentration of 0.1μg/ml and cells were left for three hours. Mitotic cells were harvested, treated with hypotonic solution (KCl:H_2O, 1:1) to make them swell and then washed in a fixative solution (methanol:acetic acid, 3:1). Twenty microlitres of metaphase cells in fixative solution were dropped onto ice-cold slides coated in ethanol and left to dry. Once dry, the slides were stained with methylene blue

solution (2g methylene blue, 0.5g NaCl, 100ml H_2O) for five minutes, then rinsed

with tap water and left to dry. The metaphase chromosomes fixed to these slides were
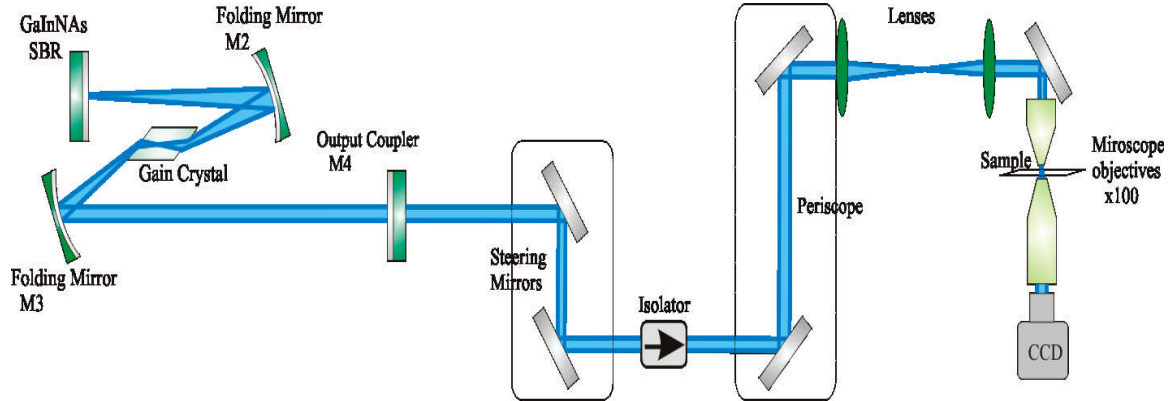
Fig. 5.12 A schematic of the experimental set-up used in the chromosome cutting experiments.

exposed to the laser in the configuration shown in Fig. 5.12.

The Cr^{4+}:forsterite laser described in Chapter 3 [8] delivered pulses of 100fs

duration, centred on 1278nm, at a pulse repetition frequency of 180MHz. The

autocorrelation and spectral traces of these pulses are displayed in Fig. 5.13.   The

typical average power of the laser in this configuration was 150mW.

Fig. 5.13 The autocorrelation trace (a) and the spectrum (b) of the mode-locked pulses used for cutting
the chromosomes.

At the sample plane these pulses had durations around 110fs at an average power of 75mW. These pulses were focused to a spot size of 1.9μm in diameter using an oil immersion X100 microscope objective. These parameters for the laser resulted in a total energy per spot of 28nJ. The peak power was 3.5kW and the peak intensity was 31GW/cm^2. The samples were held on an XYZ-stage with computer controlled 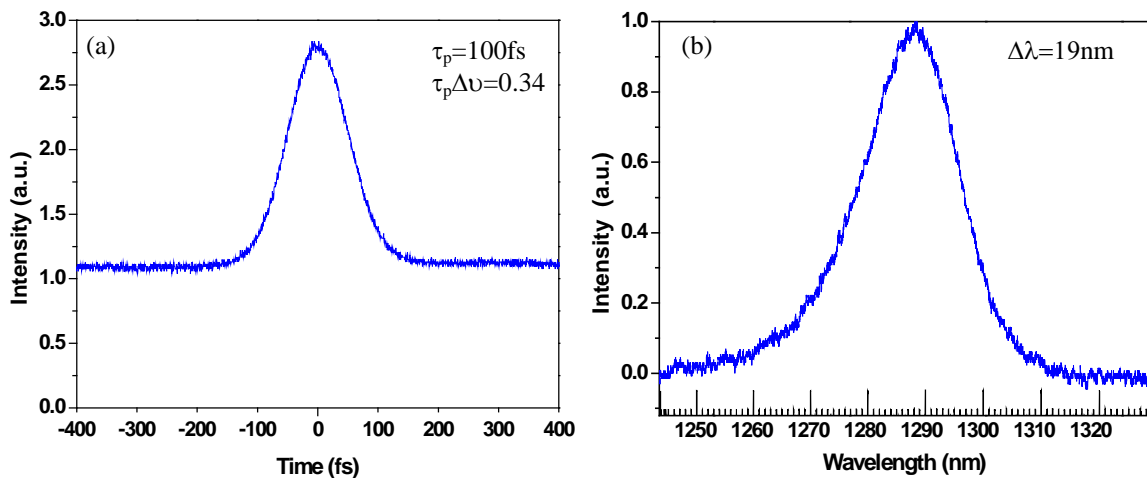actuators. The sample was scanned in the x-direction with a scan speed of 5μm/s and changes in the z-direction were made in steps of 200nm. Image capture was achieved using a long working distance X100 microscope objective with a numerical aperture of 0.7 and a working distance of 6mm. A camera with sensitivity into the 1300nm spectral region was used to record the images.

The final step before chromosome cutting could be attempted was to find the area over which the beam was effective for two-photon interactions. This was achieved using a crystal of methylene blue, the dye used to stain the chromosomes. The crystal was placed at the focus of the beam at the sample plane (Fig. 5.12). Due to the absorption in the crystal at 650nm, a two-photon process took place that produced a hole in the crystal. This was the area over which the two-photon process would occur and could be easily measured using a microscope. The profile of this hole is reproduced as Fig. 5.14 with the corresponding beam profile included for comparison.
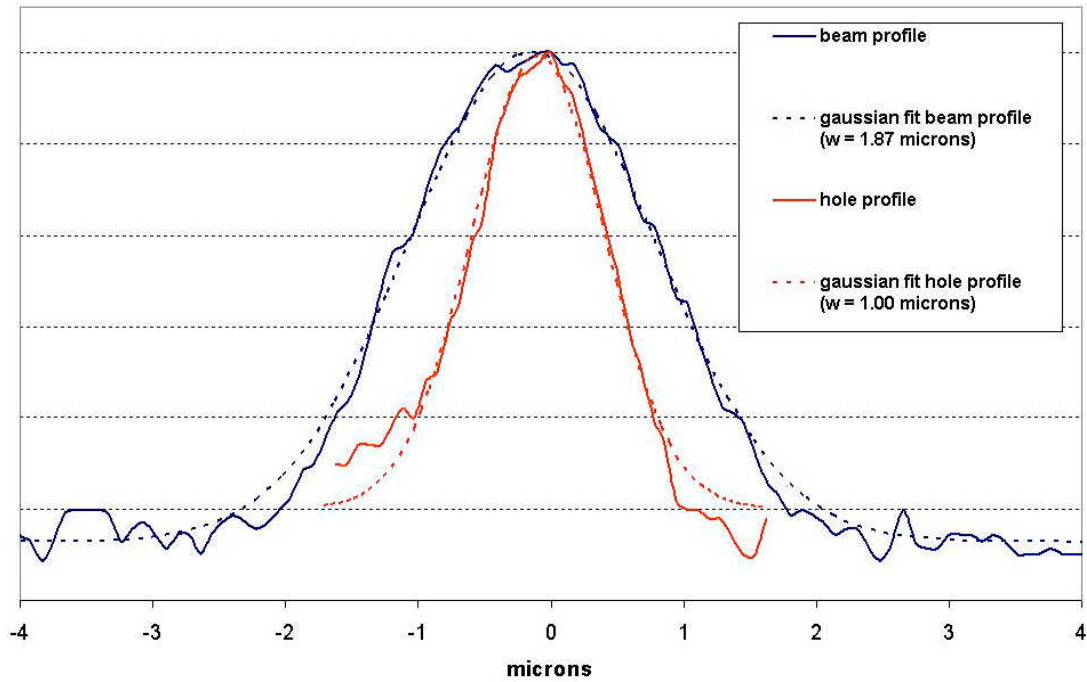
Fig. 5.14 The beam and hole profiles from the dye crystal.

The hole radius has a waist of 1μm whereas the beam radius has a waist of 1.87μm. It should be noted that no hole was produced when the laser was operating in an unmode-locked regime at the same power level. Therefore the hole formed in the crystal while the laser was mode locked could be unambiguously attributed to the two-photon process. Moreover, the interaction of the radiation with the dye crystal showed that the two-photon absorption process was sensitive to the focal position of the beam to less than 1μm. Thus the incremental steps of 200nm in the z-direction of the translation stage were appropriate.

This was the final piece of information needed to undertake the chromosome cutting experiments. The Muntjac deer chromosomes stained with methylene blue were placed into the experimental set-up (Fig. 5.12) at the sample plane and stepped through the focus in increments of 200nm to allow for the greatest likelihood of a two-photon interaction. Fig. 5.15 shows the spread of chromosomes before and after

the two-photon cutting[22], where the red arrows indicate the sites of successful two-photon cutting.
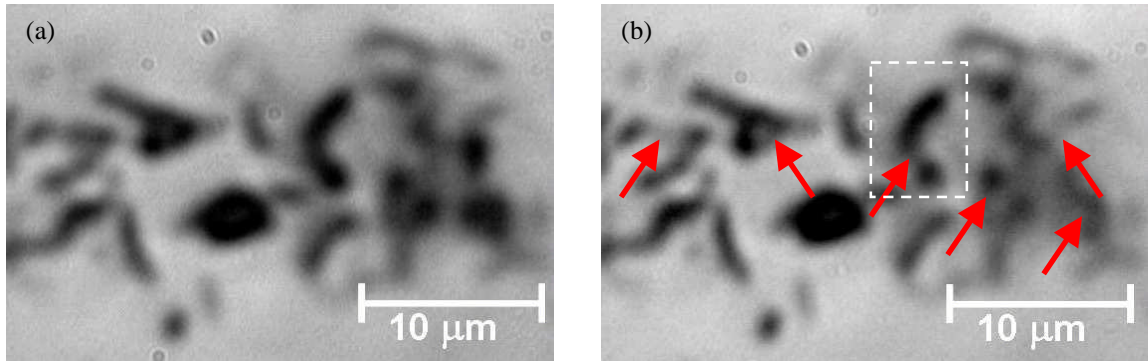
Fig. 5.15 Before (a) and after (b) two-photon cutting of the Muntjac deer chromosomes, the red arrows indicating cuts.

This shows that multiple cuts were achieved across the full spread of the chromosomes. If the chromosome in the white box is singled out and displayed as a false colour rendering from a micrograph of the chromosome, then the cut becomes all the more obvious (Fig. 5.16).
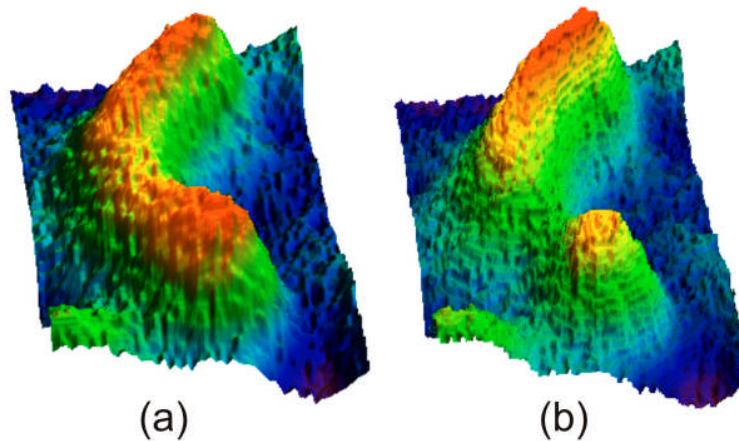
Fig. 5.16 A false colour rendering from a micrograph of a chromosome before and after two-photon cutting.

It is believed that the observations of Figs. 5.15 and 5.16 show the first example of successful two-photon cutting of chromosomes using a Cr^{4+}:forsterite laser [23].

5.3.3 Conclusions

The research undertaken in this part of the project confirms for the first time that a Cr^{4+}:forsterite femtosecond laser can be used for the two-photon cutting of chromosomes. The wavelength at which the laser operates exploits the low dispersion window for the optical components involved. This bodes well for the delivery of essentially undispersed ultrashort pulses through even the most complex of relay optics. Also, because the single-photon absorption is extremely low in biological tissue in the 1300nm spectral region, this allows the two-photon process to remain highly localised to a precise 3-D area of the tissue providing accurate cutting. This initial work thus represents a highlight for the capabilities of a femtosecond Cr^{4+}:forsterite laser when deployed in such biophotonics research. The localisation of the two-photon cutting to within 1μm of the focus of the beam is in fact much greater than was expected, with the distance expected to be much closer to the Rayleigh range (~8.6μm). This coupled with the low single-photon interaction therefore points to a much wider range of implementations of this type of laser in biology.

Future experiments with this laser aimed at a more general exploitation of 1300nm laser light in tissue interactions. By placing a thin layer of tissue, possibly a monolayer of cells or blood smeared across a glass slide, in the path of the beam it is believed that the radiation will pass through these cells without significant change to the properties of the pulse or the cells. The beam should then be able to continue to propagate and perform two-photon cutting at the sample plane. It would be particularly interesting to determine of the depth of tissue that the beam could pass through while still performing two-photon cutting. This could decide ultimately whether two-photon absorption could be exploited realistically in the treatment or diagnosis of disease. Where appropriate, implementations that involve the delivery of

light by optical fibres can take advantage of the low dispersion of these fibres in the 1300nm region.

A further extremely interesting experiment would be to attempt using two-photon absorption to cut or destroy intracellular bodies within a living cell. If a chromosome could be stained inside the cell to absorb at 650nm without harming the rest of the cell, then this chromosome could be targeted and destroyed by the Cr^{4+}:forsterite laser radiation without subjecting the surrounding material to any damage from single-photon absorption. Whether or not this cell could then continue to divide after the removal of a chromosome or with a cut chromosome would be an enlightening result.

5.4 References

1. Tai, S.P., W.J. Lee, D.B. Shieh, P.C. Wu, H.Y. Huang, C.H. Yu, and C.K. Sun, "*In vivo optical biopsy of hamster oral cavity with epi-third-harmonic-generation microscopy",* Optics Express, 2006. **14**(13): p. 6178-6187.

2. Pogue, B.W. and T. Hasan, "*Targeting in Photodynamic Therapy and Photo-imaging"*, in *Optics and Photonics News*. 2003. p. 37-43.

3. Durnin, J., "*Exact-Solutions for Nondiffracting Beams .1. The Scalar Theory",* Journal of the Optical Society of America a-Optics Image Science and Vision, 1987. **4**(4): p. 651-654.

4. Durnin, J., J.J. Miceli, and J.H. Eberly, "*Diffraction-Free Beams",* Physical Review Letters, 1987. **58**(15): p. 1499-1501.

5. Hecht, E., "*Optics"*. 3rd ed. 1998: Addison Wesley Longman Inc.

6. MacDonald, R.P., S.A. Boothroyd, T. Okamoto, J. Chrostowski, and B.A. Syrett, "*Interboard optical data distribution by Bessel beam shadowing",* Optics Communications, 1996. **122**(4-6): p. 169-177.

7. Bouchal, Z., J. Wagner, and M. Chlup, "*Self-reconstruction of a distorted nondiffracting beam",* Optics Communications, 1998. **151**(4-6): p. 207-211.

8. McWilliam, A., A.A. Lagatsky, C.G. Lebum, P. Fischer, C.T.A. Brown, G.J. Valentine, A.J. Kemp, S. Calvez, D. Burns, M.D. Dawson, M. Pessa, and W. Sibbett, "*Low-loss GaInNAs saturable Bragg reflector for mode-locking of a femtosecond Cr4+: Forsterite-laser",* IEEE Photonics Technology Letters, 2005. **17**(11): p. 2292-2294.

9. Liebert, A., H. Wabnitz, H. Obrig, R. Erdmann, M. Moller, R. Macdonald, H. Rinneberg, A. Villringer, and J. Steinbrink, "*Non-invasive detection of fluorescence from exogenous chromophores in the adult human brain"*, Neuroimage, 2006. **31**(2): p. 600-608.

10. Ma, X.Y., J.Q. Lu, H.F. Ding, and X.H. Hu, "*Bulk optical parameters of porcine skin dermis at eight wavelengths from 325 to 1557 nm",* Optics Letters, 2005. **30**(4): p. 412-414.

11. Du, Y., X.H. Hu, M. Cariveau, X. Ma, G.W. Kalmus, and J.Q. Lu, "*Optical properties of porcine skin dermis between 900 nm and 1500 nm",* Physics in Medicine and Biology, 2001. **46**(1): p. 167-181.

12. Wood, K. and J.S. Mathis, "*Monte Carlo photoionization simulations of diffuse ionized gas",* Monthly Notices of the Royal Astronomical Society, 2004. **353**(4): p. 1126-1134.

13. Fischer, P., A. McWilliam, C.T.A. Brown, K. Wood, M. MacDonald, W. Sibbett, and K. Dholakia, "*Deep Tissue Penetration of Radiation: Modelling and Experiments",* Paper CL-4-Wed, European Conference on Lasers and Electro-Optics (ECLEO), Munich, Germany, 2005.

14. Vogel, A., J. Noack, G. Huttman, and G. Paltauf, "*Mechanisms of femtosecond laser nanosurgery of cells and tissues",* Applied Physics B-Lasers and Optics, 2005. **81**(8): p. 1015-1047.

15. Chen, I.H., S.W. Chu, C.K. Sun, P.C. Cheng, and B.L. Lin, "*Wavelength dependent damage in biological multi-photon confocal microscopy: A micro-spectroscopic comparison between femtosecond Ti : sapphire and Cr : forsterite laser sources",* Optical and Quantum Electronics, 2002. **34**(12): p. 1251-1266.

16. Walmsley, I., L. Waxer, and C. Dorrer, "*The role of dispersion in ultrafast optics",* Review of Scientific Instruments, 2001. **72**(1): p. 1-29.

17. Liang, H., W.H. Wright, S. Cheng, W. He, and M.W. Berns, "*Micromanipulation of Chromosomes in Ptk2 Cells Using Laser Microsurgery (Optical Scalpel) in Combination with Laser-Induced Optical Force (Optical Tweezers)",* Experimental Cell Research, 1993. **204**(1): p. 110-120.

18. Liang, H., W.H. Wright, C.L. Rieder, E.D. Salmon, G. Profeta, J. Andrews, Y.G. Liu, G.J. Sonek, and M.W. Berns, "*Directed Movement of Chromosome Arms and Fragments in Mitotic Newt Lung-Cells Using Optical Scissors and Optical Tweezers",* Experimental Cell Research, 1994. **213**(1): p. 308-312.

19. Konig, K., I. Riemann, and W. Fritzsche, "*Nanodissection of human chromosomes with near-infrared femtosecond laser pulses",* Optics Letters, 2001. **26**(11): p. 819-821.

20. Agrawal, G.P., "*Nonlinear Fiber Optics".* 1995: Academic Press.

21. Anderson, R.R. and J.A. Parrish, "*The Optics of Human-Skin",* Journal of Investigative Dermatology, 1981. **77**(1): p. 13-19.

22. Fischer, P., A. McWilliam, L. Paterson, C.T.A. Brown, W. Sibbett, K. Dholakia, and M. MacDonald. "*Two-photon ablation with1278nm laser radiation".* in *QEP-17.* 2006. Manchester, UK.

23. Fischer, P., A. McWilliam, L. Paterson, C.T.A. Brown, W. Sibbett, K. Dholakia, M. MacDonald *"Two Photon ablation with 1278nm laser radiation",* Journal of optics A: Pure and applied optics (accepted November 2006)

Chapter 6 – General conclusions

6.1 Summary

The work presented in this thesis was undertaken within the framework of the *Ultrafast Photonics Collaboration*, one of the key objectives of which, was the development of a femtosecond laser that operated around 1300nm. This involved the use of novel GaInNAs [1] or quantum-dot-based saturable absorbers [2]. Due to the success of this work, the Cr^{4+}:forsterite laser was used subsequently in several biophotonics applications [3,4]. Both telecommunications and biophotonics applications exploit the wavelength of operation of the Cr^{4+}:forsterite laser.

A comparison of the results obtained with the GaInNAs and a QD-based device when used as alternative saturable absorber candidates is included below as Table 6.1.

	GaInNAs	Quantum-dots
Saturable Absorption	7nm thick GaInNAs Quantum well	20/35 layers of InAs Quantum-dots
Bragg Stack Reflectivity	1250nm-1400nm	1250nm-1400nm
Pulse Duration (shortest)	62fs	158fs
Output Power (Highest)	215mW	85mW
Tuning Range	25nm	10nm
Saturation Fluence	$980\mu J/cm^2$	$280\mu J/cm^2$
Modulation Depth	1%	3%
Recovery Time	69ps	<50ps

Table 6.1 A comparison of the Cr^{4+}:forsterite laser performance incorporating the GaInNAs and QD based saturable absorbers.

A comparison of the results from the Cr^{4+}:forsterite laser incorporating the GaInNAs and quantum-dot based saturable absorbers raises the obvious question: which provides the superior performance? In terms of the laser output (pulse durations, output powers and tuning ranges) the performance of the GaInNAs SBR obviously surpasses that of the QD-based saturable absorber. Sub-100fs pulse durations with mode-locked output powers of 215mW with a 25nm tuning range were obtained. However, the device performance may paint a different picture. Lower saturation fluences [5] and faster recovery times potentially allow QD-based devices to be more versatile than their quantum-well counterparts. With the inhomogeneous broadening of the device permitted through the distribution of dot sizes, an enhanced spectral bandwidth greater than that available from quantum-well devices becomes accessible [6]. This will, in theory, allow shorter pulses to be accessible with quantum-dot-based devices rather than quantum-well devices.

It is noteworthy that both of these devices were previously untested in the mode locking of solid-state lasers into the femtosecond regime. In fact, this is the first published work of any quantum-dot-based saturable absorber producing femtosecond pulses from a solid-state laser. Continuing work on these devices will inevitably lead to an improved laser performance to that reported in this thesis, as others build upon this foundation.

6.2 Future work

Future work has been discussed on the basis of research reported in each individual chapter, and so in this section a brief overview is presented of the main highlights of this work as a whole. A specific area of research needed for successful future developments of ultrafast lasers that can be suitable for data-communications or

biophotonics relates to device designs that offer more compact and rugged laser configurations. This will undoubtedly require the replacement of the prism pair with dispersion compensating mirrors [7]. A reduced cavity size will naturally result in a higher pulse repetition frequency from the laser. This is desirable for applications in data-communications but can be detrimental for potential applications in biophotonics as the peak power (and energy) of each pulse is reduced, making two-photon interactions more difficult to generate for example.

The Cr^{4+}:forsterite laser could be designed to become a femtosecond module, essentially a box containing the femtosecond laser. This box would provide stable mode locked operation at the turn of a key, ideal for use over a number of disciplines and applications. The work presented in this thesis is the first step towards this goal and highlights some practical advances in components that might be incorporated into such a module. Variable pulse durations as described in Chapter 4 could be provided, as well as a tunable output over a range of wavelengths around 1300nm, as shown by the results presented in Chapter 3. If both these effects could be provided at the turn of a dial then this type of laser design would afford exceptional practicality and versatility.

Given that the zero-dispersion window is located around 1300nm for conventional optical fibres, a data-communications network based on femtosecond pulses could perhaps be well suited to this wavelength of operation. However, the future of this laser as an ultrashort pulse source for a data/tele-communications network will depend on the development of the associated equipment needed for such a network to operate. Amplifiers, for example, have been developed for superb performance at 1550nm, where current long-range networks operate. Such devices will require further development if a network based at 1300nm is to be created.

In the area of biophotonics, numerous experiments are still to be attempted with lasers of this type. Optical tweezing [8,9], photo-poration [10] and activation of caged compounds [11] represent just a few areas for their implementation. A major question is whether any of these applications can be undertaken satisfactorily after passing the laser beams through a thickness of tissue. One of the most exciting experiments to be attempted with the laser will involve the cutting of chromosomes that are still inside a living cell. The low single-photon absorption at this wavelength and the highly localised two-photon process should allow this to be achieved successfully without killing the cell. How this cell would then continue to divide and live after the cutting, or indeed the destruction, of a chromosome would be an extremely interesting area to research.

In the long term, Cr^{4+}:forsterite solid-state lasers, because of their wavelengths of operation, have a huge potential. This laser provides a source that can be applied to several very different and dynamic areas of research. The versatility of this laser will allow for its continued development and probable commercialisation. Indeed commercial companies are already beginning to offer Cr^{4+}:forsterite lasers [12].

Whether as an ultrafast source for a future in a femtosecond network meeting the ever-growing demand on the data/tele-communications industry, or in a hospital used for diagnostic or therapeutic purposes. I believe that a Cr^{4+}:forsterite laser will lay claim to an important place in our future society.

6.3 References

1.   McWilliam, A., A.A. Lagatsky, C.G. Lebum, P. Fischer, C.T.A. Brown, G.J. Valentine, A.J. Kemp, S. Calvez, D. Burns, M.D. Dawson, M. Pessa, and W. Sibbett, "*Low-loss GaInNAs saturable Bragg reflector for mode-locking of a femtosecond Cr4+: Forsterite-laser",* IEEE Photonics Technology Letters, 2005. **17**(11): p. 2292-2294.

2.   McWilliam, A., A.A. Lagatsky, B. C.T.A., W. Sibbett, A.E. Zhukov, V.M. Ustinov, A.P. Vasil'ev, and E.U. Rafailov, "*Quantum-dot-based saturable absorber for femtosecond mode-locked operation of a solid-state laser",* Optics Letters, 2006. **31**(10): p. 1444-1446.

3.   Fischer, P., A. McWilliam, C.T.A. Brown, K. Wood, M. MacDonald, W. Sibbett, and K. Dholakia, "*Deep Tissue Penetration of Radiation: Modelling and Experiments",* Paper CL-4-Wed, European Conference on Lasers and Electro-Optics (ECLEO), Munich, Germany, 2005.

4.   Fischer, P., A. McWilliam, L. Paterson, C.T.A. Brown, W. Sibbett, K. Dholakia, and M. MacDonald. "*Two-photon ablation with1278nm laser radiation".* in *QEP-17.* 2006. Manchester, UK.

5.   Unold, H.J., D. Lorenser, D.J.H.C. Mass, A. Rudin, R. Bellancourt, U. Keller, E. Gini, and D. Ebling. "*50GHz mode-locked VESCSELs: an integrable alternative to high-repitition-rate solid-state lasers".* in *Advanced Solid-State Photonics.* 2006. Lake Tahoe, California.

6.   Ustinov, V.M., A.E. Zhukov, A.Y. Egorov, and N.A. Maleev, "*Quantum Dot Lasers",* in *Series on Semiconductor Science and Technology*, O.S. publications, Editor. 2003.

7.   Stormont, B., I.G. Cormack, M. Mazilu, C.T.A. Brown, D. Burns, and W. Sibbett, "*Low-threshold, multi-gigahertz repetition-rate femtosecond Ti : sapphire laser",* Electronics Letters, 2003. **39**(25): p. 1820-1822.

8.   Agate, B., C.T.A. Brown, W. Sibbett, and K. Dholakia, "*Femtosecond optical tweezers for in-situ control of two-photon fluorescence",* Optics Express, 2004. **12**(13): p. 3011-3017.

9.   Paterson, L., M.P. MacDonald, J. Arlt, W. Sibbett, P.E. Bryant, and K. Dholakia, "*Controlled rotation of optically trapped microscopic particles",* Science, 2001. **292**: p. 912-914.

10.   Paterson, L., B. Agate, M. Comrie, R. Ferguson, T.K. Lake, J.E. Morris, A.E. Carruthers, C.T.A. Brown, W. Sibbett, P.E. Bryant, F. Gunn-Moore, A.C. Riches, and K. Dholakia, "*Photoporation and cell transfection using a violet diode laser",* Optics Express, 2005. **13**(2): p. 595-600.

11.   Carr, J.L., K.N. Wease, M.P. Van Ryssen, S. Paterson, B. Agate, K.A. Gallagher, C.T.A. Brown, R.H. Scott, and S.J. Conway, "*In vitro photo-release of a TRPV1 agonist"*, Bioorganic & Medicinal Chemistry Letters, 2006. **16**(1): p. 208-212.

12.   Del Mar Photonics *http://www.femtosecondsystems.com*

Publications

1. **Two Photon ablation with 1278nm laser radiation**
   P. Fischer, A. McWillam, L. Paterson, C.T.A. Brown, W. Sibbett, K. Dholakia, M. MacDonald
   Journal of optics A: Pure and applied optics (accepted November 2006)

2. **Quantum-dot Based Saturable Absorber for Femtosecond Modelocked Operation of a Solid-state Laser**
   A. McWilliam, A.A. Lagatsky, C. T. A. Brown A. E. Zhukov, V.M. Ustinov and A.P. Vasil'ev, E.U. Rafailov, W. Sibbett,
   Optics Letters Vol. 31 (10) page 1444-1446 May 2006

3. **Up to 30 mW of broadly tunable CW green-to-orange light, based on sum frequency mixing of Cr4+:forsterite and Nd:YVO4 lasers**
   Jesper L. Mortensen, Alan McWilliam, Christopher G. Leburn, Peter Tidemand-Lichtenberg, Morten Thorhauge, Jirí Janousek, Christian T. A. Brown, Alexander A. Lagatsky, Preben Buchhave, Wilson Sibbett
   Optics Communications Vol. 260 (2) page 637-640 April 2006

4. **Low-loss GaInNAs saturable Bragg reflector for modelocking of a femtosecond Cr^{4+}:forsterite-laser**
   A. McWilliam, A. A. Lagatsky, C. G. Leburn, P. Fischer, C. T. A. Brown, W. Sibbett, G. J. Valentine, A. J. Kemp, S. Calvez, D. Burns, M. D. Dawson, J. Kontinnen, T. Jouhti, M. Pessa
   IEEE Photonics Technology Letters, Vol. 17 (11) page 2292-2294 November 2005

5. **Femtosecond Cr:forsterite laser modelocked with a GaInNAs saturable Bragg reflector**
   A. McWilliam, C. G. Leburn, A. A. Lagatsky, C. T. A. Brown, W. Sibbett, G. J. Valentine, A. J. Kemp, S. Calvez, D. Burns, M. D. Dawson, J. Kontinnen, T. Jouhti, M. Pessa
   Trends in Optics and Photonics, 2005 Vol .98 Page 663-668 2005

Conference Presentations

6. **Quantum-dot based saturable absorberfor femtosecond mode-locked operation of a solid-state laser**
   A. McWilliam, A.A. Lagatsky, C. T. A. Brown, A. E. Zhukov, V.M. Ustinov and A.P. Vasil'ev, E.U. Rafailov, W. Sibbett
   QEP-17 Manchester, UK, September 2006

7. **Two-photon ablation with 1278nm laser radiation**
   P. Fischer, A. McWillam, L. Paterson, C.T.A. Brown, W. Sibbett, K. Dholakia, M. MacDonald
   QEP-17 Manchester, UK, September 2006

8. **Quantum-Dot Based Saturable Absorber for Femtosecond Mode-locked Operation of a Solid-State Laser**
   A. McWilliam, A.A. Lagatsky, C. T. A. Brown, A. E. Zhukov, V.M. Ustinov and A.P. Vasil'ev, E.U. Rafailov, W. Sibbett
   Paper CMJJ1 Conference on Lasers and Electro-Optics (ECLEO) Long Beach, California, USA May 2006

9. **Photonic analogue to digital conversion system using broadband modelocked laser with 20GHz bandwidth**
   P Jiang , Y Chai, I White , R Penty , J Heaton, A Kuver, S Clements , C G Leburn , A McWilliam , A Lagatsky , C Brown, W Sibbett
   European Conference and Exhibition on Optical Communication, Glasgow, Scotland, September 2005

10. **Femtosecond Cr:forsterite laser modelocked with a GaInNAs saturable Bragg reflector**
    A. McWilliam, C. G. Leburn, A. A. Lagatsky, C. T. A. Brown, W. Sibbett, G. J. Valentine, A. J. Kemp, S. Calvez, D. Burns, M. D. Dawson, J. Kontinnen, T. Jouhti, M. Pessa
    2nd International Symposium on Ultrafast Photonic Technologies, St Andrews, August 2005

11. **Low-loss GaInNAs saturable Bragg reflector for femtosecond modelocking of a Cr4+:forsterite laser**
    A. McWilliam, C.G. Leburn, A.A. Lagatsky, P. Fischer, C.T.A. Brown, W. Sibbett, G.J. Valentine, A.J. Kemp, S. Calvez, D. Burns, M.D. Dawson, M. Pessa
    Paper CP3-1-Thu, European Conference on Lasers and Electro-Optics (ECLEO) 2005, Munich, Germany, June 2005

12. **Deep tissue penetration of radiation: 3D modelling and experiments**
    P. Fischer, A. McWilliam, C. T. A. Brown, K. Wood, M. MacDonald, W. Sibbett, K. Dholakia
    Paper CL-4-Wed, European Conference on Lasers and Electro-Optics (ECLEO) 2005, Munich, Germany, June 2005

13. 80 GSPS Photonic Analogue to Digital Conversion
P. Jiang, Y. J. Chai, C. G. Leburn, A. McWilliam, I. H. White, R. V. Penty, J. Heaton, A. Kuver, S. Clements, A. A. Lagatsky, C. T. Brown, W. Sibbett
Conference on Lasers and Electro-Optics, Baltimore, USA, paper CTuN4, May 2005

14. Femtosecond Cr:forsterite laser modelocked with a GaInNAs saturable Bragg reflector
A. McWilliam, C. G. Leburn, A. A. Lagatsky, C. T. A. Brown, W. Sibbett, G. J. Valentine, A. J. Kemp, S. Calvez, D. Burns, M. D. Dawson, J. Kontinnen, T. Jouhti, M. Pessa
Advanced Solid State Photonics, Vienna, Austria, February 2005

15. Experimental demonstration of femtosecond switching of a fully packaged all-optical switch
C. K. Yow, Y. J. Chai, C. G. Leburn, A. McWilliam D. Reading-Picopoulos, A. A. Lagatsky, G. Maxwell, R. McDougall, C. T. A. Brown, W. Sibbett, R. V. Penty, I. H, White
Optical Fibre Communications, Anaheim, USA, paper OThE4 March, 2005.

Acknowledgements

I'd like to begin by thanking Professor Wilson Sibbett who provided the opportunity for me to undertake this PhD. Your guidance, support and enthusiasm have proved invaluable during the last three years.

Also a big thank you to Alex for all his help in getting me started. Teaching me to build a laser and keeping me on the right track throughout this work. For all your patience and confidence in my work and reading through this thesis.

Tom, Chris and Pascal for all the help and answers you have provided to me during this PhD and for making me cut up that rat brain.

All the members of W-squad; Ben, Maria Ana, Doog, Edik, Abdul, Will, Barry, Helen, Lyn, Mike and everyone else who was regularly in our office making it such a fantastic place to "work", including those infamous whisky Wednesdays!

From Strathclyde Alan, Gareth and Stephan for supplying the GaInNAs SBR and your enthusiasm and help getting the GaInNAs results.

Everyone at the Centre for Photonic Systems at Cambridge University for their welcome while I was there helping in experiments and Jesper Mortensen for coming over from Denmark and working on some fantastic yellow light experiments.

Last but certainly not least my family and fiancée for all their love and support during this time. I could not have done it without you.